University of Stavanger

Faculty of Science and Technology

MASTER'S THESIS

Study program: MSc in Petroleum Engineering Specialization: Reservoir Engineering	Spring semester, 2011 Open
Writer: Ursula Lee Norris	…… (Writer's signature)
Faculty supervisor: Dimitrios G. Hatzignatiou External supervisor(s): Arne Stavland	
Titel of thesis: Core-Scale Simulation of Polymer Flow through Porous Media	
Credits (ECTS): 30	
Key words: Polymer flooding Simulation of experimental data History matching Bulk flow rheology/Carreau Model Polymer shear thickening Polymer shear thinning Polymer degradation	Pages: …… + enclosure: …… Stavanger, June 15, 2011

ABSTRACT

From a multitude of laboratory studies conducted by various researchers during roughly the last 40 years (e.g. Hirasaki and Pope 1974, Heemskerk et al. 1984, Stavland et al. 2010), it has been identified that the behavior of partially hydrolyzed polyacrylamide (HPAM) polymer solutions in porous media is more complicated than what the bulk rheology might suggest. For decades, laboratory studies have reported the existence of shear thickening and degradation flow regimes when HPAM polymers have been exposed to high frontal velocities during corefloods. Recently developed models have displayed the capacity to accurately predict numerical values for the apparent viscosity behavior of HPAM polymers in the shear thickening and degradation flow regimes without in-depth data from coreflood experiments.

Having the ability to simulate this polymer behavior is valuable for selecting effective polymer flood design parameters, but doing this would be impossible if the simulation technology does not accurately reflect the experimental findings. This thesis sought to determine whether or not a commercially available simulator could accurately simulate results from both single- and two-phase polymer coreflood experiments conducted for a range of injection rates, which included rates that exhibiting polymer degradation behavior. The adherence to physically realistic input values with respect to experimentally derived parameters was of primary importance during the development of the models. When specific values were not available for certain simulation parameters, a reasonable range of values were investigated, and the best fitting results were selected. Through a methodical approach used to identify the best input values, two simulation models were created which produced results that were well matched with the experimental data. In the single phase simulation, the shear thinning, shear thickening, and degradation flow regimes were successfully modeled, but numerical issues arose for injection rates larger than 7.5 mL/min. In the two phase water-wet simulation, the modeled polymer behavior spanned from the shear thinning to the shear thickening flow regimes, but did not include the degradation behavior. With this model, both the pressures and cumulative oil production were successfully matched. Ultimately, understanding how to simulate the polymer behavior on a core-scale will improve the ability to model polymer floods on the field-scale.

ACKNOWLEDGMENTS

First and foremost, I would like to thank Dr. Dimitrios G. Hatzignatiou for his very generous assistance with this work. His willingness to make time for me and his interest in the success of this undertaking has benefited me immensely. I am especially grateful for his patience, knowledge, guidance, and support.

I would also like to sincerely thank Arne Stavland for his support, expertise, and time. His explanation of the experimental proceedings proved to be an invaluable resource, and I greatly appreciate his willingness to help with this work.

Additionally, I would like to extend many thanks to my fellow student, Hojatollah Moradi, whose experimental work was the basis for one of my simulations. I greatly appreciate his willingness to take the time necessary to explain his experiments so that I could be successful with my simulations. I wish him all my best with his future endeavors after graduating.

It is also my pleasure to offer a very grateful word of thanks to Hess Corporation for their generous sponsorship of my education at the University of Stavanger.

Finally, I would like to thank my close friend, Margaret Luthar, who I am so happy to have met in Stavanger.

TABLE OF CONTENTS

LIST OF FIGURES

CHAPTER 5 FIGURES

LIST OF TABLES

CHAPTER 1 - INTRODUCTION

For most oil reservoirs, primary depletion only produces 20-30% of the initial hydrocarbon content. The oil production that occurs during this primary depletion phase is produced as a result of the reservoirs natural energy, and it comes to an end as the natural energy tapers off. Because such a large percentage of the initial oil remains even after the reservoir no longer has the energy required to recover it, a lot of research has been dedicated to enhanced oil recovery, improved oil recovery, and reservoir pressure maintenance.

Water injection was one of the original methods used to revive a pressure depleted reservoir and provide pressure support such that production could be continued. The fact that all reservoirs produce some sort of brine in conjunction with their hydrocarbons made water injection an ideal operation with regards to convenience, availability, and cost. Although produced water might be the most obvious injection fluid, any form of chemically compatible water which is available at the required quantity can be used.

One of the big challenges that engineers face with water flooding is related to water's tendency to travel very quickly through the reservoir. Because water has such a high mobility, it tends to by-pass large volumes of oil, and "break-through," to the producing well before adequately sweeping the reservoir (Green and Willhite 1998). This problematic characteristic of water flooding ultimately results in only part of the reservoir being contacted for a realistic time frame and injection scheme. Additionally, reservoir heterogeneities will exacerbate the injected water's tendency to only mobilize the oil that resides in high permeability conduits rather than contacting the whole reservoir (Green and Willhite 1998).

When designing a successful pressure maintenance operation, it is not just the mobility of the displacing phase that is important, the relationship between the behaviors of the displacing and displaced phases are also important. The ratio of the oil mobility and water mobility can be used to gain a general understanding about the efficiency of an injection operation. With regards to the phase mobility values, the optimal sweep efficiency occurs when the mobility of the displacing phase is less than or equal to the mobility of the displaced phase. The required reduction in the mobility of the injected phase can be achieved by increasing the viscosity of the injected phase. Undesirable behaviors such as fluid fingering and frontal instabilities can be dampened by adding polymer molecules to the injected phase which cause a decrease in the fluid mobility. Thus far, polymer flooding has been described as an effective pressure maintenance and mobility control process when used on its own, but it also has been found to be successful in conjunction with other processes that require mobility control such as CO_2 injection (Green and Willhite 1998).

From an engineering perspective which seeks economic viability and efficiency, polymer flooding is a very effective method of improving oil recovery with regards to pressure maintenance and mobility control. Adding a relatively small concentration of polymer to water will result in a sizable increase in viscosity. Additionally, since the interest in polymer augmented flooding processes has not been isolated to one geographical area; the demand for materials has led to world-wide availability of relatively low-cost polymer products.

Even though the cost of operating a polymer flood is relatively inexpensive compared to other forms of enhanced and improved oil recovery, it is still an expensive endeavor and has therefore warranted attention from researchers. The behavior of partially hydrolyzed polyacrylamide (HPAM) macromolecules has been of special interest due to their somewhat complex behavior in a porous media. A recent study conducted by Stavland et al. (2010), which focused on developing a model to describe some of the complex behaviors that appear when HPAM is core flooded for a range of injection rates, has resulted in a relationship that uses bulk rheological parameters to calculate the apparent viscosity of the polymer solution in the porous media. The newly created model is especially important in that it can handle the whole range of polymer flow regimes from Newtonian to degradation. The ability to model the degradation regime, which occurs at very high flow rates, is particularly of interest since previous models have only succeeded in modeling up to the shear thickening regime.

The purpose of studying these fluids is to develop an understanding of their intricate behaviors which can then be used for practical field applications. Since all field operations are ultimately studied through simulation models of some form, it is important that the simulation technology is on par with all relevant experimental findings. The objective of the following work is to see if a realistic model which simulates these experimental results can be developed using the technology currently available in a commercial simulator.

CHAPTER 2 - LITERATURE REVIEW

2.1 - GENERAL POLYMER BEHAVIOR

The two main types of polymer which have been most widely studied by the petroleum industry are polyacrylamides and biopolymers. Since the focus of this thesis is on the modeling of HPAM (partially hydrolyzed polyacrylamide) experimental corefloods, biopolymers will only be mentioned briefly in this chapter.

Unhydrolyzed polyacrylamides are strongly predisposed to adsorbing onto mineral surfaces such as those present in geologically created porous mediums. For this reason, the macromolecules are hydrolyzed in a process where the polyacrylamide molecules are reacted

with a base which converts some of the amide groups to carboxyl groups. Since both the carboxyl groups and the mineral surfaces are negatively charged, HPAM adsorption on the rock surface is reduced (Green and Willhite 1998, Hirasaki and Pope 1974). Typical bases used for this hydrolysis process include sodium hydroxide, sodium carbonate, and potassium hydroxide (Green and Willhite 1998). While it is important to hydrolyze the polymer to prevent massive amounts of adsorption, it is also imperative that the polymer not be over hydrolyzed since this will result in decreased polymer solubility in water when divalent cations are present. The optimum degree of hydrolysis tends to fall in the range of 15% to 33% (Green and Willhite 1998).

The dynamic structure of polyacrylamide molecules is best described as a flexible coil. This characteristic plays an important role in understanding the HPAM's viscosity behavior which does not occur in rigid bodied polymers such as bioploymer. Many researchers have noted the occurrence of shear thickening behavior and polymer degradation in experiments with porous media (Green and Willhite 1998, Heemskerk et al. 1984, Hirasaki and Pope 1974, Maerker 1976, Morris 1978, Southwicke and Manke 1988). The presence of this behavior is directly related to the dynamic structure of the HPAM macromolecule. Later sections in this thesis will cover this behavior in more detail as it applies to the different flow regimes.

2.2 - BULK RHEOLOGY AND THE CARREAU MODEL

The stability and viscosity of a polymer solution depends on multiple parameters, some of which include: polymer concentration, salinity effects, intrinsic viscosity, presence of oxygen, reservoir temperature, and shear rate. The relationship between the intrinsic viscosity and the polymer viscosity is such that as the intrinsic viscosity increases, so does the polymer viscosity (Green and Willhite 1998). The polymer concentration also has a direct relationship with the polymer viscosity where an increase in the polymer concentration results in an increase in the polymer viscosity. A polymer solution can become unstable and lose viscosity if it is exposed to high salinities or high temperatures. Oxidative attacks can also negatively affect the polymer viscosity and result in a loss of polymer stability (Green and Willhite 1998). The effect of the shear rate on the polymer viscosity determined by bulk rheology varies in a predictable manner as described by the Carreau model which is discussed below.

The most common experiments preformed on polymers are aimed at determining their bulk rheological properties. When the apparent viscosity values from bulk rheology experiments are plotted against shear rate, both HPAM and biopolymer display shear thinning behavior. As the shear rate increases from low to high values, the fluid behavior will go from Newtonian, to shear thinning, and then back to Newtonian. The first Newtonian regime is referred to as the lower Newtonian and is characterized by constant apparent viscosity. This apparent viscosity will remain constant for increasing shear rates until the shear thinning regime is reached (Green

and Willhite 1998). Although this transition occurs gradually, for the purposes of modeling, it is demarcated by a single shear rate, τ_r.

The shear thinning regime is characterized by a decreasing apparent viscosity for increasing shear rates. The rate of viscosity decrease follows a power-law model, and the power-law exponent, n, is a rheological characteristic of the polymer. In the last Newtonian region, which is also known as the upper Newtonian regime, the apparent viscosity asymptotically approaches the solvent viscosity for increasing values of shear rate (Green and Willhite 1998). The rheogram in Figure 2.1 depicts the three flow regimes typically seen in bulk rheology experiments.

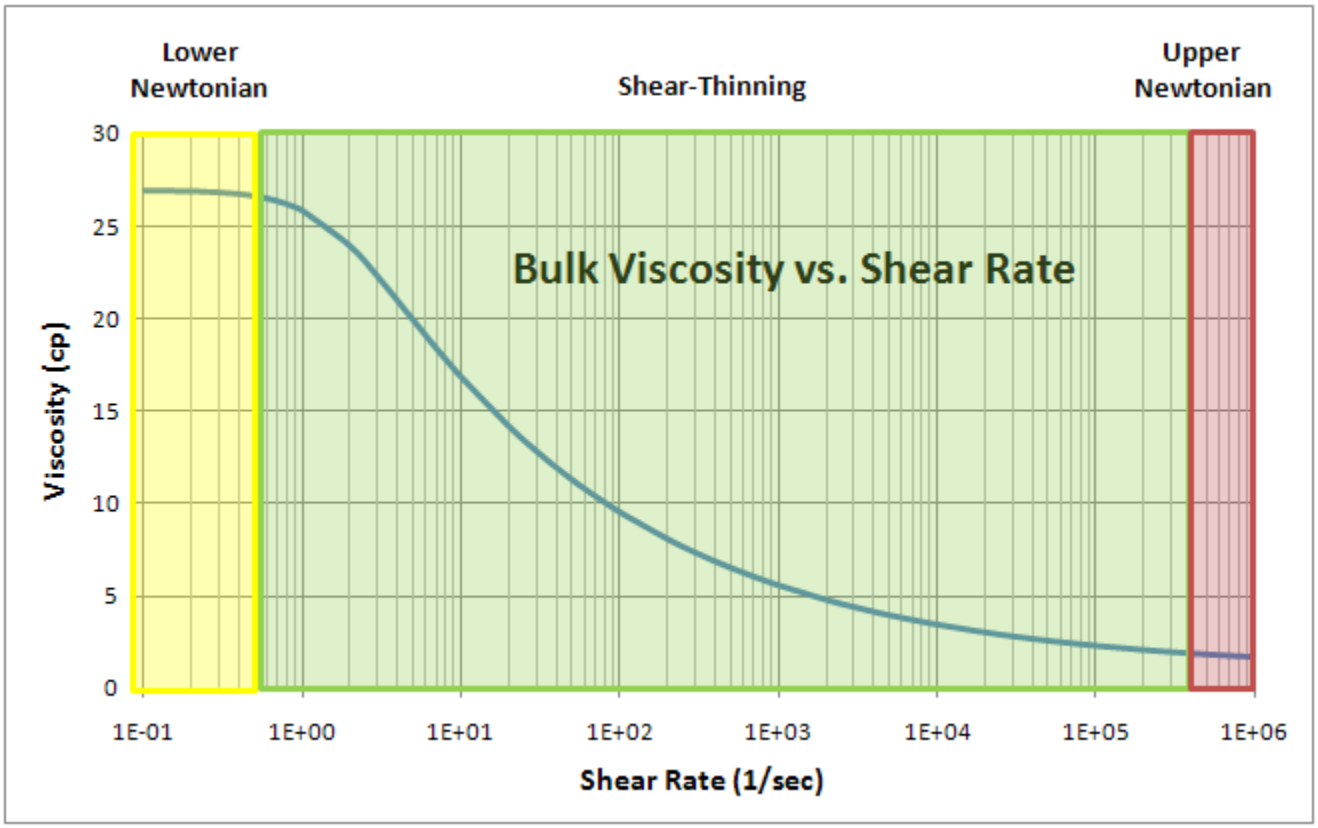

Figure 2.1: Flow regimes for typical polymer bulk rheology behavior as a function of shear rate

The Carreau model combines all of these regimes into a single equation which can be fit to experimental results by determination of the critical shear rate for shear thinning flow (τ_r), and the power law exponent (n) (Green and Willhite 1998). The bulk viscosity according to the Carreau model is calculated as:

$$\mu - \mu_U = (\mu_L - \mu_U)\left(1 + \left(\dot{\gamma}/\tau_r\right)^2\right)^{\frac{n-1}{2}} \qquad \text{(Equation 1)}$$

Where μ_U is the viscosity in the upper Newtonian regime, μ_L is the viscosity in the lower Newtonian regime, and $\dot{\gamma}$ is the shear rate associated with the viscosity of interest. τ_r is determined by identifying the shear rate associated with the intersection of lines fit through experimental data for the lower Newtonian and shear thinning regimes. Figure 2.2 gives a graphical example of this method.

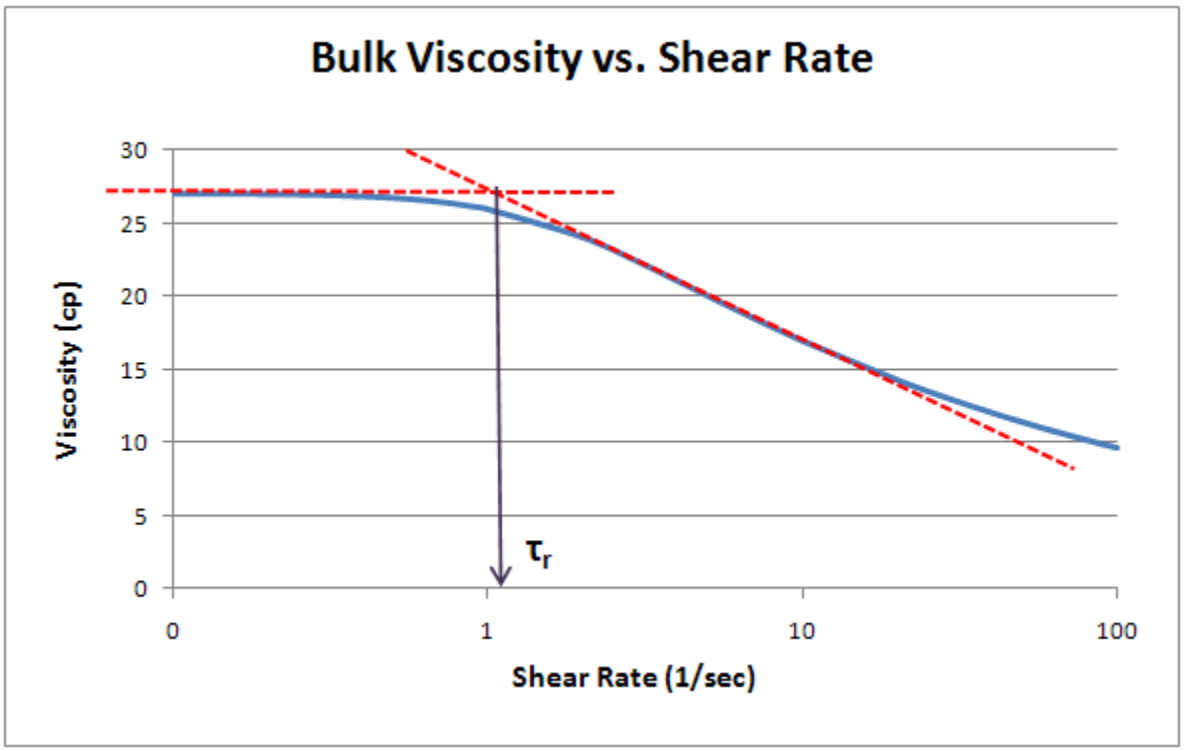

Figure 2.2: A graphical representation of how to determine the transition shear rate

The inverse of this shear rate is the relaxation time, λ_1, which will be discussed later in this chapter. The power-law exponent is also determined from experimental data by calculating the slope of a regression line through the experimental shear thinning data on a log-log plot (Green and Willhite 1998).

2.3 - BEHAVIOR IN POROUS MEDIA: SHEAR THICKENING

The behavior of HPAM in porous media is not well predicted from the rheological behavior without the help of a correlation. For a given shear rate, it is not uncommon for polymer to exhibit shear thinning or upper Newtonian regimes in rheological tests while exhibiting shear thickening or degradation in a core experiment. Shear thickening is a physical response that polyacrylamides exhibit when exposed to high frontal velocities in a porous media (Hirasaki and Pope 1974). In comparison to the rigid, rod-like molecular structure of biopolymers (which do not produce shear thickening behavior), polyacrylamides are better described as flexible coils

that take on random configurations (Green and Willhite 1998). The flexible nature of the coil structure of polyacrylamide molecules lends to their ability to produce viscoelastic responses in high shear environments (Green and Willhite 1998, Heemskerk et al. 1984, Hirasaki and Pope 1974, Southwick and Manke 1988).

There are two primary characteristics at play when considering the onset of shear thickening. The first one, which is a characteristic of the porous media, is the time it takes for a polymer molecule to travel from one pore throat to another which is effectively dependent on the space between pore throats (Green and Willhite 1998, Heemskerk et al. 1984, Hirasaki and Pope 1974). This characteristic can be calculated as the inverse of the stretch rate where the stretch rate is defined as:

$$\dot{\mathcal{E}} = \frac{v}{d_{p/2}} \qquad \text{(Equation 2)}$$

In this equation, v is the average interstitial velocity and d_p is the average grain diameter. For the purpose of this work, the Carman-Kozeny equation is used to determine the average grain diameter (Delshad et al. 2008, Stavland et al. 2010).

$$d_p = \frac{1-\phi}{\phi}\sqrt{\frac{72\tau k}{\phi}} \qquad \text{(Equation 3)}$$

Where k is permeability, ϕ is porosity, and τ is the formation tortuosity.

The second characteristic, which affects the presence of viscoelastic behavior and is related to the polymer solution, is the amount of time required for the polymer molecules go from an elongated form back to a relaxed coil configuration (Green and Willhite 1998, Heemskerk et al. 1984). This is referred to as the relaxation time, λ_1, and is measured in the lab with rheological equipment.

In order for shear thickening to occur, the polymer relaxation time must be of the same order of magnitude or larger than the time it takes for the polymer to travel between one constriction to another. The Deborah Number, which is a dimensionless relationship between the stretch rate and the polymer solution relaxation time, is useful in correlating the properties of the fluid-rock system with the onset of viscoelastic or shear thickening effects (Heemskerk et al. 1984, Hirasaki and Pope 1974, Southwick and Manke 1988). Previous research has linked the onset of viscoelastic behavior to a Deborah Number of approximately .5 (Heemskerk et al. 1984). The experimental research which this thesis aims to simulate found the onset of elongation to correspond with a Deborah Number of .22 (Stavland et al 2010).

$$N_{De} = \dot{\mathcal{E}}\lambda_1 \qquad \text{(Equation 4)}$$

The high apparent viscosity caused by the elastic strain due to polymer elongation can be modeled as a function of the Deborah Number (Green and Willhite 1998, Heemskerk et al. 1984, Hirasaki and Pope 1974, Southwick and Manke 1988). Of the multiple models that have been proposed in the past, two of the most recent models will be discussed for this work. The first model, which was developed by Delshad et al. (2008), calculates the additional viscosity due to elongation as:

$$\mu_{el} = \mu_{max}[1 - \exp(-(\lambda_2 N_{De})^{n_2 - 1})] \quad \text{(Equation 5)}$$

Here, μ_{max}, λ_2, and n_2 are described as empirical constants (Delshad et al. 2008). One of the advantages of this model compared to its predecessors is that the apparent viscosity associated with elongation is restricted by the value of μ_{max}. In previous models the elongation viscosity was not restricted to a maximum value and could increase indefinitely as the Deborah Number increased (Delshad et al. 2008).

The second method, developed by Stavland et al. (2010), aims to model the shear thickening viscosity using the critical shear rate as shown in Equation 6.

$$\mu_2 = (\lambda_2 \dot{\gamma})^m \quad \text{(Equation 6)}$$

Where m, a tuning parameter known as the elongation exponent, depends on the molecular weight of the polymer. This tuning parameter must be larger than zero (Stavland et al. 2010). The critical shear rate, λ_2 in the viscosity model proposed by Stavland et al. (2010) is dependent on the Deborah Number and can be calculated as follows:

$$\frac{1}{\lambda_2} = N_{De} * \left(\frac{1-\phi}{\phi}\right) * \left(\frac{6\alpha\sqrt{\tau}}{\lambda_1}\right) \quad \text{(Equation 7)}$$

Here τ is the formation tortuosity.

2.4 - BEHAVIOR IN POROUS MEDIA: POLYMER DEGRADATION

The viscosity associated with shear thickening will eventually reach a maximum value after which the viscosity will decrease with increasing shear rate. Polymer begins to degrade when the time required for the polymer to pass from one constriction to the next grows to be larger than the polymer's relaxation time, λ_1 (Green and Willhite 1998, Maerker 1976). When the polymer molecules are exposed to very high flow rates, they start to degrade due to the large viscoelastic stresses which are present in the elongational flow fields (Maerker 1976, Seright 1983, Southwick and Manke 1988). The occurrence of polymer shredding and mechanical degradation is especially severe in porous media that have a low permeability (Maerker 1975).

One of the ways that polymer degradation occurs is by polymer rupture and polymer chain halving (Maerker 1975, Southwick and Manke 1988). Each polymer solution has a certain distribution of molecular weights in accordance with the polydispersivity of the mixture. When polymer rupture occurs, the very heavy molecular weights are affected the most (Seright et al. 2010). The preferential shredding of longer polymer chains results in the higher molecular weights becoming more like the average molecular weight of the polymer (Green and Willhite 1998). It should be pointed out that if the shear rate is increased, shredding of the polymer molecules will result in a lower molecular weight polymer, and the polymer viscosity will behave according to the new molecular weight (Stavland et al. 2010).

Just as there is a critical shear rate associated with the onset of shear thickening, there is also a critical shear rate associated with the onset of degradation. This shear rate, $1/\lambda_3$, can be determined by analyzing the viscosity of core flood effluent (Stavland et al. 2010). A modified Carreau model has been used to match the Newtonian viscosity of the effluent. This model is as follows:

$$\mu_3 = \mu_\infty + (\mu_0 - \mu_\infty) * (1 + (\lambda_3 \dot{\gamma})^x)^{\frac{k}{x}} \qquad \text{(Equation 8)}$$

Where k is the experimentally matched shear thinning exponent, and x is a tuning parameter. In accordance with the experimental findings by Stavland et al. (2010), and for the purposes of this thesis, k is taken to be -1/2, and x is taken to be 4.

2.5 - BEHAVIOR IN POROUS MEDIA: POLYMER RETENTION AND THE LANGMUIR ISOTHERM

Although the process of partially hydrolyzing polyacrylamide molecules reduces the adsorption tendency of the polymers, it does not completely mitigate the issue. Polymer retention, which is primarily caused by adsorption to mineral surfaces, can also occur by other means such as mechanical entrapment, hydrodynamic retention, and gel formation (Green and Willhite 1998, Hirasaki and Pope 1974, Zaitoun and Kohler 1987). The degree of polymer retention is typically determined by flow experiments in conjunction with material balance calculations. Since the amount of surface area available for retention affects the levels of adsorption, results for retention tests in consolidated and unconsolidated samples are not interchangeable (Green and Willhite 1998).

It is also important to keep in mind that the molecular weight which is used to describe a particular polymer is merely an average value and does not represent the polydispersivity, or wide range of macromolecule sizes present in the specimen (Green and Willhite 1998). Since higher molecular weight polymers have a greater likelihood of becoming mechanically trapped, it is important to conduct the necessary flow tests in representative porous media (Chauveteau et al. 2002, Seright et al. 2010, Zaitoun and Chauveteau 1998, Zaitoun and Kohler 1987).

Because of the relationship between pore throat size and permeability, it is not surprising that results from published retention data show a trend of increased polymer retention in low permeability samples (Hirasaki and Pope 1974, Zaitoun and Chauveteau 1998, Zaitoun and Kohler 1987, Zitha et al. 1995). Just as the permeability of the porous medium affects the transport of the polymer, the adsorption of polymer on the pore walls causes a decrease in permeability (Hirasaki and Pope 1974, Chauveteau et al. 2002). Often times the adsorption is conceptually modeled as a monolayer, although it has also been noted that additional polymer may adsorb via lateral compression if the rock surface has a high affinity for the polymer. For the monolayer model, the thickness of the layer has been experimentally found to be approximately equal to the diameter of the molecular coil (Hirasaki and Pope 1974).

A common method for modeling polymer retention in porous media is the Langmuir isotherm. This correlation is presented below as it is presented in the Fluid and Rock Properties section of the CMG STARS manual (STARS Users Manual 2009).

$$Adsoprtion = \frac{A_z}{1+B_z} \qquad \text{(Equation 9)}$$

Where the subscript z denotes a particular component and the maximum adsorption can be calculated as A_z/B_z. Since adsorption is expected to decreases as temperature decreases, A_z and B_z are generally temperature dependent. The model, which is based on an equilibrium relationship, assumes that polymer retention is instantaneous and reversible. It is widely believed that the actual behavior of polymer adsorption occurs in an instantaneous and irreversible manner (Green and Willhite 1998). To this end, the Langmuir model is still applicable in many cases but is not appropriate for cases where the polymer concentration is decreasing (Green and Willhite 1998).

2.6. - BEHAVIOR IN POROUS MEDIA: POLYMER RETENTION BY MECHANICAL ENTRAPMENT

Mechanical entrapment is related to the ability of a polymer to pass through a constriction in the porous media and is subject to the size of the polymer relative to the constriction (Zitha et al. 1995). The radius of a polymer coil is roughly estimated by the gyration radius which can be calculated from the Fox-Flory equation as follows:

$$[\eta_0] = \Phi' \times \frac{R_g^{\,3}}{M_w} \qquad \text{(Equation 10)}$$

Where $[\eta_0]$ is the polymer intrinsic viscosity, M_w is the polymers' average molecular weight, R_g is the gyration radius, and Φ' is a universal constant equal to 4.2×10^{24} in CGS units (Zitha et al. 1995).

An alternative method for calculating the gyration radius, which was suggested for the research which this thesis aims to model, is as follows (Stavland et al. 2010):

$$R_g = A \times {M_w}^b \qquad \text{(Equation 11)}$$

Where R_g is the radius of gyration, A is the cross sectional area of the capillary tubes, M_w is the molecular weight associated with the polymer, and b takes a value between .5 and .6 for random coil molecules (Stavland et al 2010). The Hagen-Poiseuille flow model, which approximates the porous media as a bundle of capillary tubes, can be used to estimate the average pore radius (Hirasaki and Pope 1974, Zitha et al. 1995). The pore radius is calculated in this method as follows:

$$r = \sqrt{\frac{8k}{\phi}} \qquad \text{(Equation 12)}$$

Where k is the permeability, and ϕ is the porosity for the porous medium.

Experimental studies have linked mechanical entrapment of flexible coiled polymers to a dependence on the flow regime via the flow rate (Chauveteau et al. 2002). At low shear rates associated with the Newtonian flow regime, the HPAM molecules remain in a coiled state and tend to pass easily through pore constrictions. As the shear rates increase and shear thinning begins, the polymers are slightly, but not permanently, deformed by the associated shear forces. Increasing the shear rates further will lead to strong enough shear forces that the polymers are elongated and shear thickening behavior is exhibited (Delshad et al. 2008, Chauveteau et al. 2002, Green and Willhite 1998). Since the polymers do not have enough time to return to their relaxed conformation between successive pore constrictions, the polymers are propagated through the reservoir in an elongated state (Delshad et al. 2008, Heemskerk et al. 1984, Hirasaki and Pope 1974). If these elongated polymers are adsorbed, especially near entrances to constrictions where hydrodynamic forces are the largest, the result could be bridged and blocked pore throats (Zaitoun and Kohler 1987, Zitha et al. 1995).

Although some earlier works suggest the polymer concentration has little effect on the adsorption (Green and Willhite 1998), the concentration of the polymer has been demonstrated to have an effect on pore plugging (Zaitoun and Chauveteau 1998, Zitha et al. 1995). As can be expected, injecting higher concentrations of polymer will lead to larger amounts of pore plugging and pore blockage than the injection of lower concentrations of polymer (Zaitoun and Chauveteau 1998, Zitha et al. 1995). At the same time, lower polymer concentrations have larger stretched lengths than a higher polymer concentration for a give shear rate (Zitha et al. 1995). Since the retention associated with pore throat blockage is a

function of how elongated the polymer molecules are, the larger stretched lengths of the lower concentration polymer can still result in blocked pores (Zitha et al. 1995).

2.7 - BEHAVIOR IN POROUS MEDIA: THE INACCESSIBLE PORE VOLUME

The volume of the pore space that is not able to conduct polymer flow due to the large size of the molecules relative to the pore passage ways is referred to as the inaccessible pore volume (IPV). During the coreflood experiments conducted by Stavland et al. (2010), the apparent viscosity values calculated for low injection rates resulted in lower values than the bulk rheology would suggest. This behavior, which has also been reported by other researchers (Zaitoun and Kohler 1987), has been attributed to the inaccessible pore volume or a depleted layer model. Conceptually, since the polymer is not able to flow through the whole pore space, it only travels through the accessible portion which results in an accelerated arrival at the outlet. Models that reflect this concept have been developed by Sorbie (1991).

For the purpose of this work, the IPV can be calculated as follows (Stavland et al. 2010):

$$IPV = 1 - \sqrt{\frac{1}{1+B}} \qquad \text{(Equation 13)}$$

Where B is a constant with a physical meaning of (k_w/k_p) and can be derived from the pore geometry. Assuming the porous media behaves as a bundle of capillary tubes, the B factor can be calculated as:

$$B + 1 = (1 - \frac{d}{R})^{-4} \qquad \text{(Equation 14)}$$

Where d is defined as a thickness close to the wall (associated with the polymer monolayer), and R is the radius of the capillary tube. Alternatively, the B factor can be determined by its relationship to permeability reduction. An idealized way to calculate the permeability reduction or RRF, which is based on the assumptions made for Hagen-Poiseuille flow, is as follows (Zitha et al. 1995):

$$RRF = (1 - \frac{d}{R})^{-4} \qquad \text{(Equation 15)}$$

As with the equation used to calculate the B factor, d is the thickness of the layer of adsorbed polymer, and R is the capillary radius. Thus by assuming Hagen-Poiseuille flow, an association between RRF and the B factor can be made (Stavland et al 2010). This is a useful association, as will be seen later, since the permeability reduction can be determined from experimental pressure drop data.

More recent studies have demonstrated that high flow rates can result in additional adsorption of polymer to the already existing monolayer on the pore wall. Experimental results from polymer flow tests suggest that, above a critical rate the adsorbed layer thickness increases with the volumetric rate of injection (Chauveteau et al. 2002, Zitha et al. 1995).

2.8 - BEHAVIOR IN POROUS MEDIA: THE APPARENT VISCOSITY

The four flow regimes that were detailed earlier provide a general idea of how polymer solutions respond to different shear rates. Again, those regimes are Newtonian, shear thinning, shear thickening, and degradation. Understanding how experimental rheological data relates to polymer flow in porous media is of practical value which is why much time and effort is spent on developing models for properties like apparent viscosity.

The following section focuses on methods used to determine apparent viscosity in porous media. The first method utilizes core flood pressure drops to formulate parameters which can be used to calculate experimentally determined apparent viscosity values. Although this method provides correct results, it is fairly uncommon for a company to have this level of data when modeling a polymer flood. A new analytical model has recently been developed which accurately determines the apparent viscosity by means rheological data along with minimal core flood data (Stavland et al. 2010). The experimental data that was used to develop this new model is also used as input for the simulation described later in this paper.

2.9 - APPARENT VISCOSITY FROM CORE FLOODS

In core flood experiments, it is not possible to directly measure the apparent viscosity in a flooding experiment. Instead the apparent viscosity is determined by equations that depend on the mobility reduction (RF) and the permeability reduction (RRF). The permeability reduction has been found to depend on the size of the polymers (Zitha et al. 1995). The relationship between the two is such that, as the molecular weight of the polymers increases, the permeability reduction also increases (Hirasaki and Pope 1974). The mobility reduction and the permeability reduction utilize pressure drop ratios to create a non-dimensional representation of the altered permeability and mobility due to polymer flooding (Chauveteau et al. 2002, Green and Willhite 1998, Zitha et al. 1995). The equations for both parameters are as follows:

$$RF = \frac{\Delta P_{polymer}}{\Delta P_{brine^0}} \qquad \text{(Equation 16)}$$

$$RRF = \frac{\Delta P_{brine^1}}{\Delta P_{brine^0}} \qquad \text{(Equation 17)}$$

Where ΔP_{brine^0} is the pressure difference due to the flow of brine before polymer is injected and ΔP_{brine^1} is the pressure difference due to the flow of brine after polymer is injected.

An assumption is made regarding the variable ΔP_{brine^1}, where the brine permeability after polymer flow is the same as the polymer permeability (Chauveteau et al. 2002, Green and Willhite 1998, Hirasaki and Pope 1974, Zitha et al. 1995). For consistency, the pressure drops used in the pressure ratios should be determined at the same flow rate. The experimentally derived apparent viscosity is calculated by taking the ratio of the mobility reduction to the permeability reduction as follows (Stavland et al. 2010):

$$\mu_{app,exp} = \frac{RF}{RRF} * \mu_{brine} \qquad \text{(Equation 18)}$$

The brine viscosity in this equation is roughly close to one.

2.10 - APPARENT VISCOSITY: GRAPHICAL RESULTS

The following plot of mobility reduction displays the aforementioned flow regimes with relation to shear rate.

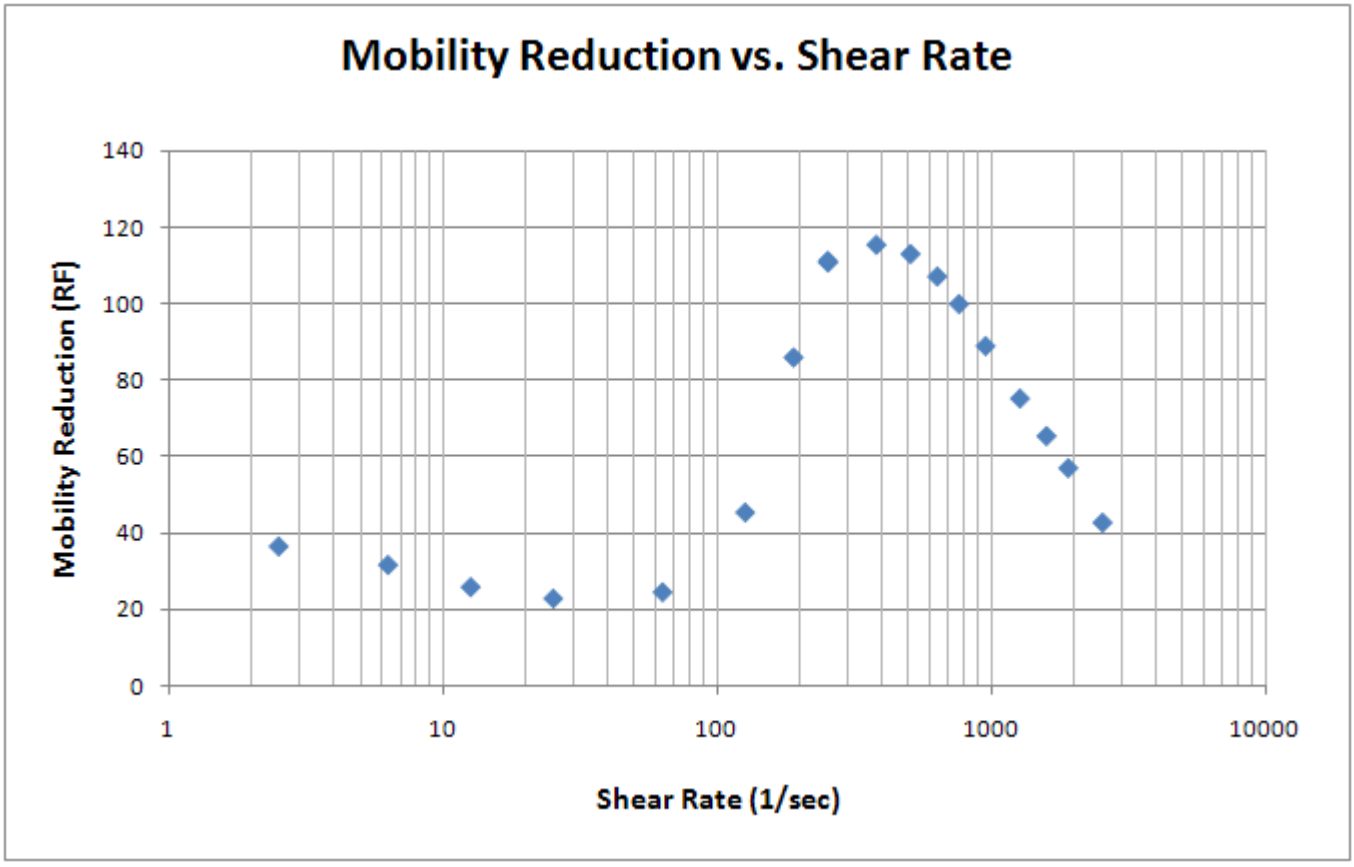

Figure 2.3: Flow regime behavior and trends in mobility reduction data as a function of shear rate

This plot exemplifies the small scale of the shear thinning behavior compared to the shear thickening behavior. The large magnitude of the shear thickening behavior relative to the shear thinning behavior has been previously reported by Seright et al. (2010). In the following plot the shear thickening and degradation regimes are very prominent compared to the shear thinning regime.

By calculating the apparent viscosity from the previous equation for the core flood data, the apparent viscosity can also be plotted as follows:

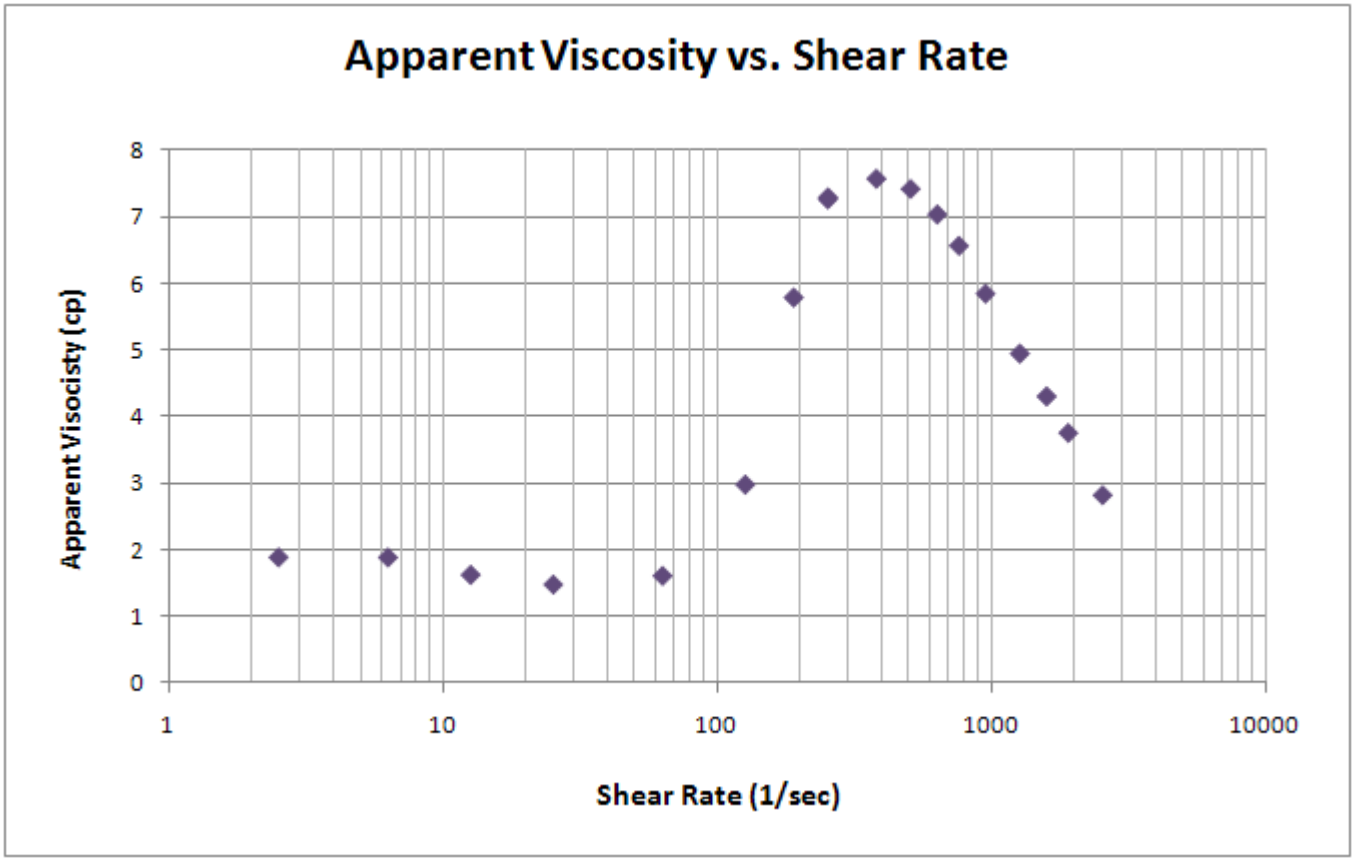

Figure 2.4: Flow regime behavior and trends in apparent viscosity data as a function of shear rate

The apparent viscosity in Figure 2.4 reaches a maximum of roughly 7.5 cp. This value is quite small compared to the apparent viscosity values which were achieved by the polymers which will be discussed later in this paper. Even so, the expected trends are present with regards to shear thickening and degradation.

2.11 – THE RELATIONSHIP BETWEEN SHEAR RATE AND INTERSTITIAL VELOCITY

For the purpose of conducting rheological experiments, it is common to record the polymers behavior with relation to the shear rate. When considering polymer behavior in porous media, it is more natural to think in terms of Darcy velocities or volumetric rates. There are many

equations that have been proposed to relate shear rate to the interstitial velocity, and it is common for tuning parameters and adjusting factors to be utilized so the data is properly aligned (Sorbie 1991). For the purpose of this paper, the following relationship was used to relate shear rate to interstitial velocity (Stavland et al. 2010):

$$\dot{\gamma} = \frac{4\alpha v}{\sqrt{\frac{8k}{\varphi}}} \qquad \text{(Equation 19)}$$

Where v is the interstitial velocity, φ is the porosity, and k is the permeability. An α-value of 2.5 was used since this value is what has been deemed appropriate for porous media with angular particles (Zitha et al. 1995).

CHAPTER 3 - EXPERIMENTAL COREFLOOD DATA

3.1 - INTRODUCTION TO THE EXPERIMENTAL DATA

The simulation work created for this thesis was based on experimental data provided by two separate sources. Both sources used a polymer which was 30% hydrolyzed, mixed into synthetic seawater, and had a molecular weight of 20 million Dalton. This polymer was also known by the name 3630SSW.

One of the data sets resulted from the experiments conducted by Stavland et al. (2010) using Berea sandstone cores. These experiments studied the polymer behavior in single phase flow, so the initial core saturations before polymer flooding were 100% synthetic seawater.

The other experiment, which was conducted using a Bentheim sandstone core, was used to study the polymer behavior in two phase flow where the initial saturations consisted of oil at a residual saturation and synthetic seawater (Moradi 2011). The rest of this chapter is dedicated to explaining the procedures and results associated with these two experiments in more detail.

3.2 – THE SINGLE PHASE EXPERIMENTS

3.2.1 – PREMISE FOR THE SINGLE PHASE EXPERIMENTS

Recently conducted research (see for example, Stavland et al. 2010) has aimed to develop an equation to model the shear degradation behavior which has been observed at very high shear rates, from a combination of bulk and core rheological data. Polymer experiments were preformed where parameters such as molecular weight, permeability, degree of hydrolysis, and brine salinity were systematically altered and the apparent viscosity was determined

experimentally. The resulting apparent viscosity values were well-matched with a theoretical model.

3.2.2 – PROCEDURE FOR THE SINGLE PHASE EXPERIMENTS

Bulk viscosity measurements were preformed for multiple polymer solutions which varied with concentration, molecular weight, and degree of hydrolysis. From the bulk experiments, relaxation times and shear thinning exponents were determined for the polymer mixtures (Stavland et al. 2010).

The core flood experiments were conducted using two serially mounted cores each of which had a 1.5 inch diameter and were 7 centimeters in length. Before the polymer injection began, the cores were initially 100% saturated with synthetic seawater (SSW). Additionally, the reference makeup water for the polymer was synthetic seawater. Once the polymer injection process began, the two cores were exposed to sequential increases and decreases in injection rate. During the injection process, atmospheric pressure was maintained at the outlet of the second core. The pressure drop in each core section was determined as a function of time by using a pressure tap located between the two cores. When the pressure drop for a given rate was assuredly stabilized, pressure data was recorded, and a new flow rate was initiated.

At the end of the series of injection rates, water was injected and the pressure drop was recorded. This pressure drop was then used to determine the permeability reduction. Since each set of the two serially mounted cores was exposed to multiple flow rates, only one value of permeability reduction (RRF) was determined for the polymer solution. Given that the first flow rate is maintained until steady-state flow is achieved, it is generally assumed that all of the adsorption will occur during this flow rate.

In some situations however, an increase in flow rate could lead to an increase in permeability reduction (Chauveteau et al. 2002). As previously discussed, in the Newtonian and the shear thinning flow regimes, the polymers are not elongated and are in a relaxed conformation. If the flow rate increases and the polymers elongate, hydrodynamic retention could result (Chauveteau et al. 2002, Zaitoun and Chauveteau 1998, Zitha et al. 1995). This might cause an increase in permeability reduction if the retention is permanent. If additional polymer adheres to the polymer that has already adsorbed, the permeability reduction may further increase (Chauveteau et al. 2002). Therefore, if fresh cores were used for each new flow rate in the experimental procedure described above, one could argue that a different RRF might be achieved for each flow rate. For the purposes of this thesis, the single RRF value associated with the polymer will be used as a guide to allow for the proper pressure drop to be achieved in the history match.

3.2.3 – RESULTS THE SINGLE PHASE EXPERIMENTS

The experimental data which was reported by Stavland et al. (2010) for the 3630SSW HPAM solution with a molecular weight of 20 million Dalton and 30% hydrolysis was of special interest for this thesis. The following section provides more details about the results from the bulk and core flood experiments for this particular polymer solution.

A summary of the core properties are as follows in Table 3.1

Core Properties				
Location	Diameter	Length	Porosity	Permeability
Front	1.5 inches	7 cm	0.22	824 mD
Back	1.5 inches	7 cm	0.22	800 mD

Table 3.1: Core properties for the single phase experiment

Both cores were comprised of Berea sandstone, but the permeability properties in the front core differed very slightly from the properties in the back core. During polymer injection, the front core experienced very high pressures due to polymer alignment and adjustment in the pore space. Since the polymer behavior was more stable as it flowed through the second core, the experimental results from the second core were the focus of the history matching simulations.

From the bulk rheology experiments, the relaxation time and shear thinning exponents were determined as a function of normalized polymer concentration. The intrinsic velocity, relaxation time, and shear thinning exponent for the 3630SSW polymer are displayed in Table 3.2

Rheological Bulk Properties for HPAM 3630SSW at 1500 ppm		
Intrinsic Viscosity, mg/l	Relaxation Time, s	Shear-thinning Exponent
3820	0,61	-0,27

Table 3.2: Bulk rheology data for the 1500 ppm polymer

By using these experimentally derived parameters in the Carreau model it was possible to create a graph of bulk viscosity as a function of shear rate which can be seen in Figure 3.1. As expected, the polymer behavior displays both lower Newtonian and shear thinning behavior. For this particular plot, the shear rates do not extend to high enough values to display the upper Newtonian behavior which would asymptotically approach the viscosity of the synthetic seawater.

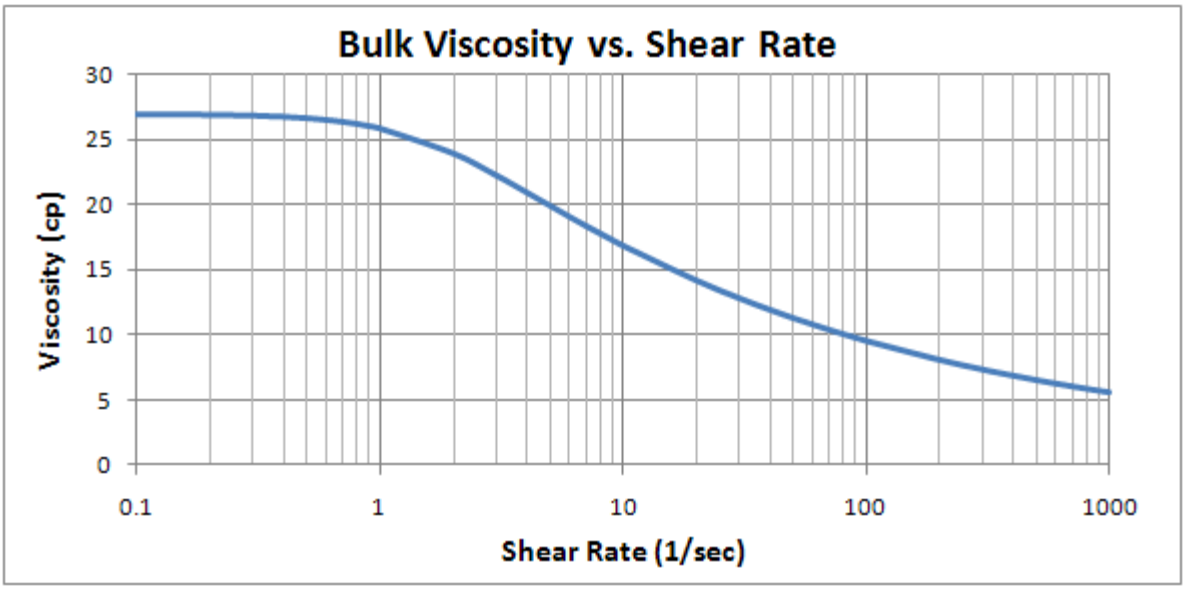

Figure 3.1: Experimental results for the bulk viscosity of the polymer as a function of shear rate

Pressure measurements in the front and back core were obtained every half minute during the flooding experiment. In Figure 3.2, the pressure drop in the back core has been plotted as a function of time along with the associated injection rate. As previously mentioned, the data from the back core was the only data considered when simulating the flooding experiment. The pressure spikes that can be seen at the beginning of each new flow rate were a result of the polymer realignment that occurred when the macromolecules elongated with increasing injection rates. For the injection rates that occur in the degradation regime, an initial pressure spike can be attributed to an entrance pressure drop which occurs when the polymer shreds as it enters the formation (Seright 1983).

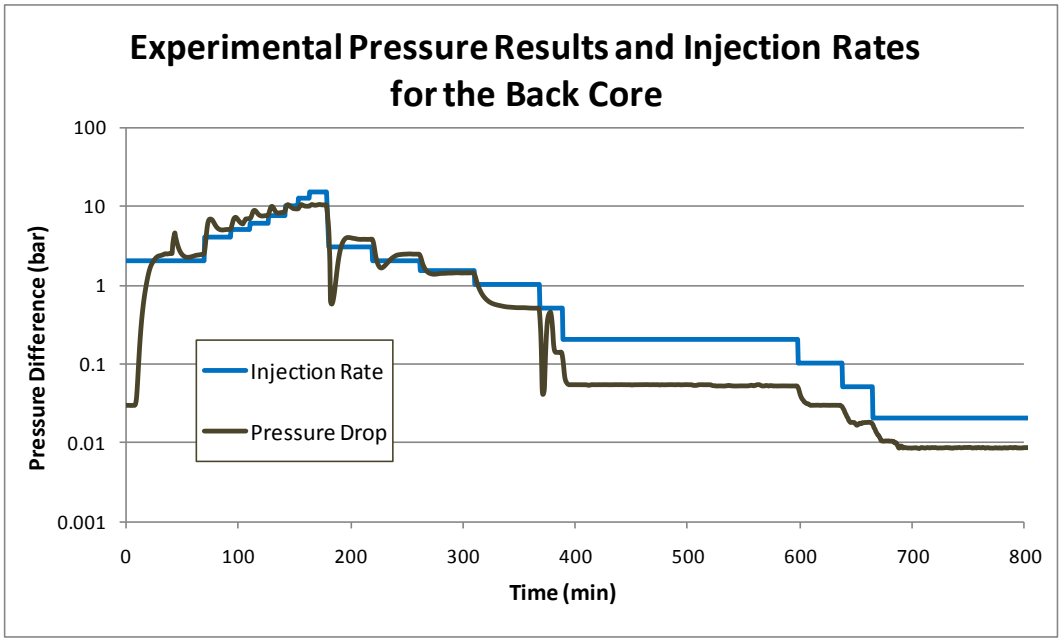

Figure 3.2: Polymer injection rates and resulting pressure differentials across the back core

The stabilized pressure drop associated with steady state flow was also recorded for each flow rate. This data is presented for the back core in Table 3.3 along with the injection rate.

Flow Rate	Pressure Drop: Back Core
ml/min	bar
2	2.49
4	5.08
5	6.02
6	6.74
7.5	7.5
10	8.46
12.5	9.2
15	9.63
20	9.64
3	3.89
2	2.5
1.5	1.45
1	0.512
0.5	0.139
0.2	0.0519
0.1	0.0293
0.05	0.0179
0.02	0.00825

Table 3.3: Stabilized pressure difference for various flow rates in the second core

The polymer-related pressure drops in the second core for a given flow rate were used in conjunction with water-related pressure drops to determine the mobility reduction. The plot in Figure 3.3 displays the mobility reduction data with respect to volumetric flow rate.

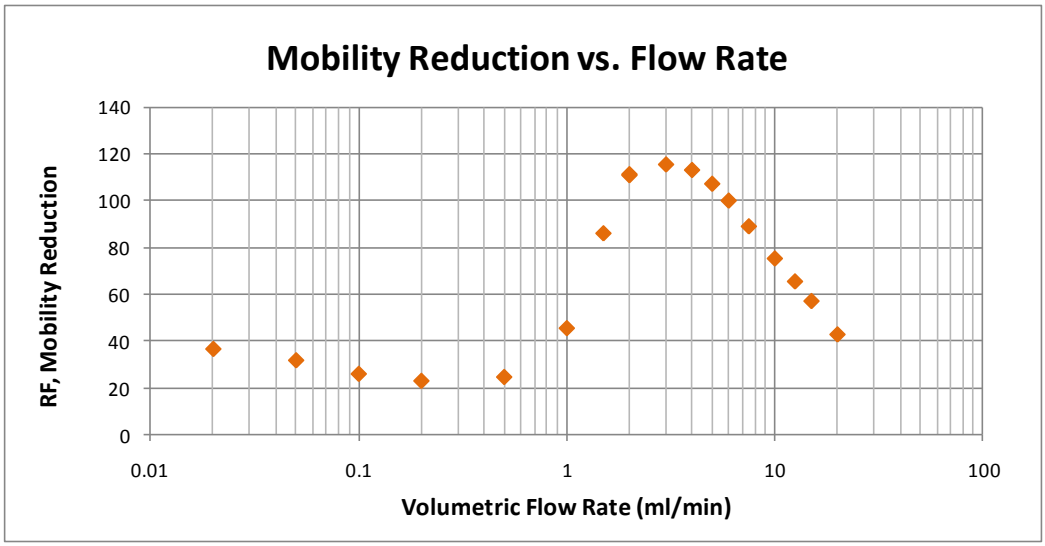

Figure 3.3: Flow regime trends in experimentally determined mobility reduction data as a function of flow rate

The pressure drop values associated with each flow rate for water were calculated using Darcy's Law and the core properties of the back core. These water flood pressure drop values were also modeled in the simulator for the aforementioned experimental core set-up. The values determined from the Darcy's Law calculations matched very well with the values from the water flood simulation. The procedure taken to model the simulated water flood will be discussed in more detail in Section 4.3.2.

In the experiments preformed by Stavland et al. (2010), after multiple rates of polymer injection, a second water flood was preformed until steady-state flow was achieved. From the stabilized pressure drop associated with this water injection, the permeability reduction (RRF) was determined to be 3.6.

Given that the mobility reduction, permeability reduction, and water viscosity (taken to be 1.08 cp) are known, the experimentally derived apparent viscosity can be determined as described by Equation 18. The apparent viscosity calculated by this method is displayed in Figure 3.4. The mobility reduction values were initially determined with respect to the volumetric flow rate, but through the relationship presented earlier, these flow rates have been converted to shear rates.

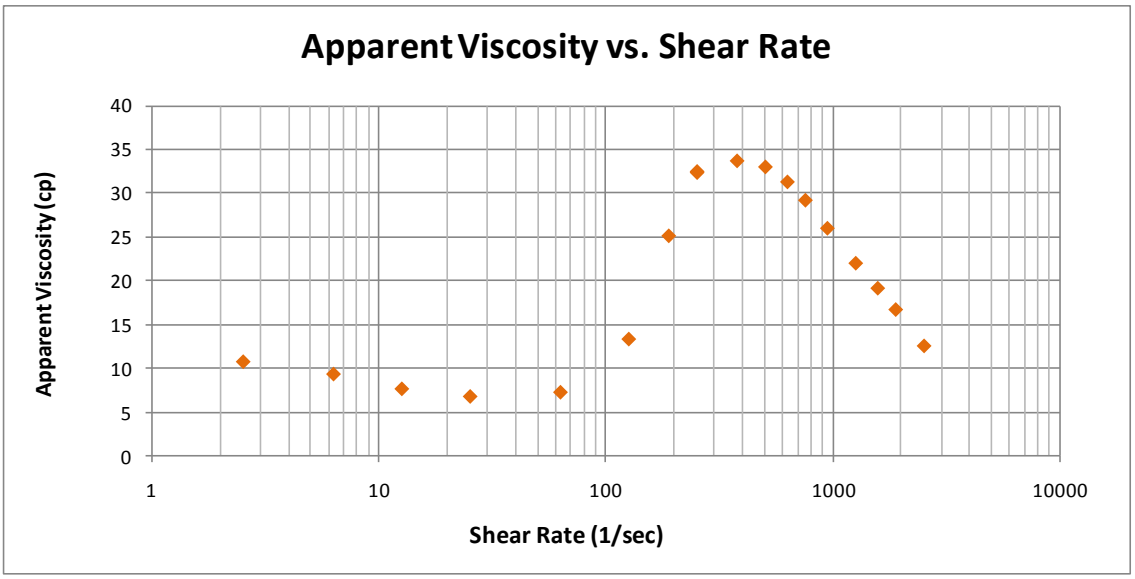

Figure 3.4: Flow regime trends in experimentally determined apparent viscosity data as a function of flow rate

The importance of displaying the apparent viscosity with respect to shear rate is that it highlights the difference in polymer behavior between the rheological results and the core flood results. For the range of shear rates presented above, shear thickening and degradation behavior is very prominent in the core flood. For a very similar range of shear rates, the rheological bulk data is dominated by a shear thinning regime.

Table 4.1 (located in the water flood simulation section), presents the mobility reduction, apparent viscosity, and pressure drop values in a consolidated form along with the injection rate.

3.2.4 – THE APPARENT VISCOSITY MODEL

In the earlier sections of this work, which covered the individual flow regimes, viscosity equations were developed based on the behavior in each regime. Recent research, which focused on relating shear degradation to rheological properties, has resulted in an equation which accurately models the behavior of all four flow regimes (Stavland et al. 2010).

As discussed in the section on shear thickening, earlier models have been developed which accurately handle the shear thickening regime. Furthermore, Delshad et al. (2008) produced a well-matched simulation of the shear thickening regime using the UTCHEM simulator.

The new developments by Stavland et al. (2010) have created a successful model of the degradation regime which occurs at very high shear rates. This model has demonstrated a capability to match apparent viscosities derived from experimental core floods. The model is as follows:

$$\mu_{apparent} = \mu_w + ((\mu_{app0} - \mu_w) * ((1 + \lambda_1\dot{\gamma})^n + (\lambda_2\dot{\gamma})^m) * (1 + (\lambda_3\dot{\gamma})^4)^{\frac{j}{4}} \qquad \text{(Equation 20)}$$

Where the time constant, λ_1, is determined from bulk viscosity measurements. Additionally, two experimentally derived relationships were used to determine λ_2 and λ_3 where λ_1/λ_2 = 17, and λ_1/λ_3 = 238. (Stavland et al. 2010)

The apparent viscosity at zero shear rate, μ_{app0} , which is associated with flow through porous media and is calculated as:

$$\mu_{app0} = \frac{\mu_0 * (1+B)}{1+B\sqrt{\frac{\mu_0}{\mu_w}}} \qquad \text{(Equation 21)}$$

Here, μ_0 is the polymer solution viscosity at zero shear rate, μ_w is the water viscosity, and B is a factor related to the inaccessible pore volume (IPV). The B-factor can be determined through a relation with the RRF as discussed in the section on retention. The relationship between the B-factor and the RRF is based on the idealized assumptions made for Hagen-Poiseuille flow. Since the B-factor cannot be determined experimentally, it may also function as a tuning parameter.

Figure 3.5 displays the resultant apparent viscosity for the 3630SSW HPAM polymer as determined by Equation 20.

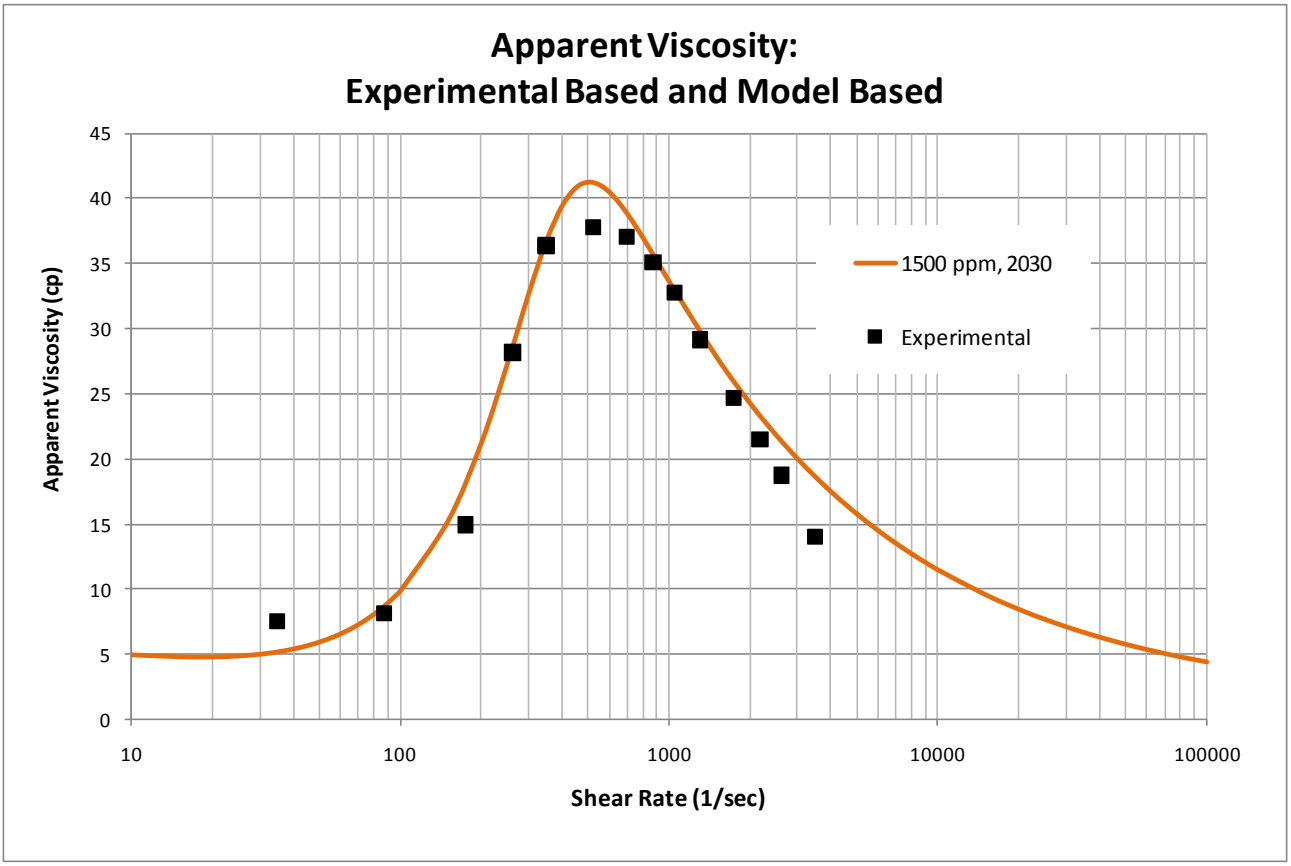

Figure 3.5: A comparison of experimental-based and model-based apparent viscosity values

The graphical results displayed above were part of the data used to investigate whether or not current simulation technology had the proper functionalities to simulate this recently modeled behavior.

3.3 – THE TWO PHASE EXPERIMENTS

3.3.1 – PREMISE FOR THE TWO PHASE EXPERIMENTS

Moradi in 2011 preformed multiple coreflood experiments of oil displacement by polymer solutions and under various core-wetting conditions. As compared to the previous experimental work which occurred as single phase flow, this new experimental work focused on the behavior that occurred when oil was also present in the core. Aside from creating new insight to the specifics of two phase polymer flooding behavior, his work also provided input data that could be used for modeling in a simulator.

3.3.2 – EXPERIMENTAL PROCEDURE FOR THE TWO PHASE COREFLOOD

The polymer which was studied in the two phase core flood was described as being 30% hydrolyzed with a molecular weight of 20 million Dalton. Synthetic seawater was used as the makeup water for the polymer solution.

A bulk rheology study was conducted for this polymer solution at multiple concentrations varying between 100 and 2000 ppm. For each polymer concentration, the bulk rheological behavior was observed as the shear rate was varied from low to high and high to low values of shear rate. The data from the experiments that went from high to low shear rates were the clearest, and were therefore taken to represent the bulk behavior of the polymer solution.

For this particular experiment, a single water-wet Bentheim core was used for the flooding process. After the core was loaded into the core holder and put on a vacuum, synthetic seawater was injected until the core was saturated. Once it was verified that the core was 100% saturated with synthetic seawater, the absolute permeability of the core was determined using data collected during multiple injection rates of the synthetic seawater. The core was then flooded with oil until residual water saturation was established which was then followed by another water flood using synthetic seawater to establish a residual oil saturation.

At this point the core saturations consisted of residual oil and water, which meant polymer flooding could commence. The polymer was injected at an intentionally low rate in order to maintain the residual oil saturation establish by the previous water flood. Additionally, since this was the first polymer injection the core had experienced, it is assumed that most of the irreversible adsorption and retention took place during this injection process.

After injecting about 4.2 pore volumes of polymer in the core, another injection of synthetic seawater occurred. The purpose of this flood was to remove the non-adsorbed polymer before performing a second polymer flood to study the retention of the polymer in the core. Because both polymer injection processes were conducted at the same rate, the difference in the injected pore volumes required to reach steady-state flow are attributed to the polymer retention.

Finally, a multi-rate polymer flood was conducted. For the first three increasing rates, no visible oil was produced and the residual oil saturation remained the same as it was initially. For the fourth rate and on, visible volumes of oil were produced. These volumes were recorded and used to determine the new residual oil saturation once both steady-state flow occurred and no additional oil production was seen. The experimental results that were provided as the basis for the two phase simulation are detailed in the following section.

3.3.3 – RESULTS FROM THE TWO PHASE EXPERIMENTS

The bulk rheology measurements from the experiments conducted by Moradi in 2011 are presented in Figure 3.6. The different cases, each of which has been fit with a Carreau model, represent the aforementioned polymer at different concentrations.

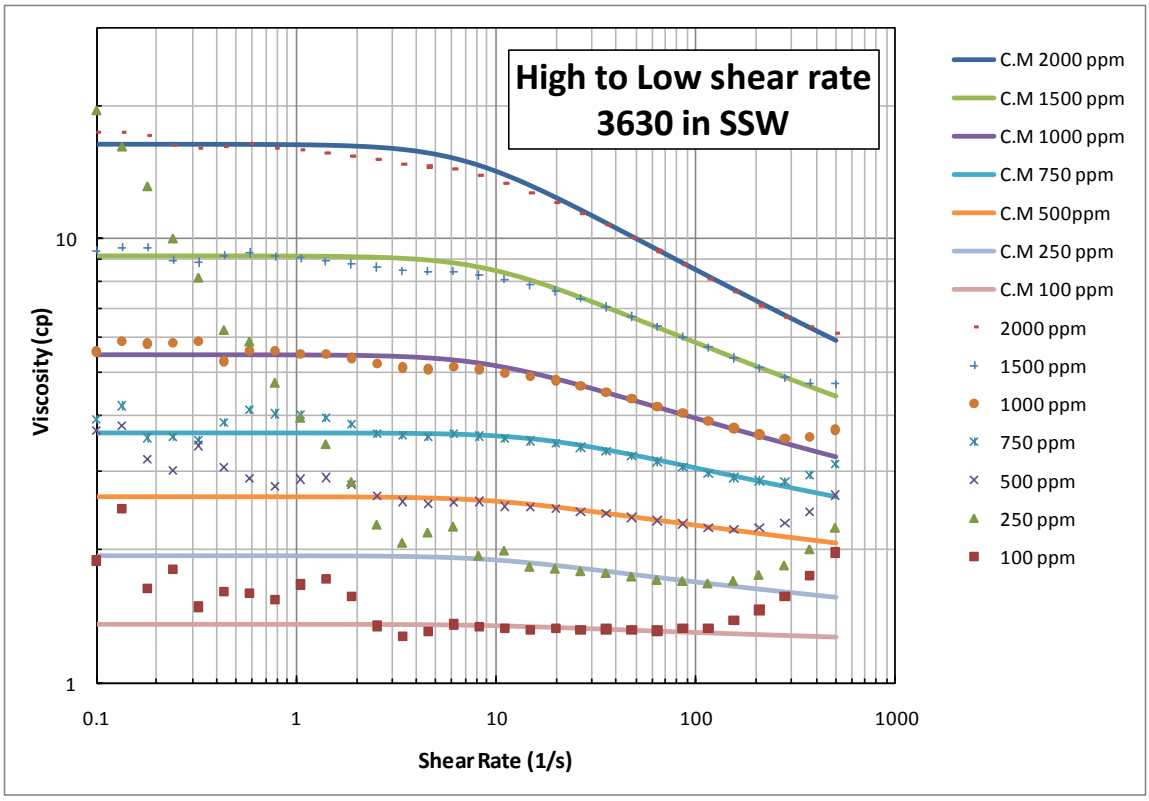

Figure 3.6: Experimental bulk rheology data and corresponding Carreau model for various polymer concentrations

The concentrations below 1000 ppm display a very small increase in viscosity towards the highest shear rates that were encountered. Although it is probably not appropriate to refer to this trend as "shear thickening," given the small magnitude of the behavior, it is an interesting occurrence. Additionally it should be noted that at lower concentrations, the polymers display erratic behavior and do not adhere to the Carreau model as well as the higher concentration polymer solutions. For the purpose of this work, the behavior of the polymers at lower concentration is of special interest since the polymer that was modeled in the simulator had a concentration of 400 ppm.

Table 3.4 contains information about the core dimensions, porosity, and absolute permeability as determined from the multi-rate water flood. This water flood occurred before polymer was injected, so the calculated absolute permeability does not reflect any effects from polymer retention.

Core Properties			
Diameter	Length	Porosity	Permeability
3.794 cm	24.3 cm	21.34%	2278.76 mD

Table 3.4: Core properties for the two phase experiment

The end-point relative permeability values were determined by conducting a water flood at residual oil saturation, and an oil flood at residual water saturation. Again, both of these injection cycles occurred before any polymer was introduced in the core, so the measurements were unaffected by polymer retention. Table 3.5 displays the end-point saturation and relative permeability information that was gathered from this experiment.

Relative Permeability and Saturation Values Before Polymer Flooding	
Oil Flooding at Interstitial Water Saturation	
Interstitial Water Saturation (Swi)	22.82%
Oil Permeability at Swi	1607.27 mD
Oil Relative Permeability at Swi	0.705327
Water Flooding at Residual Oil Saturation	
Residual Oil Saturation (Sor)	39.92%
Water Permeability at Sor	216.41 mD
Water Relative Permeability at Sor	0.09497

Table 3.5: Relative permeability and saturation values for the Bentheim core before polymer flooding

When the polymer flooding began, it was intentionally conducted at a very low rate in order to avoid oil production. By doing this, the effects from the polymer could be analyzed without any convoluting effects from two phase flow being mixed in. Plots of the pressure difference across the core from the primary and secondary polymer floods are presented in Figures 3.7 and 3.8, respectively.

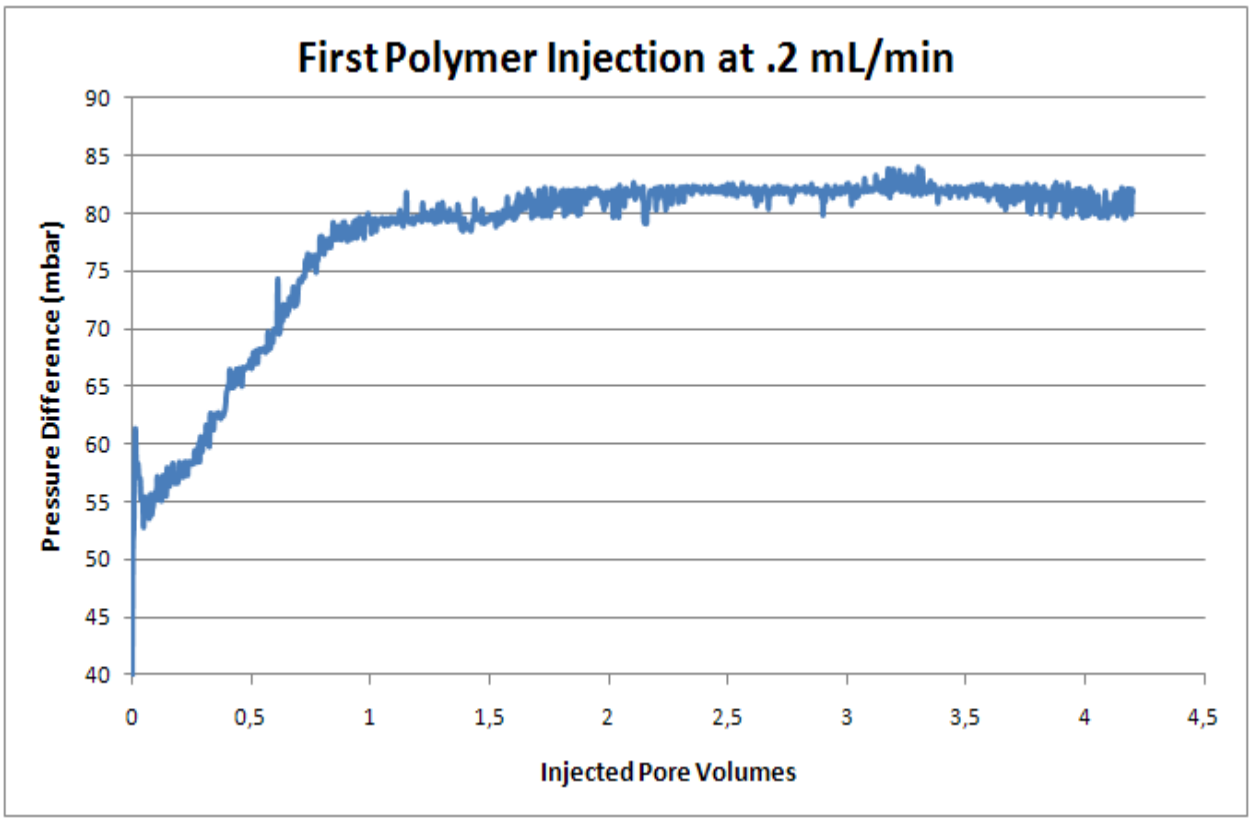

Figure 3.7: Differential pressure drop across the core during the initial polymer injection

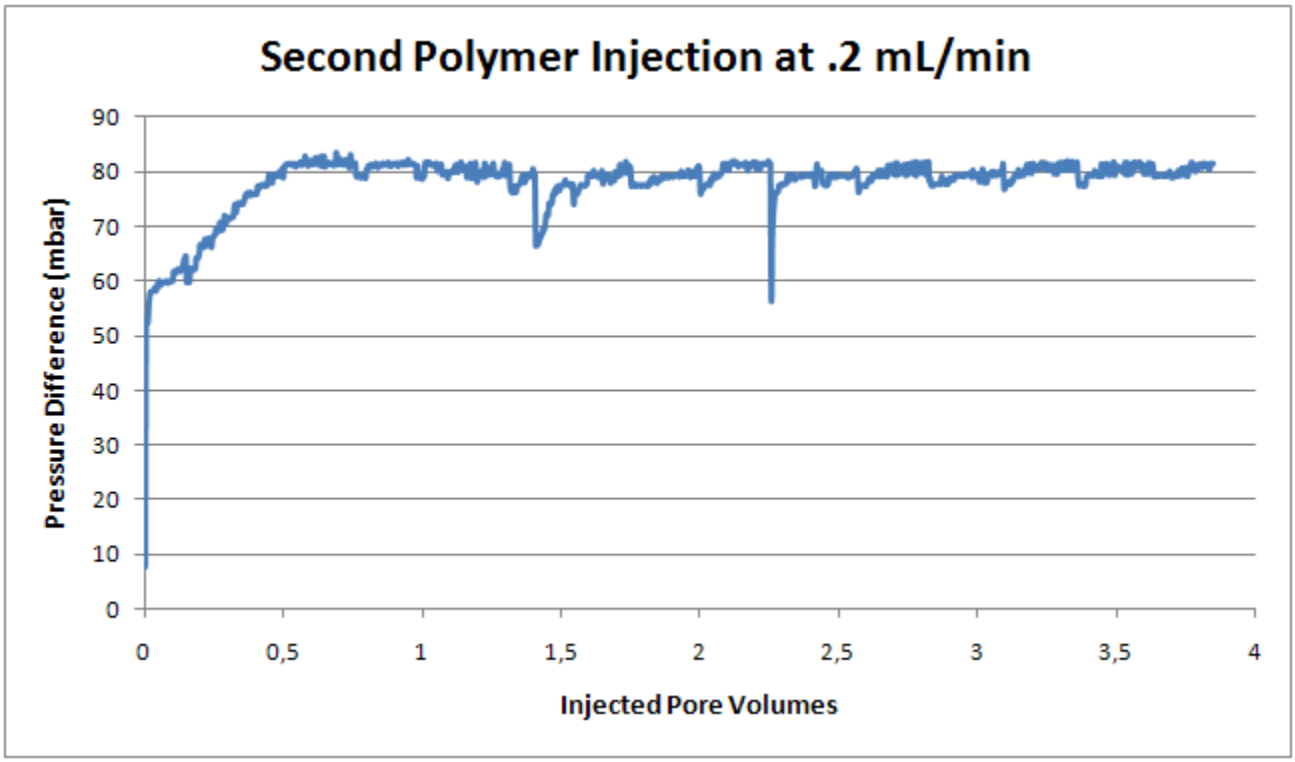

Figure 3.8: Differential pressure drop across the core during the second polymer injection

During the primary polymer flood, about one pore volume was injected at a rate of .2 mL/min before steady-state was achieved. The secondary polymer flood only required about .5 pore volumes before the pressure difference achieved steady-state. Between each of the polymer floods, a water flood was conducted to clean out the excess polymer that had not adsorbed to the rock surface. Given that both polymer floods were conducted at an injection rate of .2 mL/min, the difference between the volumes that were injected to reach steady-state was attributable to the retention that occurred during the primary polymer flood.

After the polymer flood occurred, the relative permeability was reassessed to determine the permeability properties associated with the polymer. Additionally, the permeability reduction was determined to be 1.3958 by comparing the permeability of the polymer and the water flood at residual oil saturation. Table 3.6 presents the polymer flood associated end-point results.

Relative Permeability and Saturation Values After Polymer Flooding

Polymer Flood at Residual Oil Saturation	
Residual Oil Saturation (Sor)	39.92%
Polymer Permeability at Sor	155.041 mD
Polymer Relative Permeability at Sor	0.068038

Table 3.6: Relative permeability and saturation values for the Bentheim core after polymer flooding

A series of multi-rate polymer injections were conducted right after the second .2 mL/min polymer flood. The order of the injection rates for the multi-rate polymer flood was as follows: .4, .8, 1.6, 3.2, 6.4, 9.6, 12, 14, and 18 mL/min. No delay occurred between the second polymer flood at an injection rate of .2 mL/min and the .4 mL/min injection rate. The experimental data that was recorded during these injection rates is presented in two separate figures. The first plot (Figure 3.9) shows the data collected for the flow rates varying from .2 mL/min to 3.2 mL/min and the second plot (Figure 3.10) shows the data collected for the flow rates varying from 6.4 mL/min to 18 mL/min.

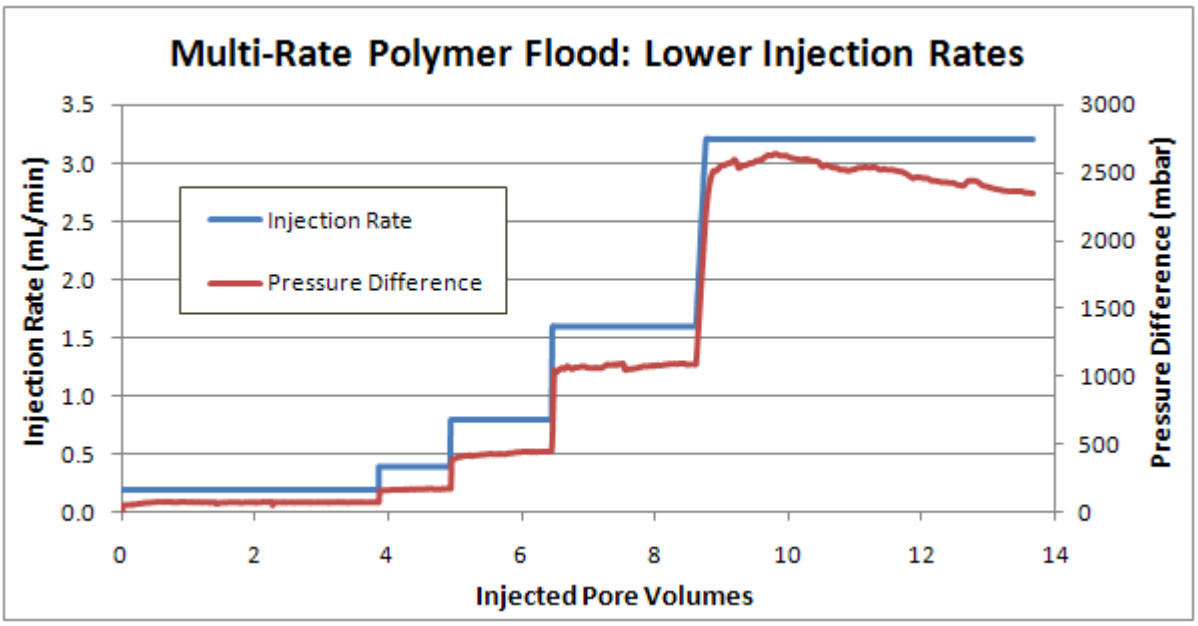

Figure 3.9: Differential pressure drop across the core for the first five injection rates

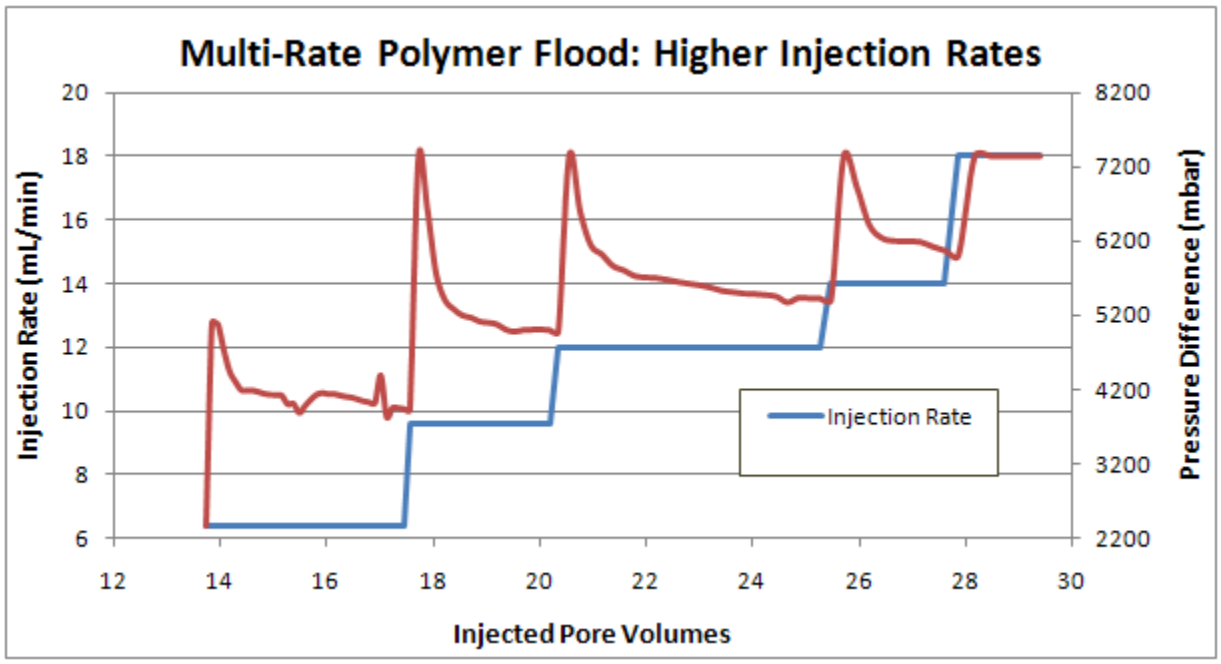

Figure 3.10: Differential pressure drop across the core for the last five injection rates

All of the injection rates that occurred before the injection rate of 3.2 mL/min resulted in single phase flow and were therefore conducted at the same residual oil saturation as the one posted in the previous table. The larger injection rates, starting with the injection rate of 3.2 mL/min , produced oil along with the injected polymer which meant a new residual oil saturation was established during each of these flow rates.

For the purpose of this thesis, the largest injection rate that was considered for simulation work was 3.2 mL/min. The oil produced during this rate amounted to 1.1 mL which resulted in a decrease of the residual oil saturation from its previous value of 39.92 % to a value of 38.04%.

CHAPTER 4 - SIMULATION WORK AND RESULTS

4.1- SELECTING A SIMULATOR

Before any simulation work could take place, a simulator had to be selected. There were two main qualities which were sought after when deciding which simulator was most applicable. First, it was necessary that the simulator had the capacity and the functionalities necessary for modeling the polymer behavior of interest. For example, since the degradation behavior was of particularly important, it was necessary that the selected simulator could model this behavior. It was also desirable for the simulator to be commonly used within the industry. Since the ultimate purpose of conducting the polymer experiments was to gain a better understanding of the polymer behavior for what would eventually be field purposes, it is also important that a commonly available simulator could model the experimental findings.

The three simulators which were investigated for potential use were Eclipse which has been created by Schlumberger, STARS which has been created by CMG, and UTCHEM which has been created for research application at the University of Texas at Austin. The ability of UTCHEM to model a polymer solutions shear thickening behavior had already been demonstrated by Delshad et al. (2008). Other attractive features of this simulator included the availability of the source code, its specialized ability to model lab scale experiments, and the fact that it was specially designed to model very specific and complex chemical and polymer behavior. The obvious downfall of this simulator is the fact that it is not commonly used outside of the academic realm.

The Eclipse simulator is by far one of the most well known reservoir simulation tools in the petroleum industry. Because it is so commonly used in the industry for field applications, it could have been an ideal simulator for modeling the experiments. Unfortunately, this very popular simulator did not contain the technical functionalities required to model the recent experimental findings that were the focus of this work. At the time of the investigation, the polymer viscosity related capabilities of the Eclipse simulator were restricted to shear thinning behavior. Although the simulator also had the capacity to model salinity effects, adsorption behavior, and polymer concentration mixing behavior, without the ability to model the shear thickening and degradation regimes, a successful simulation could not be produced.

The final simulation tool which was considered and subsequently selected to model the experimental data was the STARS simulator by CMG. This simulator, which is implemented by multiple companies in the petroleum industry, is known for its ability to model both laboratory and field scale models while also having the capability to handle complicated chemical behavior. One of the main attractive features of this simulator was option to input the polymer apparent viscosity in a tabular format. Although it was not certain from the outset, the hope was that the tabular input would be able to handle all four flow regimes if necessary. Further details regarding the polymer-related keywords which were applicable for this work are discussed in the following section.

4.2- KEYWORDS FOR THE CMG STARS SIMULATOR

An important preliminary step towards creating a successful simulation model required gaining a better understanding of the simulator and how it functioned. Given that the STARS simulator operates through the usage of keywords, it was important to understand which keywords were applicable to the polymer model, how the keywords worked, and what inputs were required for the keywords to function properly. The keywords discussed here are presented in the order in which they appear in the simulator. It is important to note that the simulation model was developed via a data file rather than through the interface provided by STARS.

The first polymer-related keyword that is encountered in the simulation code is “VSMIXFUNC,” which handles the non-linear viscosity behavior that results from the changes in the polymer concentration. The manner in which the water phase viscosity increases as the polymer concentration increases can be modeled from bulk rheology data if experiments are conducted for multiple polymer concentrations. The concentration mixing behavior affects how quickly the viscosity builds in the polymer front, which in turn affects how quickly the pressure builds in the model. By default, the simulator assumes a linear mixing behavior when the user does not supply input values.

When a linear mixing behavior is not realistic, the keyword allows for eleven inputs, each of which will be associated with equally spaced polymer concentrations varying from zero to a given concentration of interest. The polymer concentration range is specified with the associated keyword, “VSMIXENDP.” The eleven inputs used with the “VSMIXFUNC,” keyword are used to correct the curvature of the actual viscosity-concentration behavior to that of a linear trend. The specific linear trend to which the data is fit is described by a line connecting the viscosity associated with zero polymer concentration, and the viscosity associated with the maximum polymer concentration of interest.

Once the mixing behavior is accounted for, the “SHEARTAB,” keyword is used to model the apparent viscosity that occurs for a given flow rate and reflects the behavior associated with

the maximum polymer concentration as set by “VSMIXENDP.” The keyword, which allows for 40 input values, allows the user to define the polymer viscosity as a function of the Darcy velocity. The data is input as two columns, the first of which is for the Darcy velocity, and the second of which is the associated apparent viscosity. In this work, there were two methods used to create the apparent viscosity data. As previously discussed, the apparent viscosity can be determined from experimental data as a function of the permeability and mobility reduction values. If this data is not available, and only a single phase is flowing, the Darcy equation can be used to create an approximation for these inputs.

The remaining pertinent keywords which have yet to be discussed are all related to the adsorption behavior and are grouped together in the simulator. The first of these adsorption keywords is “ADSTABLE,” which essentially provides a tabular method for inputting data related to the Langmuir isotherm. The input table consists of two columns of data. The first column contains the polymer concentration values and the second column contains the adsorption values associated with each concentration. Since the Langmuir isotherm is a commonly used method for attributing adsorption behavior to specific polymer concentrations, the STARS simulator also offers the option of specifying the Langmuir model according to the isotherm coefficients. Additionally, the simulator allows for the “ADSTABLE,” and the “ADSLANG,” keywords to reflect temperature dependence, but this feature was not used for this thesis.

Since the adsorption parameters can vary for different rock types, and it is possible to have multiple rock types in a reservoir, the simulator is capable of defining different rock types within a single model. Although it was not necessary to define multiple rock types for this thesis, the following adsorption keywords could have been used in a manner that defined multiple rock types. For the purpose of this thesis, they were used accordingly to represent a single rock type.

The first of these parameters is the maximum adsorption capacity which is accounted for by the keyword “ADMAXT.” The irreversible adsorption behavior, which is related to the maximum adsorption capacity, is modeled with the keyword “ADRT.” Both the maximum adsorption and the irreversible adsorption used the same units.

The inaccessible pore volume was handled with the “PORFT,” keyword which is more accurately described as the percentage of accessible pore volume. The “PORFT,” input value can be calculated as (1-IPV). The final adsorption keyword was the permeability reduction or “RRFT.” In the STARS simulator, when the “RRFT,” is set equal to one, there is no permeability reduction effect. The “PORFT,” and “RRFT,” keywords operate as a function of how much polymer has been adsorbed compared to the stated maximum adsorption. Once the maximum adsorption is achieved, the full effect of the “PORFT,” and “RRFT,” values are seen in the simulator. For

adsorption values smaller than the maximum adsorption, the “PORFT,” and “RRFT,” are only seen as a fraction of the input values.

4.3 – SINGLE PHASE SIMULATION WORK

4.3.1 – INTRODUCTION TO THE SINGLE PHASE SIMULATION WORK

Using the data that was collected as a result of the single phase flow experiment, which was described in the previous chapter, the following simulation work was created. While obtaining a well matched simulation was considered an important task, it was imperative that the input for the simulated model did not deviate too much from the experimentally determined parameters. For this reason, only parameters such as adsorption, which was not well defined, and the permeability reduction value, which might vary slightly with flow rate, were considered to be tuning parameters.

4.3.2 – MODELING A WATERFLOOD

A water flood was simulated before attempting to simulate and history match the polymer flood data. This exercise was useful for gaining a better understanding of the simulator, ensuring that the initialization parameters were set properly, and obtaining the pressure difference in the core due to water injection at multiple rates. The water injection rates studied with the simulator were the same rates the cores experienced during the experimental polymer flood.

The water flood simulation was based on an example file provided by CMG STARS. The original example file (see ‘stflu036,’ in the 2009 STARS example database) demonstrated how the polymer-related key words were used to model an example polymer flood. By inhibiting the irrelevant key words, setting the core parameters and initial conditions to be representative of the experimental parameters, and adjusting the injection fluid to pure water, a successful water flood was simulated.

The two serially mounted cores were modeled with 30 blocks each, or 60 blocks in total. Injection and production wells were located in blocks one and 60, respectively. The pressure tap which recorded the pressure between the first and second core in the lab experiment was modeled by setting the simulator to record the block pressures in blocks 30 and 31. The average pressure from these two blocks was taken to be the pressure recorded by the pressure tap which is also the entrance pressure to the second core. The pressure drop in the second core was determined from the difference between the average pressures in blocks 30 and 31, and the pressure in the block 60, where the producing well was located.

The results from the water flooding simulations are located in Figure 4.1. The graph displays the pressure difference between the inlet and outlet of the second core as well as the water injection rate. As can be seen, the difference in the pressure increases or decreases immediately for each increasing or decreasing flow rate.

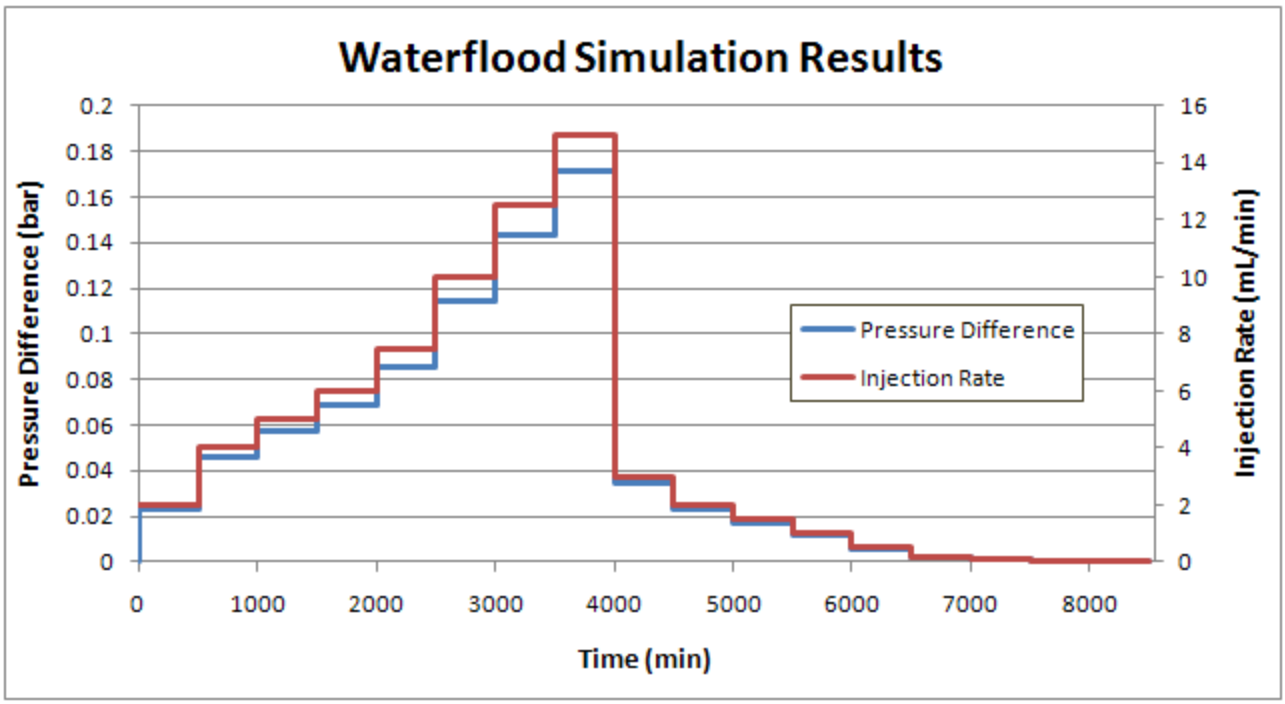

Figure 4.1: Injection rates and pressure results for the simulated multi-rate water flood

The following table summarizes the results for the water flood pressure drop, mobility reduction, and apparent viscosity values for different flow rates.

Flow Rate	Pressure Drop: Back Core	Simulation Waterflood	Darcy-Based Waterflood	RF	Calculated Apparent Viscosity
ml/min	bar	bar	bar	Unitless	cp
2	2.49	2.251E-04	2.250E-04	36.66	10.69125607
4	5.08	5.626E-04	5.626E-04	31.82	9.279695656
5	6.02	1.125E-03	1.125E-03	26.04	7.594834713
6	6.74	2.250E-03	2.250E-03	23.06	6.726839757
7.5	7.5	5.626E-03	5.626E-03	24.71	7.206402483
10	8.46	1.125E-02	1.125E-02	45.50	13.27201231
12.5	9.2	1.688E-02	1.688E-02	85.91	25.05779161
15	9.63	2.250E-02	2.250E-02	110.65	32.27302088
20	9.64	2.250E-02	2.250E-02	111.09	32.4026314
3	3.89	3.376E-02	3.376E-02	115.24	33.61229997
2	2.5	4.501E-02	4.501E-02	112.87	32.92107351
1.5	1.45	5.626E-02	5.626E-02	107.01	31.21026416
1	0.512	6.751E-02	6.751E-02	99.84	29.11929329
0.5	0.139	8.439E-02	8.439E-02	88.88	25.92227447
0.2	0.0519	1.125E-01	1.125E-01	75.19	21.93035652
0.1	0.0293	1.406E-01	1.406E-01	65.41	19.07899077
0.05	0.0179	1.688E-01	1.688E-01	57.06	16.64235295
0.02	0.00825	2.250E-01	2.250E-01	42.84	12.49485843

Table 4.1: A summary of the water flooding results, mobility reduction, and apparent viscosity calculation

4.3.3 – SENSITIVITY STUDY: ADSORPTION PARAMETERS

After the water flood was correctly simulated, the polymer flood became the focus of the simulation work. Although very good data was available to model the apparent viscosity, there was not any experimental adsorption data available. Additionally, viscosity data was only available for one concentration, so the viscosity behavior of the polymer at lower concentrations was relatively unknown. Because a mixing front is developed as the polymer front travels through the core, understanding the viscosity effects for the lower concentrations allows for the viscosity of the front to be simulated accurately. As previously mentioned, the B-factor can behave as a tuning parameter and therefore the IPV (or PORFT with respect to the STARS nomenclature) was considered a tuning parameter for the simulation.

The following list summarizes the parameters that were not known, and were considering tuning parameters for the simulation.

- The effect of polymer concentrations lower than 1500 ppm on the viscosity (i.e.: the viscosity mixing rule)
- Adsorption parameters including: the maximum adsorption, the adsorption associated with different polymer concentrations (Langmuir isotherm), the amount of reversible adsorption, and the resultant inaccessible pore volume (IPV).

Sensitivity studies were conducted for a range of realistic values in order to gain a better understanding of how greatly these unknown parameters affected the simulation results. Since the first flow rate used in the experimental procedure was 2 ml/min, the sensitivity study was also conducted at this flow rate. This first flow rate was decidedly the most critical flow rate for the purpose of achieving a proper history match since all of the effects from the polymer adsorption and the mixing of polymer concentrations occur during this flow rate.

The initial sensitivity study was designed in order to gain a better understanding of the polymer adsorption. It is understood that there is a maximum level of adsorption after which no more polymer can be adsorbed. For the purposes of this work, it was assumed that most if not all of the adsorption had occurred once the pressure drop achieved steady state. The maximum adsorption, adsorption associated with the injected polymer concentration, and the irreversible adsorption all used input units of moles per pore volume. The sensitivity study was conducted assuming that a reasonable range of adsorption would be 5 to 30% of the injected polymer moles. These adsorption percentages correspond to adsorption values (in units of moles per pore volume) of 1.18×10^{-11} and 7.06×10^{-11}, respectively. This range was studied in increments of 5%.

The first sensitivity that was to be executed would have investigated the effect of varying the percentage of adsorption, while keeping the maximum adsorption, the adsorption associated with polymer concentration, and the irreversible adsorption equal to each other. Unfortunately the Langmuir isotherm-based adsorption table in STARS requires that the difference between each entry not be smaller than 1×10^{-10} moles of polymer per pore volume. With respect to the volume of solution injected, an adsorption of 1×10^{-10} moles per pore volume would mean that around 42.5% of the injected polymer was adsorbed. Since the polymer adsorption associated with the injected polymer concentration could not go low enough to realistically model the adsorption behavior, it was set constant at 1×10^{-10} moles per pore volume while the maximum adsorption and irreversible adsorption were varied.

Table 4.2 displays the inputs for the first sensitivity study, and Figure 4.2 displays the simulation results from these input values. Each of the cases in the table corresponds, as labeled, to a graphical simulation result. The experimental pressure difference for 2 ml/min flow rate is also plotted with the simulation results as a dark charcoal colored line.

Adsorption Trials for Maximum and Irreversible Adsorption Between 5-30%							
Case	Polymer Concentration	Adsorption Associated with Concentration	Maximum Adsorption	Irreversible Adsorption	Fraction of Available Pore Space	Viscosity Mixing Function	RRF
1	1.87E-09	1.00E-10	1.18E-11	1.18E-11	0.85	no	3.2
2	1.87E-09	1.00E-10	2.35E-11	2.35E-11	0.85	no	3.2
3	1.87E-09	1.00E-10	3.53E-11	3.53E-11	0.85	no	3.2
4	1.87E-09	1.00E-10	4.71E-11	4.71E-11	0.85	no	3.2
5	1.87E-09	1.00E-10	5.89E-11	5.89E-11	0.85	no	3.2
6	1.87E-09	1.00E-10	7.06E-11	7.06E-11	0.85	no	3.2

Table 4.2: Input data for the maximum and irreversible adsorption study - all adsorption parameters are in units of moles per pore volume

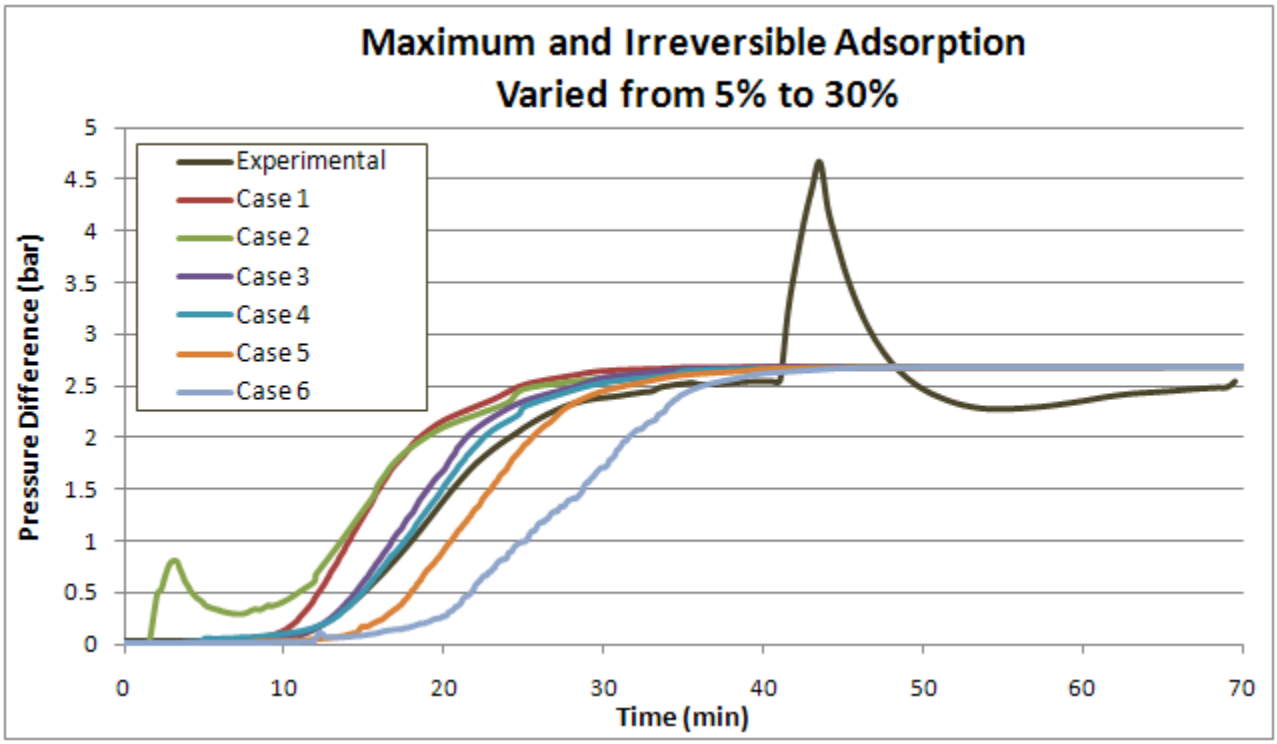

Figure 4.2: Simulation results for the study which investigated the effect of the adsorption parameters where the maximum and irreversible adsorption were assumed to be equal

As can be seen, increasing the amount of adsorption leads to a delay in the pressure build up. This can be understood by recognizing that the adsorbed polymer does not add to the viscosity of the injected fluid, which results in injecting a larger volume of fluid to accomplish the same

viscosity behavior of a less absorptive polymer. This same behavior has been seen in experimental results where polymer adsorption was responsible for the delay in fluid break through (Zaitoun and Kohler 1987). As seen from these simulation results, the way the adsorption keywords operate is such that the final pressure drop is unaffected by the maximum adsorption value.

The various adsorption scenarios in Figure 4.2 show that the adsorption that occurred during the experiment fell within the expected range. In particular, the true experimental adsorption behavior appears to be such that 20 to 25% of the injected moles are adsorbed during the initial injection stage.

Upon closer inspection, an adsorption value of 4.68×10^{-11} moles per pore volume was found to closely simulate the experimental results. The simulation results for this adsorption can be seen in Figure 4.3.

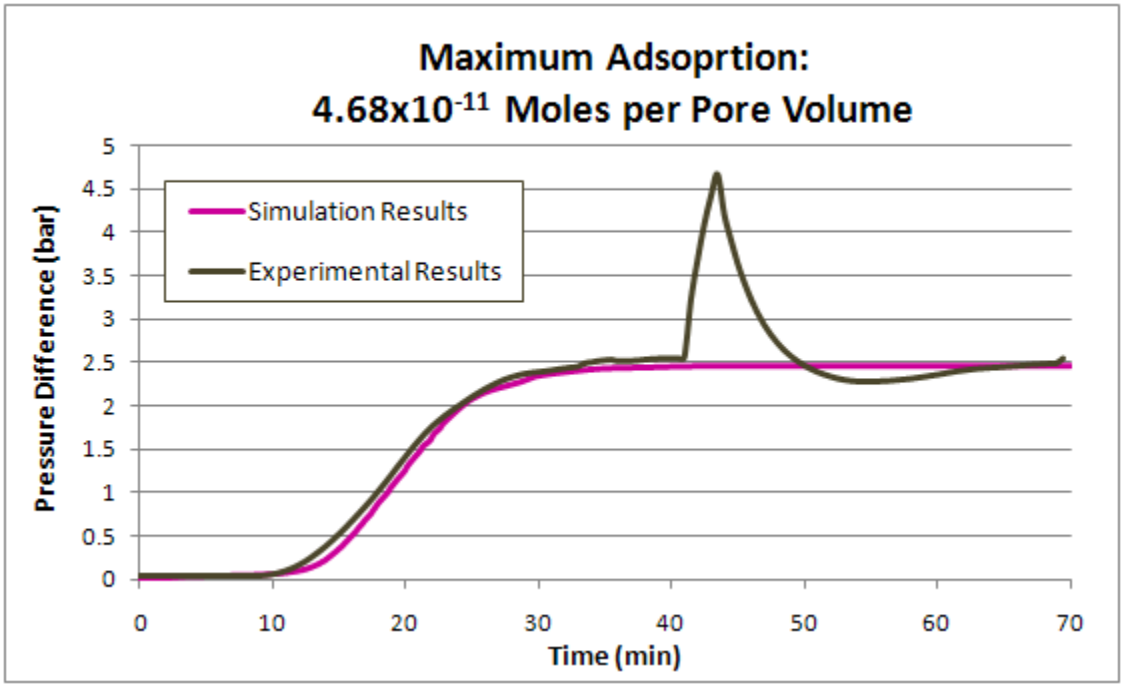

Figure 4.3: Simulation results for the best fit maximum adsorption value

Although the simulation results in Figure 4.3 show that the pressure build up can be well matched when the maximum and irreversible adsorption are equal to 4.68×10^{-11} moles per pore volume, the behavior of the individual adsorption parameters needed to be investigated to see if a better fit could be obtained and to understand the effect of the other parameters.

The next sensitivity study was run to determine whether or not the polymer concentration associated adsorption used in the STARS keyword, 'ADSTABLE,' had any effect on the adsorption behavior or the pressure response. This keyword, which is based on the Langmuir

isotherm, allows the user to input a table of polymer concentrations and associated adsorption values. For this particular case, the adsorption value is associated with the injected polymer concentration which, in units of mole fraction, is 1.87×10^{-9}. As previously noted, this value could not be lower than 1×10^{-10}, and was therefore set as a constant in the previous sensitivity study. Since the way the simulator handles adsorption is related to the amount of fluid being injected, the limiting value in the adsorption table could be an issue for modeling small scale situations such as a coreflood. In a reservoir scale situation however, this would not be expected to be a problem since the volume of injected fluid, and therefore the number of adsorbed moles of polymer would be significantly larger. Table 4.3 and Figure 4.4 display the input parameters and corresponding results which were used to study the effect of the polymer adsorption associated with the polymer concentration. The specific parameter that is being varied in this case is the polymer adsorption (in units of moles per pore volume) that has been input for the STARS keyword 'ADSTABLE.'

Adsorption Trials for Adsorption Associated with Polymer Concentration							
Case	Polymer Concentration	Adsorption Associated with Concentration	Maximum Adsorption	Irreversible Adsorption	Fraction of Available Pore Space	Viscosity Mixing Function	RRF
1	1.87E-09	1.00E-10	4.68E-11	4.68E-11	0.85	no	3.2
2	1.87E-09	2.00E-10	4.68E-11	4.68E-11	0.85	no	3.2
3	1.87E-09	3.00E-10	4.68E-11	4.68E-11	0.85	no	3.2
4	1.87E-09	4.00E-10	4.68E-11	4.68E-11	0.85	no	3.2
5	1.87E-09	1.00E-09	4.68E-11	4.68E-11	0.85	no	3.2

Table 4.3: Input data for the Langmuir isotherm adsorption study - all adsorption parameters are in units of moles per pore volume

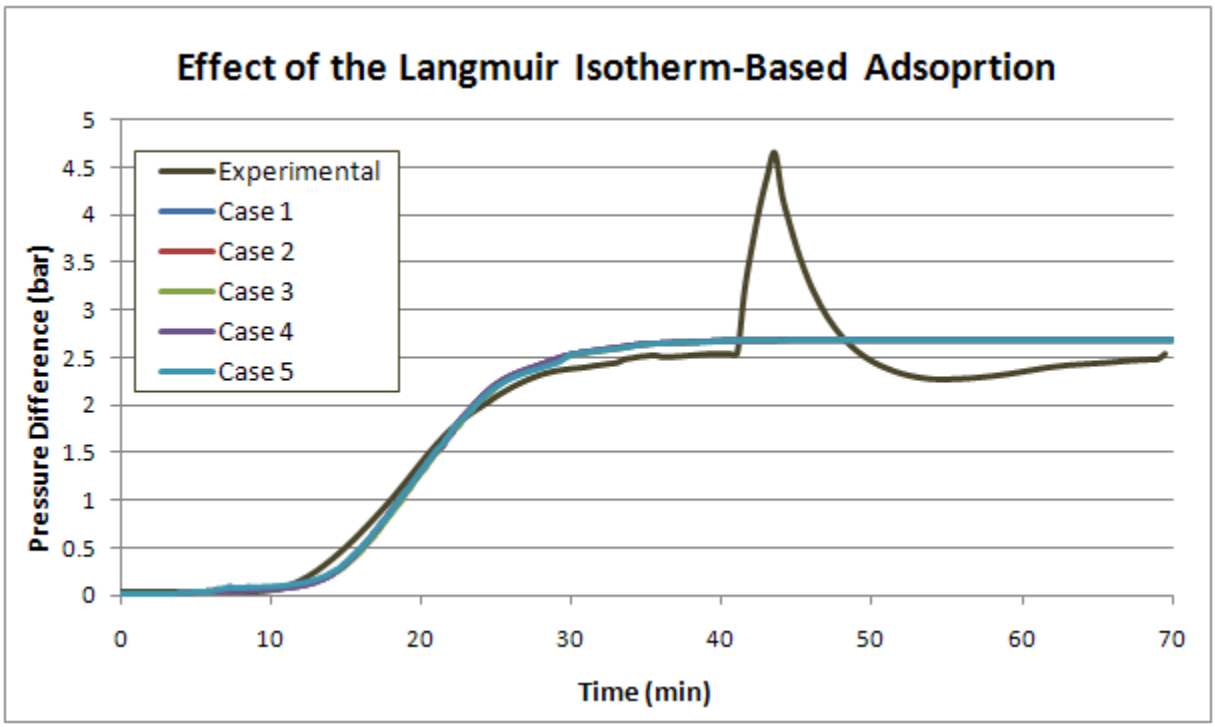

Figure 4.4: Simulation results for the study which investigated the effect of the keyword related to the Langmuir isotherm

As can be seen from the graph, despite the broad range of adsorption values that were investigated in this study, all of the cases resulted in very similar pressure behavior. Since the adsorption associated with the polymer concentration did not appear to affect the pressure results, the original value of $1x10^{-10}$ was selected as the default for the rest of the sensitivity studies.

In the two previous sensitivity studies, it was assumed that all of the adsorption was permanent and irreversible. Since there was no experimental data to confirm whether this assumption was correct or not, the irreversible adsorption was treated as a sensitivity parameter. Using a maximum adsorption value of $4.68x10^{-11}$ moles per pore volume, the irreversible adsorption was varied as a function of the maximum adsorption value from 75% to 95%. The input values are presented in Table 4.4, where irreversible adsorption was studied in 5% increments. The simulation results for each case are located in Figure 4.5.

Adsorption Trials for Irreversible Adsorption							
Case	Polymer Concentration	Adsorption Associated with Concentration	Maximum Adsorption	Irreversible Adsorption	Fraction of Available Pore Space	Viscosity Mixing Function	RRF
1	1.87E-09	1.00E-10	4.68E-11	4.44E-11	0.85	no	3.2
2	1.87E-09	1.00E-10	4.68E-11	4.21E-11	0.85	no	3.2
3	1.87E-09	1.00E-10	4.68E-11	3.97E-11	0.85	no	3.2
4	1.87E-09	1.00E-10	4.68E-11	3.74E-11	0.85	no	3.2
5	1.87E-09	1.00E-10	4.68E-11	3.51E-11	0.85	no	3.2

Table 4.4: Input data for the irreversible adsorption study – all adsorption parameters are in units of moles per pore volume

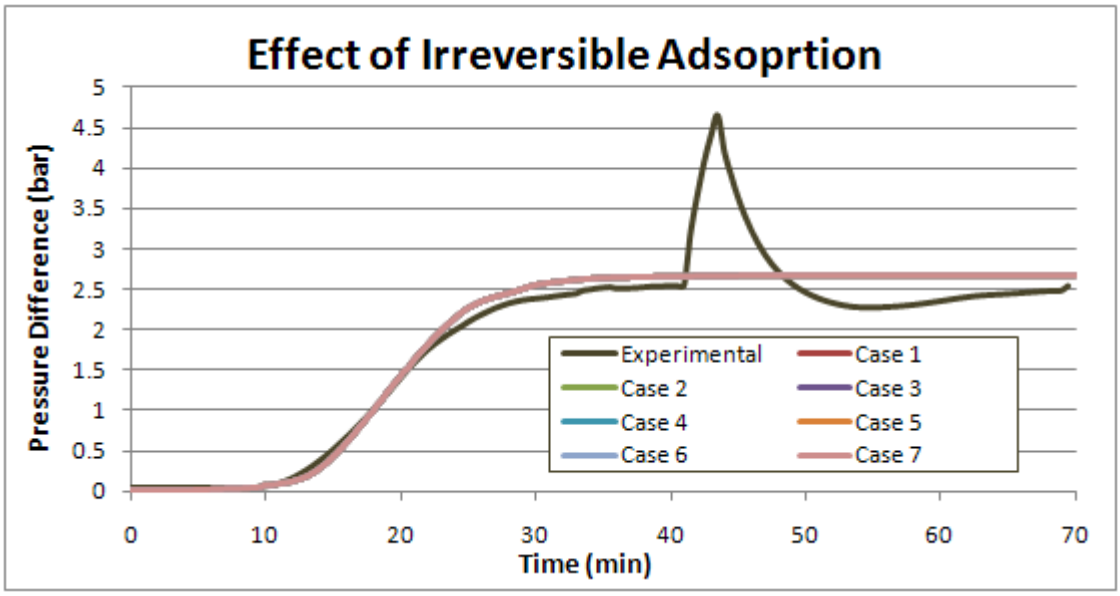

Figure 4.5: Simulation results for the study which investigated the effect of the irreversible adsorption parameter

Just as varying the adsorption associated with the polymer concentration had no effect on the pressure response, varying the irreversible adsorption as a function of the maximum adsorption displayed a negligible effect. For the rest of the simulations, it was decided that it would suffice to assume that all adsorption was permanent and irreversible.

The final sensitivity that was conducted for this flow rate investigated the effect of the inaccessible pore volume. Until now, an inaccessible pore volume of 15% had been used in all of the previous sensitivities. It was assumed that a range of reasonable inaccessible pore volume values was somewhere between 10% and 20%. For the purpose of studying the simulators behavior, this range was expanded to study inaccessible pore volumes ranging from 5% to 30%. This study was conducted in increments of 5%. The input values and graphical results are located in Table 4.5 and Figure 4.6, respectively.

Adsorption Trials for Inaccessible Pore Volume							
Case	Polymer Concentration	Adsorption Associated with Concentration	Maximum Adsorption	Irreversible Adsorption	Fraction of Available Pore Space	Viscosity Mixing Function	RRF
1	1.87E-09	1.00E-10	4.68E-11	4.68E-11	0.95	no	3.2
2	1.87E-09	1.00E-10	4.68E-11	4.68E-11	0.9	no	3.2
3	1.87E-09	1.00E-10	4.68E-11	4.68E-11	0.85	no	3.2
4	1.87E-09	1.00E-10	4.68E-11	4.68E-11	0.8	no	3.2
5	1.87E-09	1.00E-10	4.68E-11	4.68E-11	0.75	no	3.2
6	1.87E-09	1.00E-10	4.68E-11	4.68E-11	0.7	no	3.2

Table 4.5: Input data for the inaccessible pore volume study - all adsorption parameters are in units of moles per pore volume

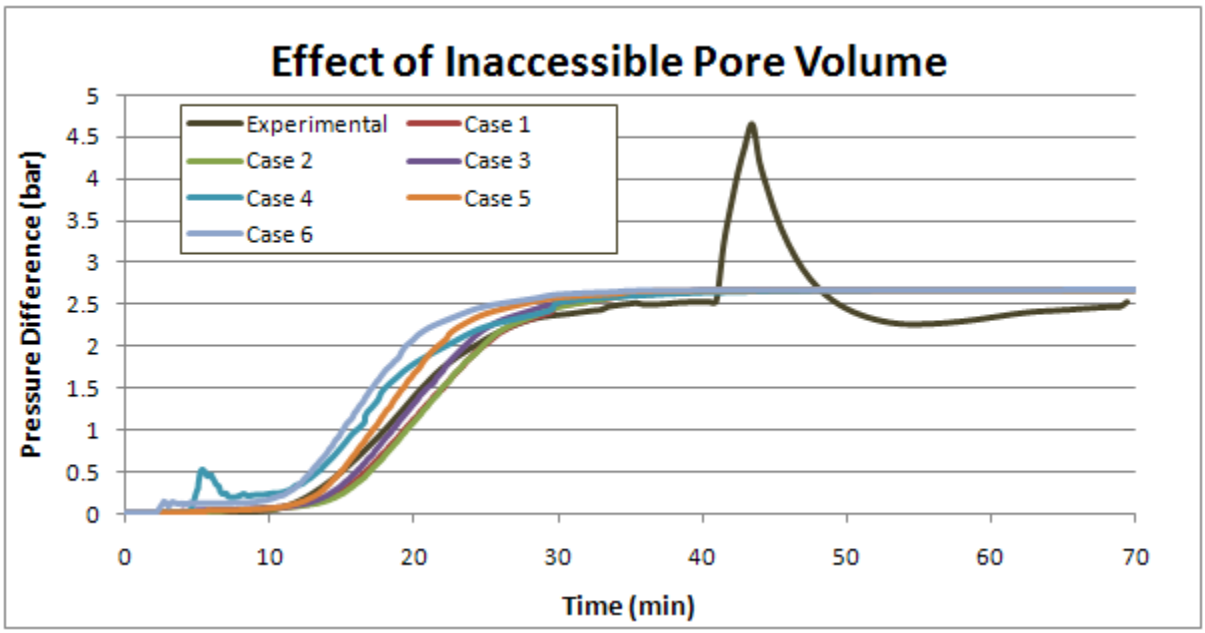

Figure 4.6: Simulation results for the study which investigated the effect of the inaccessible pore volume

From the graphical results it becomes apparent that the inaccessible pore volume does affect the pressure behavior. Although the magnitude of the effect is smaller, increasing the inaccessible pore volume affects the pressure results in a similar manner as decreasing the maximum adsorption. The pressure drop in the core is able to build faster as the percentage of the pore volume through which fluids are able to flow decreases. Although increasing or decreasing the available pore volume affects the pressure build, it does not affect the stabilized pressure result. From graphical observation it was determined that Case 3 represented the experimental data the closest. This case was created using an inaccessible pore volume of 15%, which falls within the expected range of inaccessible pore volumes and was therefore accepted as a reasonable value.

The viscosity mixing function was also investigated for the 2 ml/min flow rate. This parameter controls how quickly the maximum viscosity is achieved with relation to the polymer concentration, so the fact that the viscosity mixing parameter affected the pressure build but not the stabilized pressure difference is understandable. The results for three different cases are displayed below. The first case represents an extreme situation where the ultimate viscosity is achieved at very low polymer concentrations. The last case represents a linear mixing function, and the middle case represents something in between the two extremes. As can be seen, the pressure build can be manipulated to a decent extent by adjusting the mixing function. Since the viscosity behavior of the polymer at lower concentrations was not known, a linear mixing function was assumed.

Polymer Concentration	Viscosity Mixing Cases: Fraction of Total Viscosity Available for a Given Concentration		
Polymer Mole Fraction	Moderate Mixing	Strong Mixing	Linear Mixing
0	0	0	0
1.87E-10	0.5	0.9991	0.1
3.74E-10	0.5	0.9992	0.2
5.61E-10	0.6	0.9993	0.3
7.48E-10	0.65	0.9994	0.4
9.35E-10	0.7	0.9995	0.5
1.122E-09	0.75	0.9996	0.6
1.309E-09	0.8	0.9997	0.7
1.496E-09	0.85	0.9998	0.8
1.683E-09	0.9	0.9999	0.9
1.87E-09	1	1	1

Figure 4.6: Input data for the relationship between the polymer concentration and the viscosity behavior

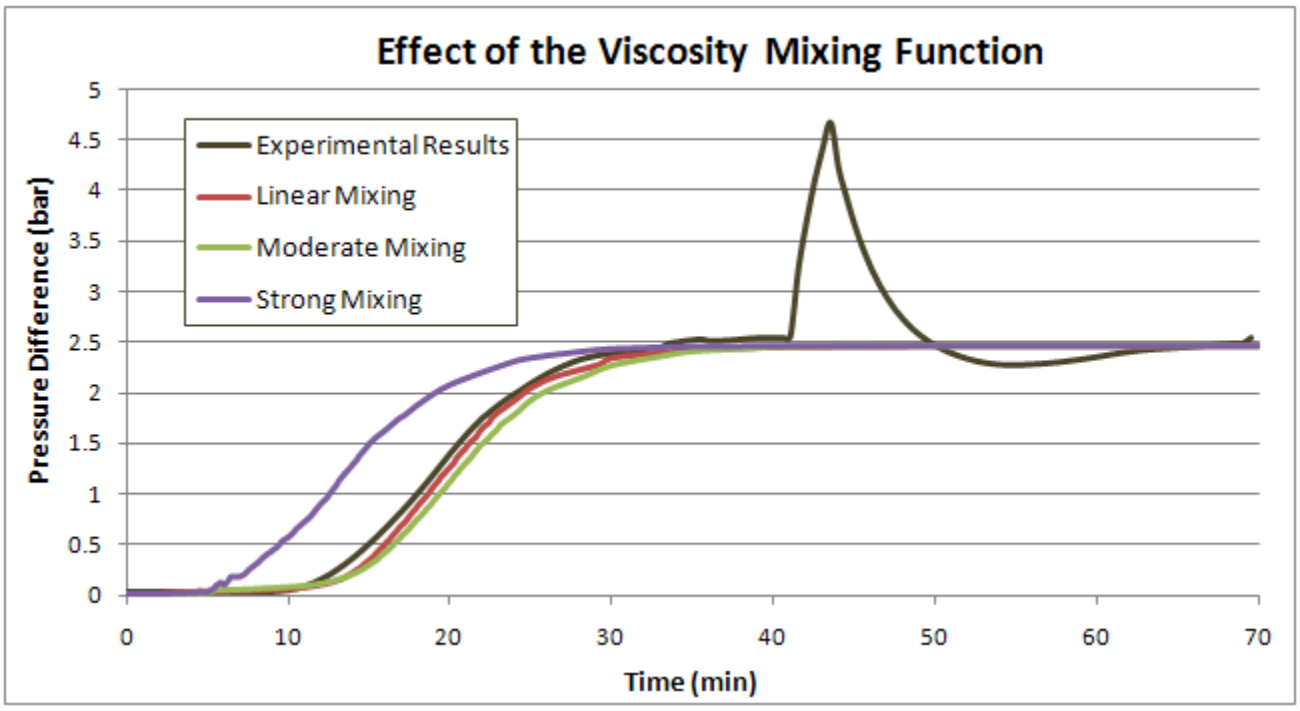

Figure 4.7: Simulation results for three different scenarios modeling the viscosity effect due to concentration mixing

The only parameters that appear to have any effect on the pressure difference that is ultimately achieved in the core when the flow reaches steady state are the permeability reduction (RRF), and the fluid viscosities. Since the fluid viscosities were well defined from experimental coreflood results, the RRF was used as a tuning parameter to obtain a better fit for the stabilized pressure result. The RRF affects the stabilized pressure in a manner such that for a simulation with a given stabilized pressure and RRF value, an estimate of the "correct," RRF can be determined as a ratio of the simulated and experimental pressures and the simulated and experimental RRF values. Formulaically this new RRF can be calculated as follows:

$$RRF_{new} = RRF_{Simulation} \Big/ \left(\frac{Stabilized\ Pressure\ Drop_{Simulation}}{Stabilized\ Pressure\ Drop_{Experimental}}\right) \qquad \text{(Equation 22)}$$

By using this method, it was determined that the pressure results could be matched more closely with an RRF value of 2.94. As previously mentioned, the RRF value was experimentally determined at the end of the series of polymer floods, so the exact permeability reduction for any given flow rate was not known. Since it is assumed that the permeability reduction varies to some degree for each of the flow rates, it was decided that an RRF value of 2.94 was reasonably acceptable for the purpose of this work.

4.3.4 – PRESSURE MATCH FOR THE 2 ML/MIN FLOW RATE

After conducting the sensitivity studies to understand how the adsorption parameters affected the simulated results, a final match was created for the 2 ml/min flow rate. Between the inaccessible pore volume, the maximum adsorption, and the effect of polymer concentration on the viscosity, there was a lot of flexibility in determining the values which provided the best pressure match. Since none of these parameters were well defined from the experimental data, the combination of the parameters was not well constrained. As a result, the values that were selected to simulate the experimental pressure behavior do not create a unique match. It is not hard to imagine that multiple combinations of values for the three aforementioned parameters could result in simulated pressure differences that were well matched with the experimental data. In a situation where the actual values for key parameters are not well known, it is important to understand and experiment with a reasonable range of values for these parameters. The input parameters and graphical results for the final match that was created are presented below in Table 4.7 and Figure 4.8.

Data for the 2 mL/min Pressure Match						
Polymer Concentration	Adsorption Associated with Concentration	Maximum Adsorption	Irreversible Adsorption	Fraction of Available Pore Space	Viscosity Mixing Function	RRF
1.87E-09	1.00E-10	4.68E-11	4.68E-11	0.85	no	3.2

Table 4.7: Input parameters selected to model the first polymer injection rate - all adsorption parameters are in units of moles per pore volume

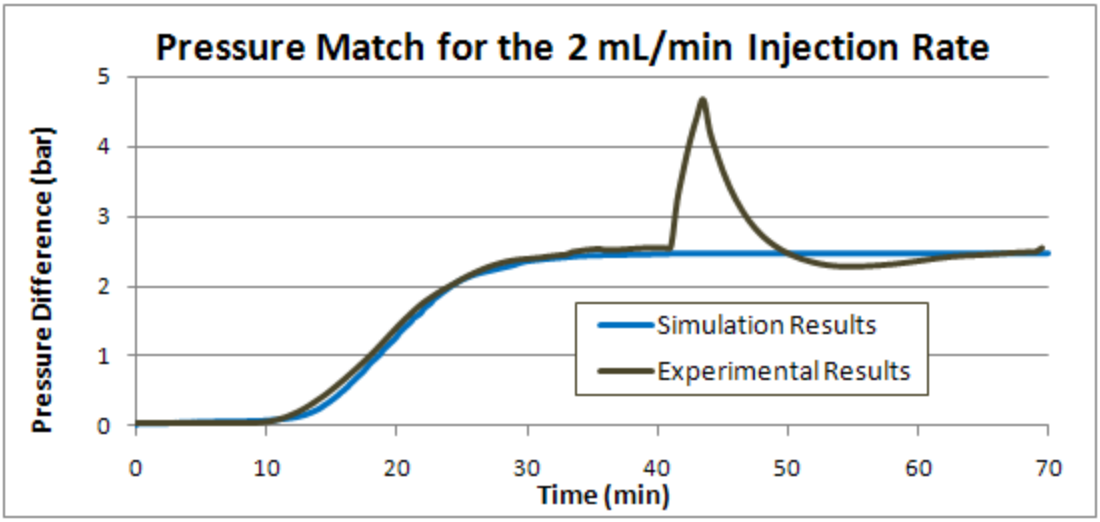

Figure 4.8: Simulation results displaying the accepted pressure match for the first injection rate

4.3.5 – PRESSURE MATCHES CREATED FOR THE OTHER FLOW RATES

After matching the first injection rate, the process of matching the other injection rates was just a matter of adjusting the permeability reduction factor. The method that was used to determine the appropriate permeability reduction value for the simulation was described earlier in Equation 17. Since STARS does not allow for multiple values of RRF to be entered in a single input file, a restart file had to be created for each new RRF value.

Problems pertaining to pressure instabilities were encountered as the flow rates increased. The first injection rate that displayed these instabilities was the 6 ml/min injection rate. By decreasing the time step associated with this injection rate it was possible to smooth out the pressure fluctuations. The problem with the pressure fluctuations became more pronounced as the injection rates increased to larger values, and it was not possible to dampen the instabilities past an injection rate of 7.5 ml/min.

Multiple methods such as decreasing the size of the time step, increasing the number of iterations, increasing the number of time cuts associated with changes in fluid saturations, and increasing the maximum allowable number of time steps were tried to remedy this problem, but they resulted in limited success beyond an injection rate of 7.5 ml/min. Because of this, it was decided that all of the flow rates larger than 7.5 ml/min would be excluded from the simulation. This meant that the decreasing injection rates, starting with the 3 ml/min rate, would be simulated directly after the 7.5 ml/min injection rate.

4.3.6 – SINGLE PHASE SIMULATION RESULTS

The final pressure match which was created by reasonable manipulation of the RRF values for the different injection rates is displayed in Figure 4.9.

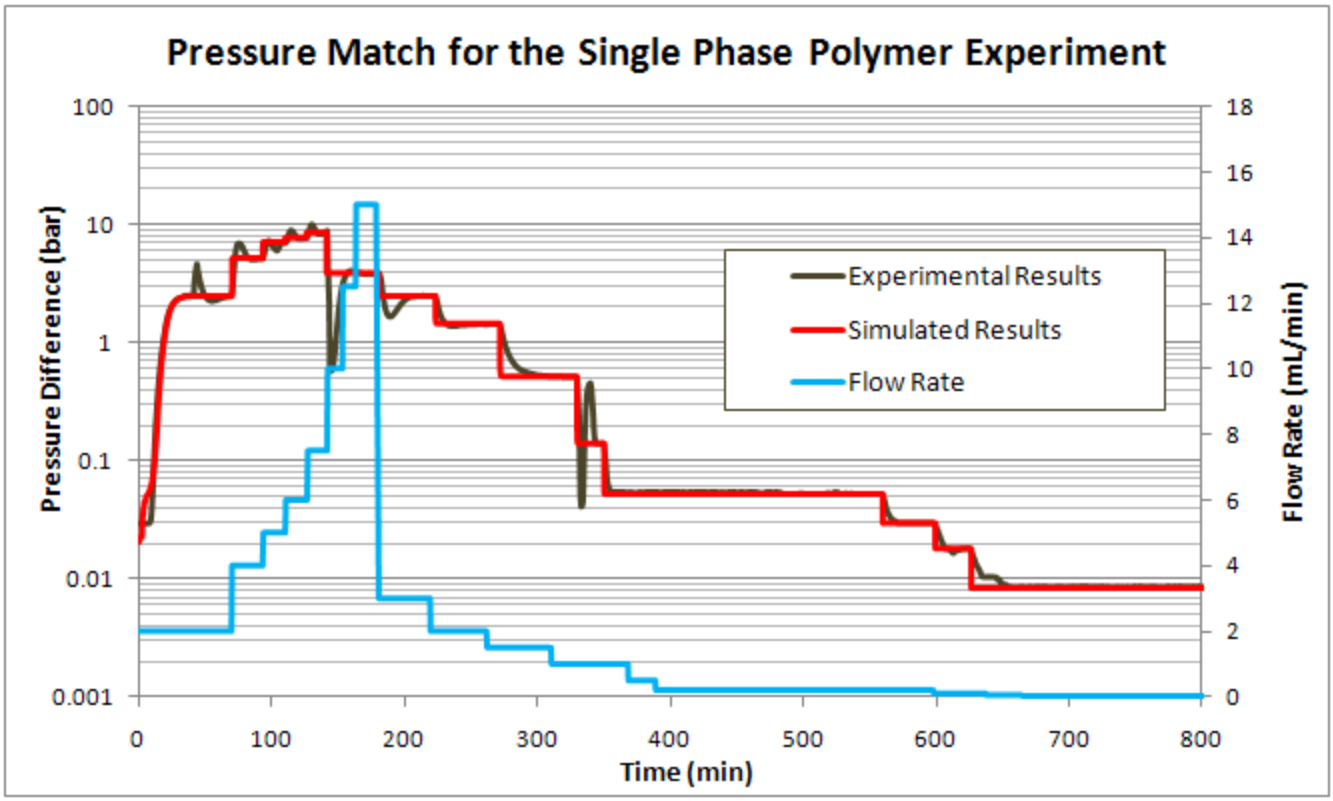

Figure 4.9: Simulation results displaying the accepted pressure matches for all of the injection rates ranging from .02 mL/min to 7.5 mL/min

Additionally, since there were some issues encountered during the process of modeling the higher injection rates, a zoomed-in version of these injection rates has been plotted in Figure 4.10. As can be seen from the ''Simulated Results,'' line, despite the steps taken to reduce the pressure fluctuations, the 7.5 mL/min flow rate still exhibits very minor oscillations.

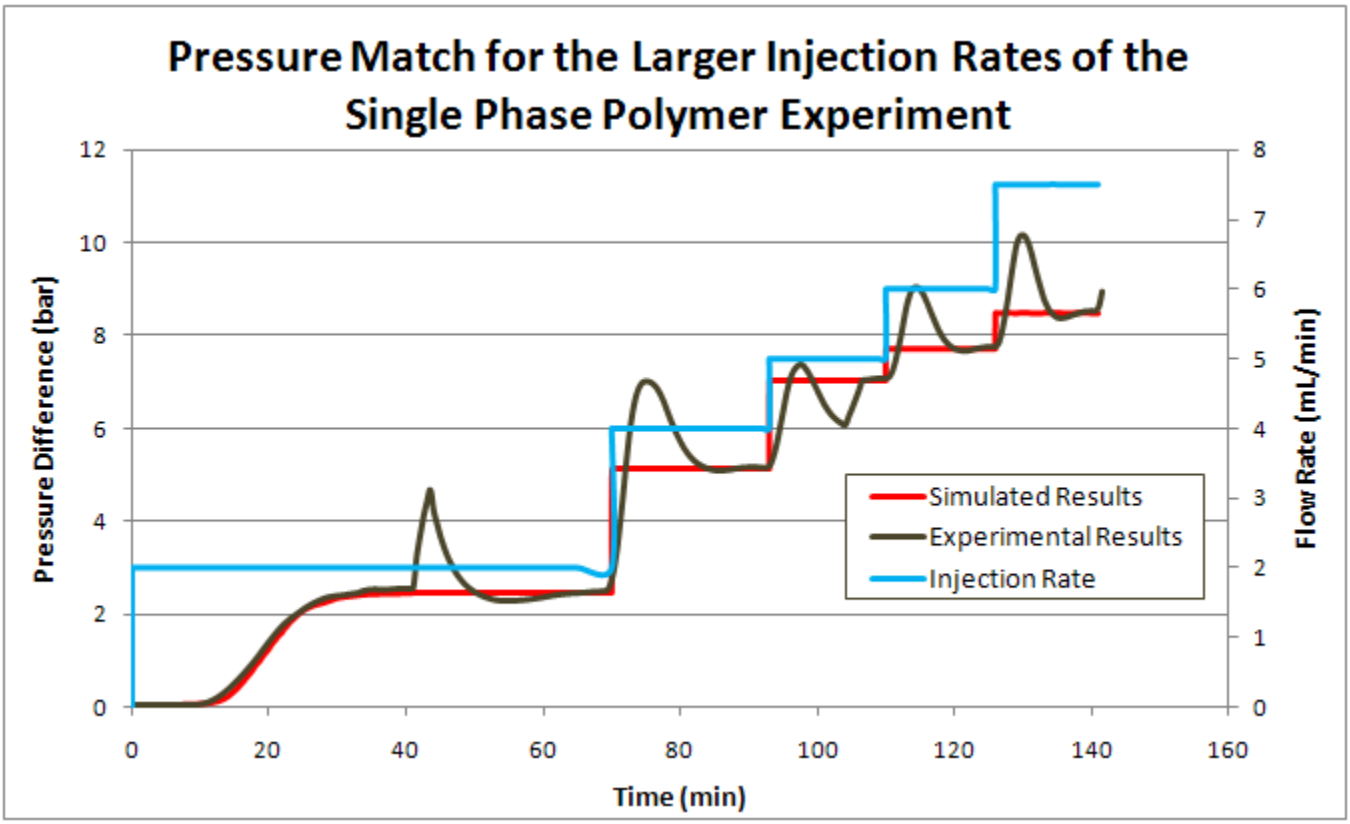

Figure 4.10: A zoomed-in view of the well-matched results from the simulation for the increasing injection rates

The following table (Table 4.8) presents a summary of the results created by the simulation of the single phase polymer flood. In this table, the final pressure differences across the second core from the experimental and simulated data are compared for different flow rates. Additionally, the RRF has been displayed for each flow rate along with the flow regime that each flow rate was located in. The red font represents the increasing injection rates and the blue font represents the decreasing injection rates.

Flow Rate	Experimental Stabilized Pressure Drop	Simulated Stabilized Pressure Drop	Percent Error	RRF	Flow Regime
ml/min	bar	bar	%	unitless	regime name
2	2.49	2.467	-0.92369	2.94	shear thickening
4	5.08	5.14144	1.209449	3.05	shear thickening-degradation
5	6.02	7.039	16.92691	3.469	degradation
6	6.74	7.7256	14.62315	3.4	degradation
7.5	7.5	8.329	11.05333	3.36	degradation
10	8.46	-		-	degradation
12.5	9.2	-		-	degradation
15	9.63	-		-	degradation
3	3.89	3.8537	-0.93316	2.94	shear thickening
2	2.5	2.46736	-1.3056	2.94	shear thickening
1.5	1.45	1.437157	-0.88572	2.94	shear thickening
1	0.512	0.511255	-0.14551	2.96	shear thickening-shear thinning
0.5	0.139	0.1388	-0.14388	2.96	shear thinning
0.2	0.0519	0.051835	-0.12524	2.96	shear thinning
0.1	0.0293	0.029262	-0.12969	2.96	shear thinning
0.05	0.0179	0.017877	-0.12849	2.96	shear thinning
0.02	0.00825	0.0082386	-0.13818	2.96	shear thinning

Table 4.8: Summarized results from the simulation for the single phase polymer flood - red indicates increasing injection rate and blue indicates decreasing injection rate

Although the simulated data appears to fit the experimental data well from the graphs in Figure 4.9 and Figure 4.10, this does not seem to be the case when comparing the stabilized pressure drop values. By viewing the results in this manner, it becomes immediately apparent that the higher injection rates incurred a significantly larger amount of error than the lower flow rates. Aside from any error associated with the pressure instabilities that occur at the higher flow rates, there is also the possibility that errors were introduced in the pressure readings. When conducting the multi-rate polymer floods the injection rates can take longer to stabilize than

expected, and it is preferable to run the whole series of injection rates in a single day. Because of this, there are sometimes erroneous pressure readings due to the fact that the pressure differential might not actually be at steady-state when the pressure measurement is taken.

While history matching the pressures for each injection rate it was noted that the higher injection rates seemed to require larger values of RRF than the lower injection rates. Additionally there seemed to be a noticeable difference in the RRF values with respect to the flow regime. The behavior of the RRF values as a function of injection rate has been plotted in Figure 4.11. As with the previous table, red indicates increasing injection rate while blue indicates decreasing injection rate.

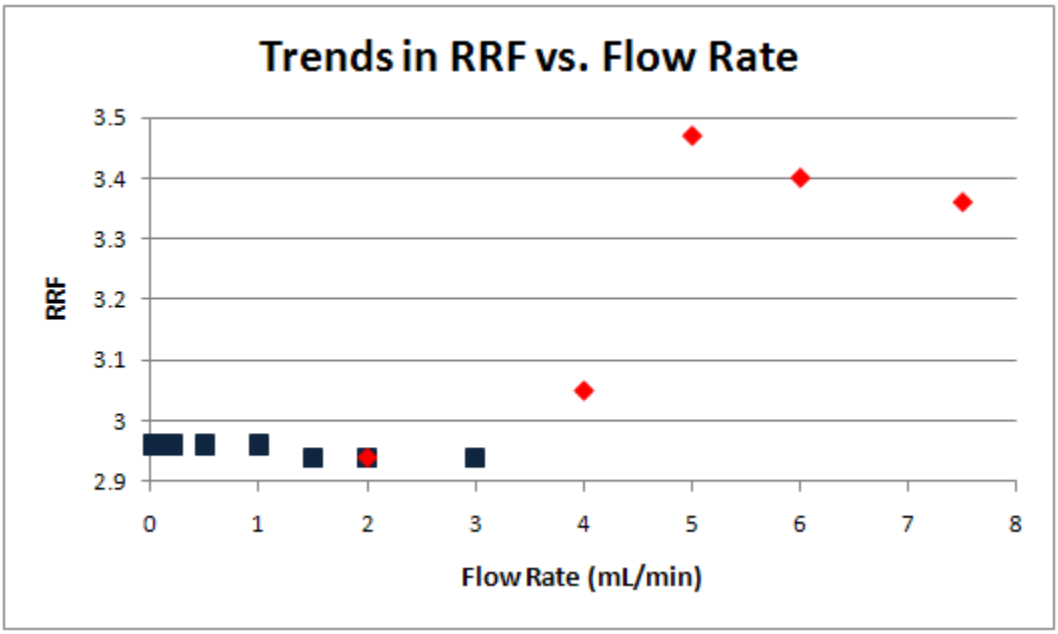

Figure 4.11: A trend in the RRF values that were used as tuning parameters - red indicates increasing injection rate and blue indicates decreasing injection rate

Upon initial inspection, the behavior of the RRF values appears to follow the same trend as the apparent viscosity. Additional comparisons and commentary on this behavior will be covered in the discussion section of this thesis.

4.4 – TWO PHASE SIMULATION WORK

4.4.1 – INTRODUCTION TO THE TWO PHASE SIMULATION WORK

The experimental results from the two phase flooding experiment were used to develop the simulation which is described in the following sections. As with the previous polymer flood model (hence forth referred to as “Simulation 1”), it was imperative that the final simulation was based on physically realistic input values. Because of time constraints, the analysis of the experimental results (preformed by Moradi 2011), and the development of the simulation

model had to take place simultaneously. This resulted in a few parameters, which could have been determined experimentally, being treated as uncertainties during the initial stages of the simulation. These parameters included the apparent viscosity of the polymer during two phase flow, the behavior of the relative permeability and saturation curves, and the adsorption behavior. Since some of the analysis of the experimental results occurred independently from the development of the simulation model, it was desirable to retrospectively confirm the validity of the uncertain parameters if and where possible.

4.4.2 – MOBILE PHASE RELATIVE PERMEABILITY CURVE

Unlike Simulation 1 where the relative permeability curves were not a point of interest, it was important to provide realistic relative permeability data for the two phase experiment. A complete description of the permeability behavior as a function of the fluid saturation was not available, but the end-point behavior was available as described in the experimental results for the two phase polymer flood. Multiple scenarios with varying curvature were created to model the relative permeability behavior. Once the curves were created, the most realistic looking curves were tested in the simulator to see if they provided a good match with the experimental data.

Since no visible oil production occurred for the first four injection rates, the oil relative permeability was sufficiently accounted for with the proper end-point values. For these rates, the shape of the curve between the oil related end-points was not of interest. Of course this changed later when the injection rate was high enough that two phase flow occurred, at which point the shape of the oil relative permeability curve became important. The most successful water relative permeability behavior, as determined by the simulation results, is presented in this section.

An initial approximation for the relative permeability behavior was created by fitting a straight line through the water related end-point data. Because this sort of data tends to display more curvature than is suggested by a straight-line model, additional variations with more curvature were created. By manipulating the relative permeability value associated with the 41.85% water saturation (which is half way between the interstitial and maximum water saturation), a range of curves displaying more realistic shapes were produced. Since a linear trend is created by setting the mid-point relative permeability to be equal to 50% of the maximum relative permeability, curves with a concave-up trend were created by setting the mid-point value to be between 10% and 40% of the maximum relative permeability. The numbers that were created from this process are presented in Table 4.9. The data in the 50% column represents the data associated with a straight line. The graphical results can be seen in Figure 4.12.

Water Relative Permeability Investigation						
Water Saturations	Relative Permeability Cases					
Sw	10%	20%	30%	40%	45%	50%
0.2282	0	0	0	0	0	0
0.4185	0.009497	0.018994	0.028491	0.037988	0.042736594	0.047485
0.6008	0.0949702	0.09497	0.09497	0.09497	0.094970208	0.09497

Table 4.9: Water relative permeability input data for varying cases of curvature

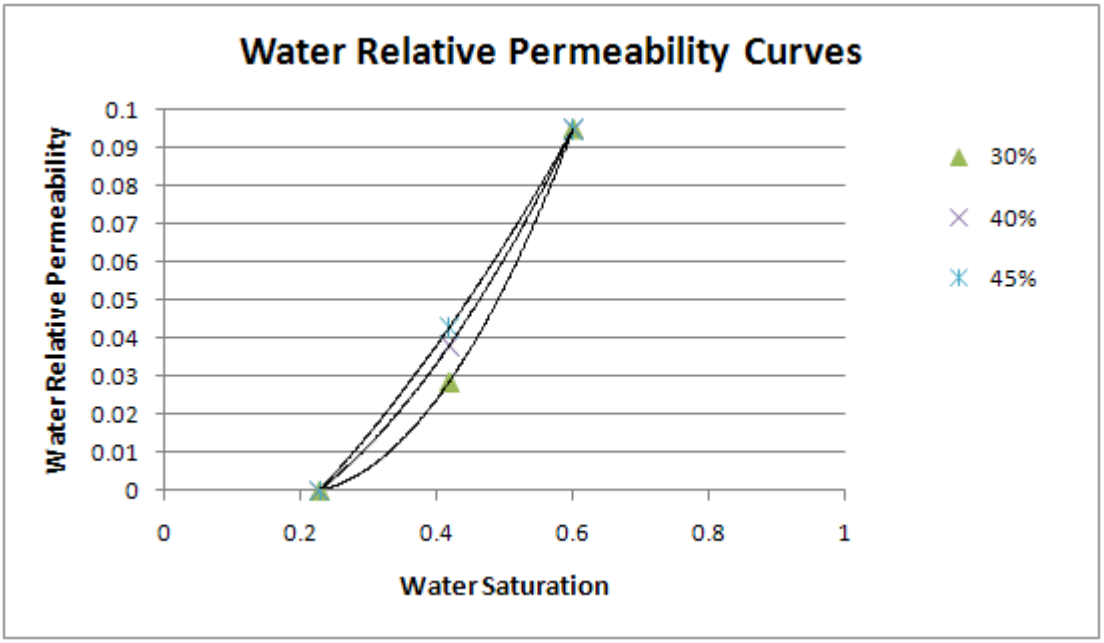

Figure 4.12: Multiple relative permeability scenarios developed by fitting a curve through the water relative permeability end-points

The "30% case" was selected for the simulation because it had a nice curvature and did not contain any negative relative permeability values. The 10% and 20% cases were not presented in the graph since they included unrealistic negative values. The curvature of the relative permeability function was treated as a tuning parameter for the model, so any realistic starting point was decidedly acceptable for the initial investigation.

4.4.3 – VISCOSITY BEHAVIOR IN THE POLYMER MIXING FRONT

From Simulation 1 it was understood that the primary polymer-related parameters which were affecting how quickly the steady-state pressure difference was achieved were the maximum adsorption, the effect of the polymer concentration on the solution viscosity, and the inaccessible pore volume.

Bulk rheology experiments were conducted for multiple polymer concentrations, so the effect of the polymer concentration on the solution viscosity was fairly well defined. Figure 4.13 displays the behavior of the polymer for concentrations varying from 0 to 2000 ppm. The polymer concentration has been displayed in units of mole fractions rather than ppm since the simulator required input units of mole fractions.

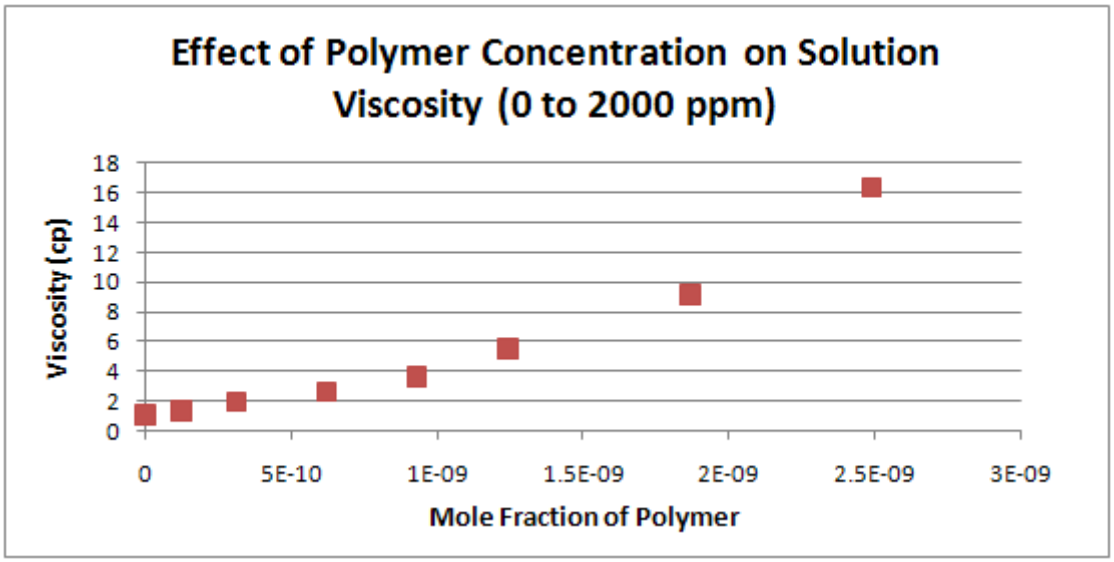

Figure 4.13: Non-linear behavior displayed in the relationship between viscosity and polymer concentration

As can be seen from the graph, the relationship between the polymer concentration and the solution viscosity is not linear. The data set presented in Table 4.10 was calculated for polymer concentrations ranging from 0 to 400 ppm from an equation that was created by fitting a polynomial trend through the experimental data points. This data was then converted into the form required by the simulator to account for the effects of non-linear mixing. A description of the process required to convert the experimental data to simulation input values can be found in the simulation manual (STARS Users Manual 2009).

Calculated Solution Viscosity for 0 to 400 ppm		
ppm	Polymer Mole Fraction	Solution Viscosity, cp
0	0.00E+00	1.048
40	4.97E-11	1.184
80	9.94E-11	1.318
120	1.49E-10	1.451
160	1.99E-10	1.583
200	2.49E-10	1.715
240	2.98E-10	1.847
280	3.48E-10	1.980
320	3.98E-10	2.115
360	4.47E-10	2.252
400	4.97E-10	2.391

Table 4.10: Polymer concentrations and associated solution viscosity values with non-linear behavior

The input values used to model the non-linear viscosity behavior due to polymer concentration variations are shown in Table 4.11. The simulation default values, which correspond to linear mixing behavior, are also presented in the table. As can be seen, the non-linear and the linear values are not significantly different from each other. The plot in Figure 4.14, which displays both data sets, further illustrates this point.

Linear and Non-Linear Mixing Values for 0 to 400 ppm			
ppm	Polymer Mole Fraction	Linear Mixing	Non-Linear Mixing
0	0.000E+00	0.0	0.000
40	4.970E-11	0.1	0.158
80	9.940E-11	0.2	0.295
120	1.491E-10	0.3	0.416
160	1.988E-10	0.4	0.525
200	2.485E-10	0.5	0.622
240	2.983E-10	0.6	0.711
280	3.480E-10	0.7	0.793
320	3.977E-10	0.8	0.867
360	4.474E-10	0.9	0.936
400	4.972E-10	1.0	1.000

Table 4.11: Input data for the linear and non-linear viscosity mixing behavior based on polymer concentration

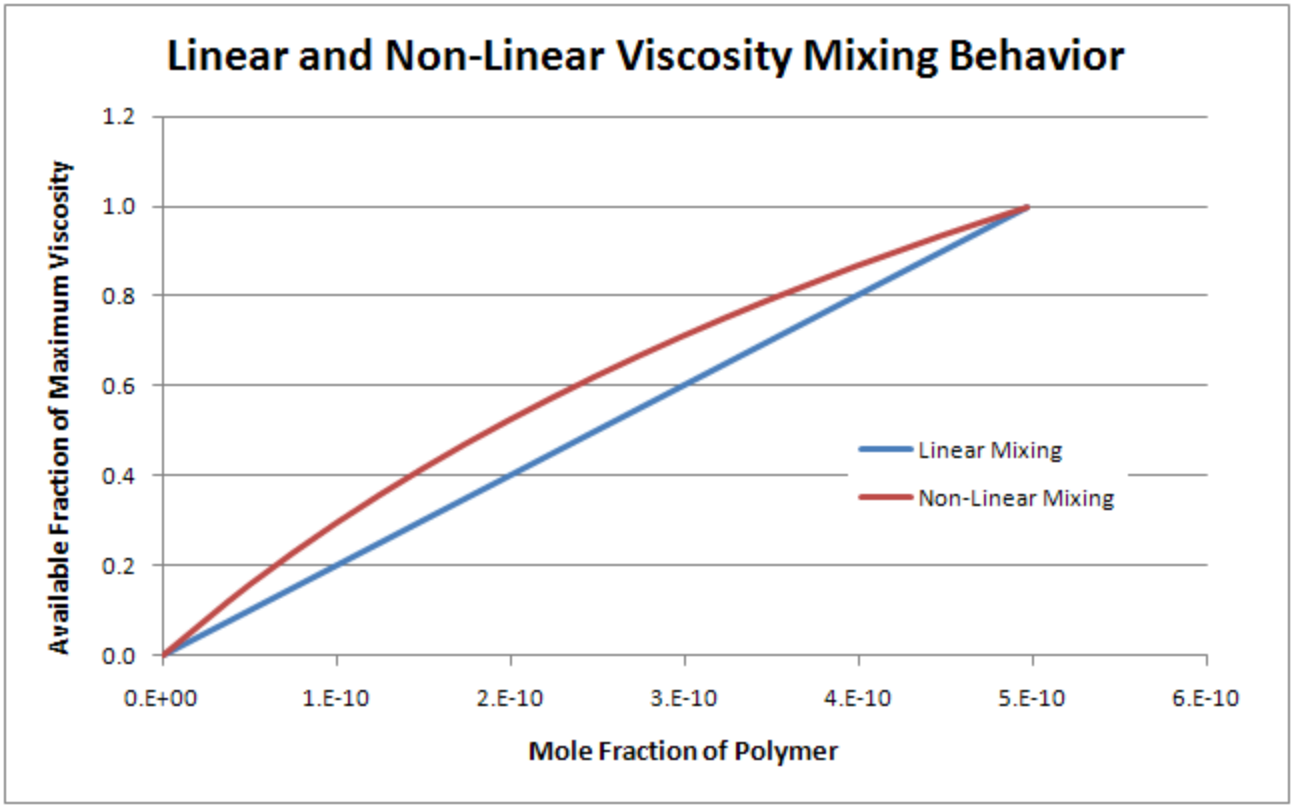

Figure 4.14: A graphical representation of the actual polymer viscosity behavior compared to the default simulation assumption

4.4.4 – POLYMER ADSORPTION BEHAVIOR - SENSITIVITY STUDY

The adsorption behavior associated with the first polymer injection rate in the two phase experiment was one of the parameters that was not well defined when the simulation modeling began. Since investigating a realistic range of values had successfully identified reasonable adsorption values for Simulation 1, it was decided that a similar approach would be used for the two phase case.

From the experimental data, the inaccessible pore volume was believed to be no more than 5%, and all adsorption was assumed to be irreversible. Additionally, as just shown previously, the viscosity behavior due to mixing polymer concentrations was defined from the bulk rheology experiments. Because two of the three factors affecting the pressure build up were fairly well constrained, it was anticipated that determining a realistic value for the maximum adsorption would be straight forward. It was also expected that the selected value could accurately reflect the experimental results that were being calculated by Moradi (2011).

Adsorption values ranging from 5% to 30% of the injected moles were investigated to identify the adsorption behavior. An experimentally determined value of 1.3958 was used to account for the permeability reduction (Moradi 2011). Since the apparent viscosity data was not available for the 400 ppm polymer concentration, the viscosity of the polymer needed to be determined before the sensitivity study could be run.

Given that the .2 mL/min injection rate resulted in single phase flow conditions, the apparent viscosity could be estimated from the Darcy equation. Using the core dimensions, the steady-state pressure difference, and the polymer relative permeability, an apparent viscosity of 1.75 cp was computed. With the polymer viscosity determined, all of the necessary inputs were accounted for and the sensitivity could be preformed. The input values used for the maximum adsorption study and the associated simulation results are presented respectively in Table 4.12 and Figure 4.15.

Adsorption Study for Maximum Adsorption					
Percent Adsorbed	Polymer Concentration	Adsorption Associated with Concentration	Maximum Adsorption	Irreversible Adsorption	Fraction of Available Pore Space
5	4.97E-10	1E-10	4.51E-12	4.51E-12	1
10	4.97E-10	1E-10	9.02E-12	9.02E-12	1
15	4.97E-10	1E-10	1.35E-11	1.35E-11	1
20	4.97E-10	1E-10	1.80E-11	1.80E-11	1
25	4.97E-10	1E-10	2.25E-11	2.25E-11	1
30	4.97E-10	1E-10	2.71E-11	2.71E-11	1

Table 4.12: Input values for the two phase maximum adsorption study

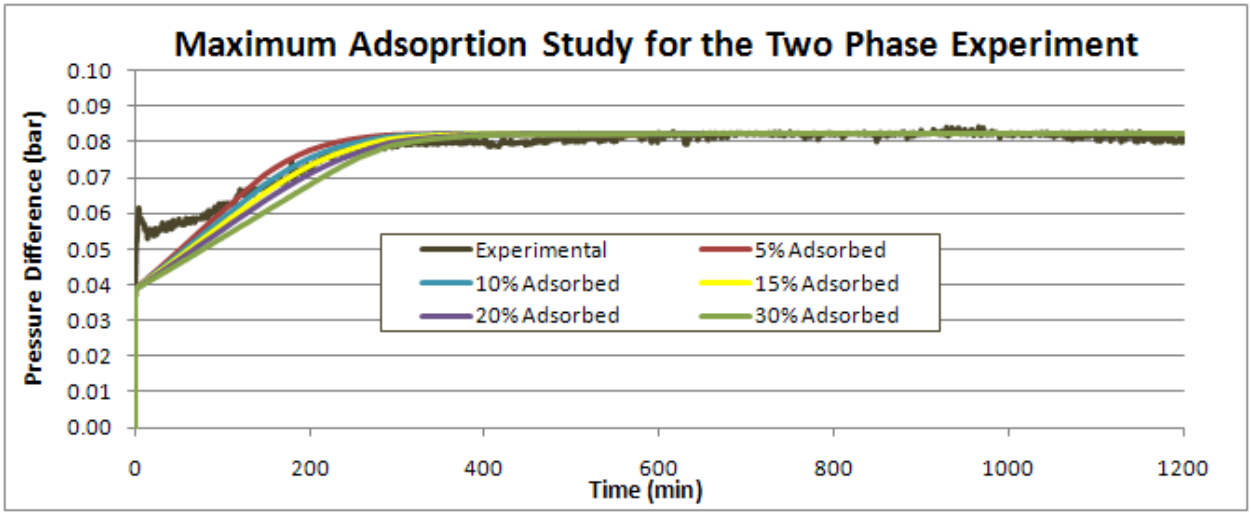

Figure 4.15: Differential pressures determined by the simulator for a range of maximum adsorption values for the two phase simulation - all adsorption parameters are in units of moles per pore volume

As can be seen, a maximum adsorption of 15% provided the best fit for the experimental results. Because the 15% case provided the best fit and seemed like a reasonable value, it was accepted as the maximum adsorption value for the simulation model.

Despite the multitude of efforts taken to achieve a better match via investigating the other simulation parameters, the experimental pressure data that was recorded before approximately 90 minutes could not be matched. Upon closer inspection it was noticed that the slope of the pressure build-up changes around 90 minutes. The nature of the experimental process, and the uncertainty associated with different pieces of equipment is such that it is not uncommon for sections of data to be neglected with reasonable cause. Since there was an unexpected change in the rate of the pressure build, and the pressure spike at the beginning of the data seemed incorrect, it was suspected that something went awry with the pumping system at the beginning of the polymer injection.

4.4.5 – PRESSURE MATCH FOR THE FIRST INJECTION RATE

As was the case with Simulation 1, creating a good match which used realistic values was considered a priority for the first polymer injection rate. Although there was some uncertainty surrounding the behavior of the initial data, the simulation results fit the experimental results quite well after 90 minutes. Since the inputs used in the simulation model were largely based on experimentally derived values or ranges of values, the simulation results were decidedly good enough to begin focusing on the other injection rates. The finalized simulation model for the first injection rate used a maximum adsorption of 15%, a water relative permeability curve that corresponded to the 30% curvature case, and an apparent viscosity value of 1.75 cp. By using these simulation-derived parameters along with the experimentally derived parameters, the pressure match displayed in Figure 4.16 was created.

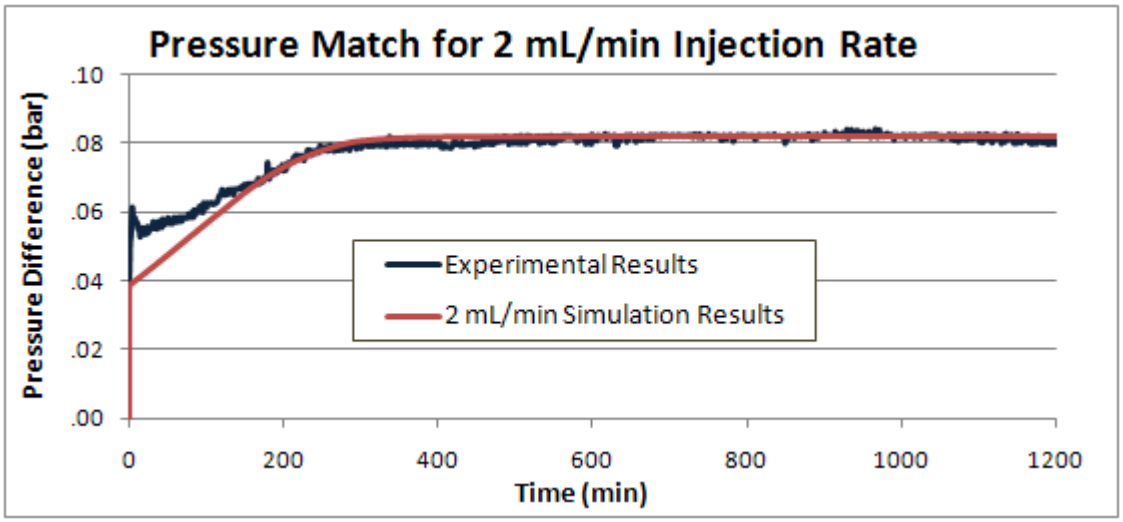

Table 4.16: Differential pressure match for the first injection rate in the two phase simulation

4.4.6 – POLYMER APPARENT VISCOSITY VALUES FOR VARIOUS SINGLE PHASE FLOW RATES

The three injection rates that followed the initial injection rate also resulted in single phase flow. Assuming that the adsorption behavior related to the initial injection rate was modeled correctly, the apparent viscosity of the polymer was the only unknown parameter for each of these flow rates. As before, the Darcy equation was applicable, as were the previously used core dimensions and permeability values. Using these parameters, the following apparent viscosity values were determined. The Darcy velocity is included in the table because the apparent viscosity is associated with the Darcy velocity rather than the injection rate in the simulator.

Injection Rate	Darcy Velocity	Apparent Viscosity
mL/min	cm/min	cp
0.2	0.01769	1.74054
0.4	0.03538	1.85325
0.8	0.07076	2.31107
1.6	0.14153	2.856

Table 4.13: Viscosity input data for the single phase flow rates

4.4.7 – INPUT DATA FOR TWO PHASE FLOW

Estimating the apparent viscosity is a straight forward procedure for single phase flow, but it becomes more complicated when two flowing phases are present. As the injection rate was increased from 1.6 mL/min to 3.2 mL/min, oil was produced along with the polymer indicating the presence of two phase flow. This meant that the Darcy-based method which was previously used to calculate the apparent viscosity would no longer work since there were too many unknowns. Instead, a basic understanding of how the apparent viscosity transitioned from one regime to another was used to create an estimate that was then refined by adjustments which were decided upon by multiple simulations.

The process to determine the apparent viscosity began by plotting the data from Table 4.13 as a function of the injection rate to see what the trend looked like. The graphical result from this is displayed below in Figure 4.17.

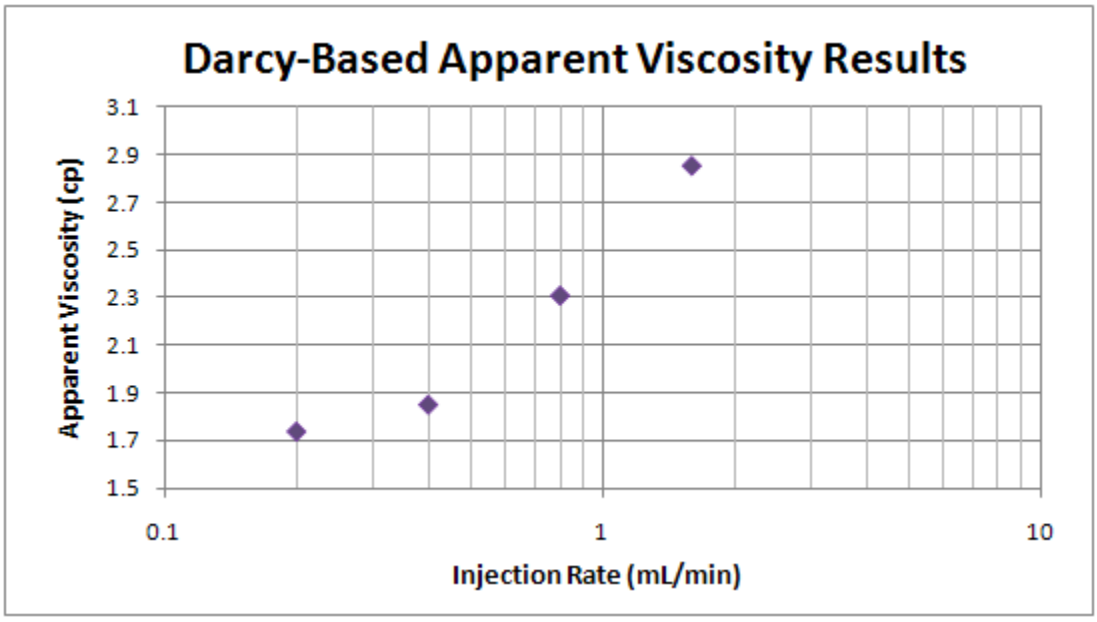

Figure 4.17: Darcy-based apparent viscosity values for the single phase flow rates of the two phase experiment

By presenting the viscosity data on a semi-log plot, as was done here, it becomes apparent that the three largest rates fall in the shear thickening regime.

The maximum achievable apparent viscosity was unknown, so it was not immediately obvious whether the 3.2 mL/min rate was in the shear thickening or the degradation regime. To determine this required running some scenarios in the simulator for representative values and observing the results. It was suspected that the injection rate of 3.2 mL/min would continue to reflect shear thickening behavior. Either way, the range of expected behavior was narrowed by understanding the realm of possible behavior based on the flow regimes.

Since a continuation of the shear thickening regime seemed most probable, a polynomial trend line was fit through the data and used to extrapolate the apparent viscosity for the rate of 3.2 mL/min. The graphical result of this process can be seen in Figure 4.18. The orange line represents the apparent viscosity model that was created for use in the simulator, and the purple points represent the apparent viscosity values that were calculated for the first four injection rates.

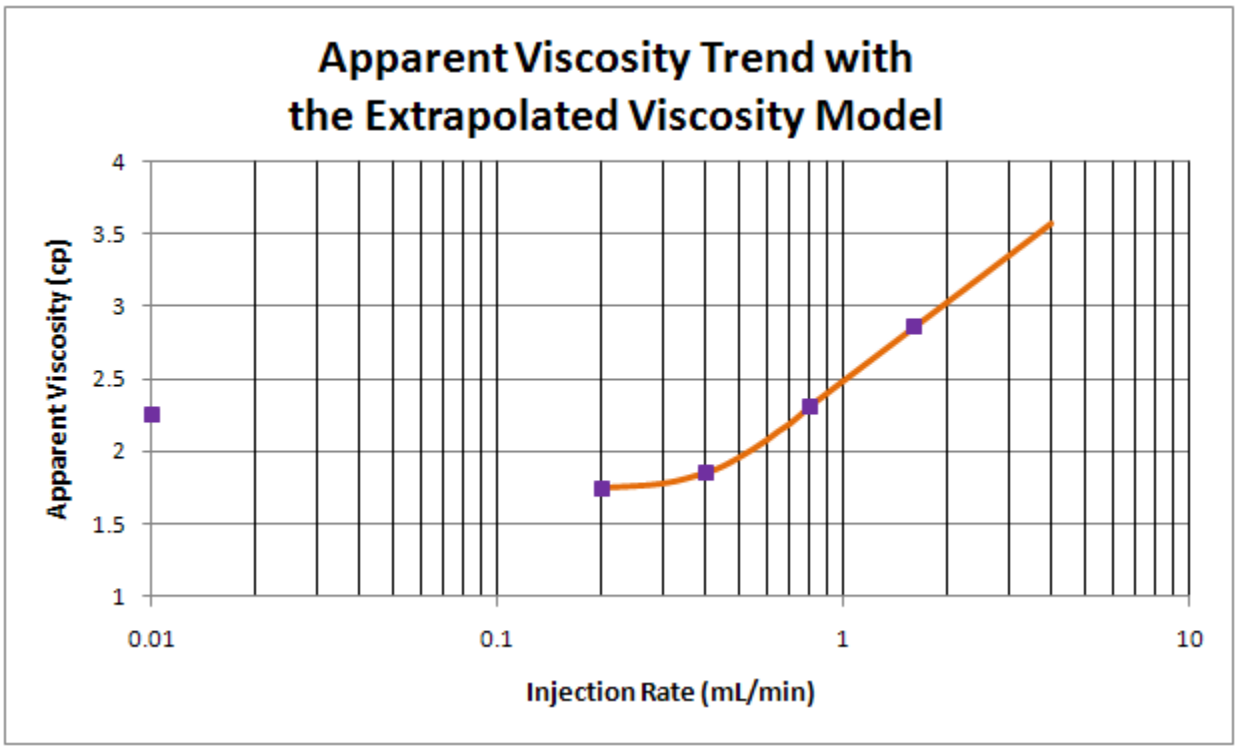

Figure 4.18: The Darcy-based apparent viscosity values and the extrapolated apparent viscosity model for the two phase experiment

Although it was not technically part of the experiment, the injection pump was left running over a weekend at a rate of .01 mL/min. This meant there was also data available to calculate the apparent viscosity associated with the .01 mL/min rate. The additional data from this rate has been added to Figure 4.18, because it provides insight about the location of the shear thinning regime.

It is not possible to discern from this single point as whether the .01 mL/min rate is in the lower-Newtonian or the shear-thinning flow regime, nor is it possible to pin-point exactly where these regimes start and stop. It is quite apparent though that the polymer is most probably in the shear thinning regime between the .01 and .2 mL/min injection rates.

With a realistic viscosity model developed, the only other parameter that needed to be addressed was the oil relative permeability curve. As previously mentioned, the behavior of this data was not considered important for the first few injection rates since they did not result in oil production. The oil production that occurred with the injection rate of 3.2 mL/min resulted in the water phase occupying additional pore space, and a small adjustment needed to be made so the water permeability curve accounted for the new incremental water saturation. This was accomplished by applying the saturation dependent polynomial equation that was developed for the first four rates to the new water saturations.

The same procedure which was used to create the water relative permeability curve was followed to create the oil relative permeability curve. As before, the initial curve was approximated by a straight line fit through the end-point data. The shape of the data was then manipulated by multiplying factors which varied from 10% to 40%. In this process, the oil relative permeability associated with the mid-point saturation, which controlled the curvature of each case, was calculated by multiplying the maximum possible oil relative permeability by these percentages. The values that were created from this procedure are presented in Table 4.14 and plotted in Figure 4.19.

Oil Relative Permeability Investigation						
Water Saturations	Relative Permeability Cases					
Sw	10%	20%	25%	30%	35%	40%
0.2282	0.70533	0.70533	0.70533	0.70533	0.70533	0.70533
0.4185	0.070533	0.141066	0.1763325	0.211599	0.2468655	0.282132
0.6195	0	0	0	0	0	0

Table 4.14: Oil relative permeability input data for varying cases of curvature

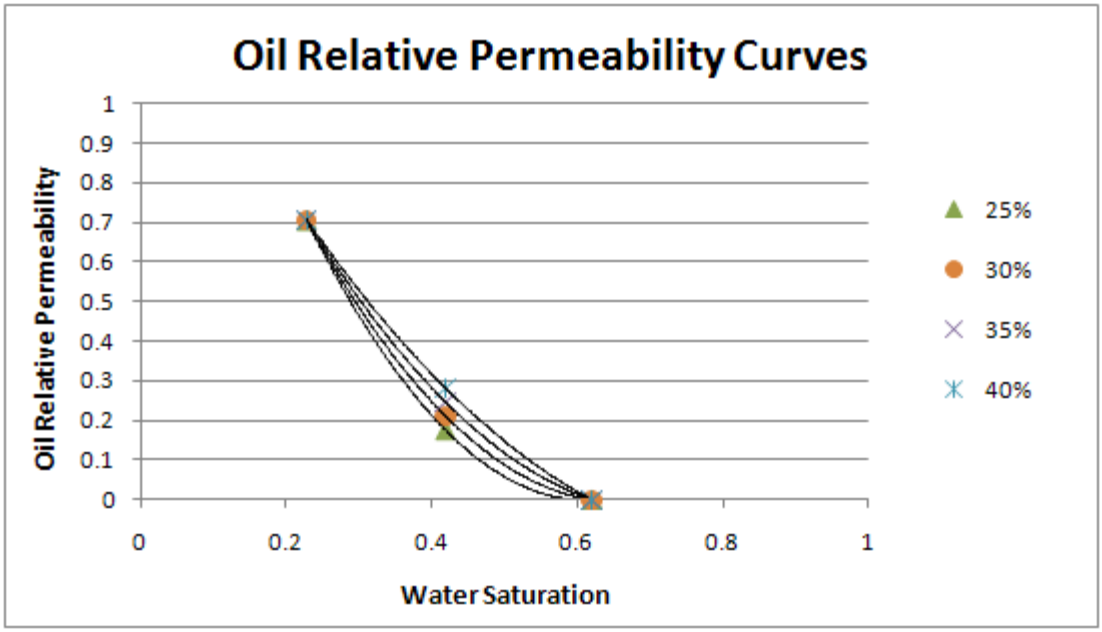

Figure 4.19: Multiple relative permeability scenarios developed by fitting a curve through the oil relative permeability end-points

Again, the 30% case was selected to be used in the simulator. Again, the 10% and 20% cases are not presented in the graph since they resulted in unrealistic negative values. Because the relative permeability curves for the first four injection rates differed from the relative permeability curve for the last injection rate that was simulated, a restart file was used. Other

than the adjustments to the injection rate, the relative permeability behavior was the only difference between the two files.

Ultimately, the data that was input in the simulator for both the oil and water relative permeability values used the 30% cases. The calculated curves were based on the end-point values from the 3.2 mL/min injection rate. These curves were then adjusted for use with the single phase flow injection rates by setting the end-points to properly reflect the experimental data. The water saturations and associated relative permeability values for each of the files are presented below in Table 4.15 and Table 4.16. The values used to model the two phase flow situation are also presented in graphical form in Figure 4.20.

Water Saturation, Sw (-)	Water Relative Permeability, krw (-)	Oil Relative Permeability, kro (-)
0.2282	0	0.705329944
0.25	0.00110625	0.634297
0.3	0.005801	0.48552232
0.35	0.01338025	0.35644808
0.4	0.023844	0.24707428
0.45	0.03719225	0.15740092
0.5	0.053425	0.087428
0.55	0.07254225	0.03715552
0.6	0.094544	0.00658348
0.6008	0.0949702	0

Table 4.15: Finalized relative permeability and saturation values for the single phase rates

Water Saturation, Sw (-)	Water Relative Permeability, krw (-)	Oil Relative Permeability, kro (-)
0.2282	0	0.705329944
0.25	0.00110625	0.634297
0.3	0.005801	0.48552232
0.35	0.01338025	0.35644808
0.4	0.023844	0.24707428
0.45	0.03719225	0.15740092
0.5	0.053425	0.087428
0.55	0.07254225	0.03715552
0.6	0.094544	0.00658348
0.6008	0.0949702	0.006254453
0.610575	0.099566921	0.002641438
0.6195	0.102	0

Table 4.16: Finalized relative permeability and saturation values for the two phase rate

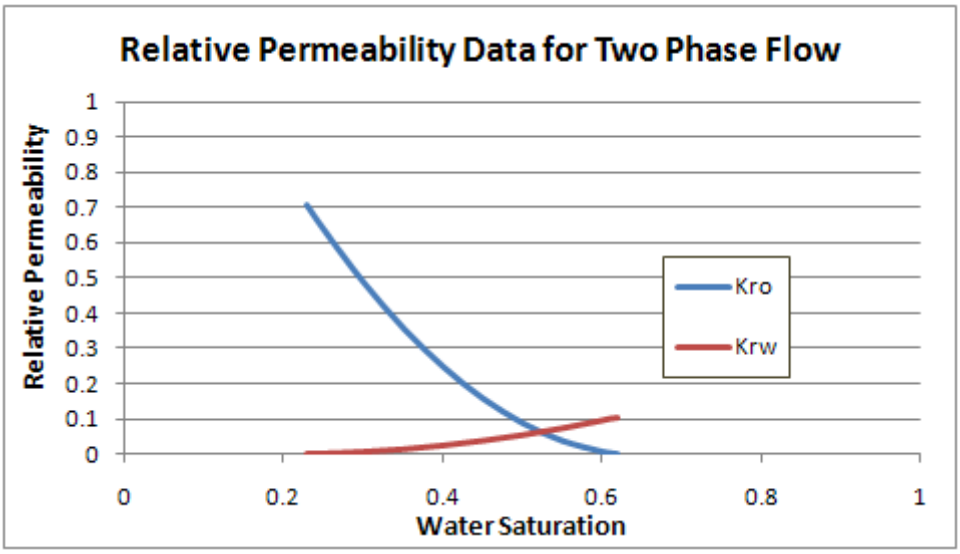

Figure 4.20: The relative permeability model for the oil and water phases

With the relative permeability behavior modeled, all of the required input parameters were accounted for and the simulation model was ready to be run and evaluated.

4.4.8 – SIMULATION RESULTS FOR THE TWO PHASE FLOW EXPERIMENT

As mentioned in Section 3.3.3, experimental results were available for both cumulative oil production and the pressure difference in the core. The oil production rate was not known since the measurement was made by observation and the oil production was too small to determine a rate. The pressure differentials which resulted from the simulator by using the previously discussed inputs for the five injection rates are displayed in Figure 4.21. As can be seen in the figure, a very good pressure match was obtained by using the input parameters that were created.

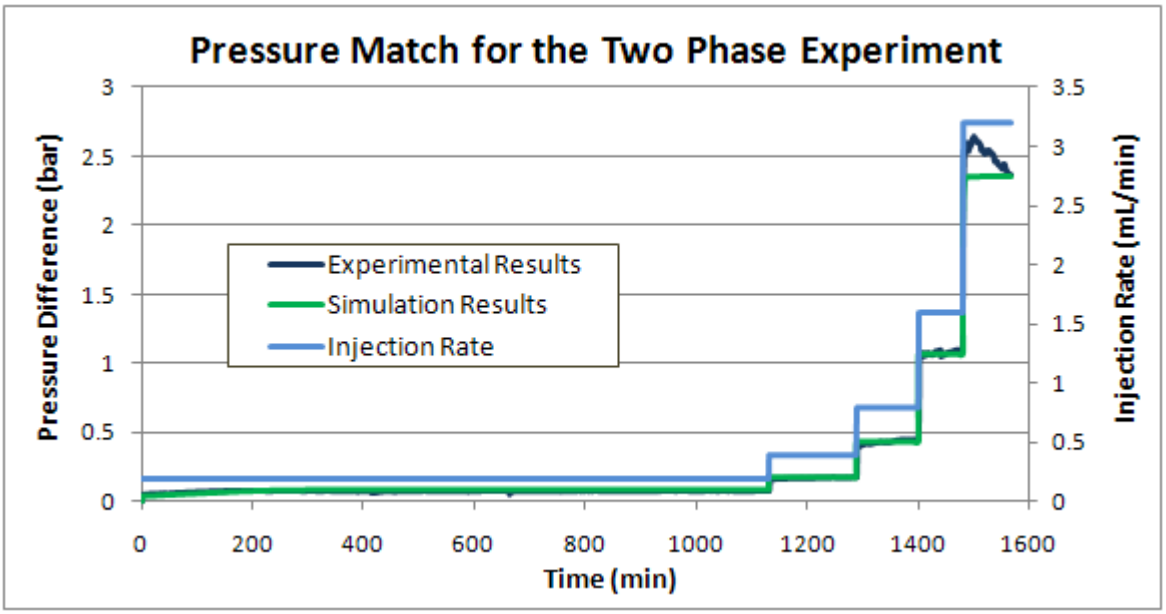

Figure 4.21: Injection rates and pressure results for all of the injection rates that were modeled for the two phase simulation

There was some uncertainty regarding the pressure match for the final injection rate. The declining behavior of the data suggests that a steady-state pressure difference had not been achieved, or if it had, it was only maintained for a short period of time before the next injection rate began. The pressure spike that is displayed is similar to pressure spikes seen in the experimental data for Simulation 1. Since the apparent viscosity associated with the final injection rate was unknown and was treated as a tuning parameter, an assumption about the stabilized pressure had to be made. From the behavior which is displayed, it was decided that a reasonable stabilized pressure could reflect the lowest pressure difference associated with the 3.2 mL/min rate, or a value slightly lower than the lowest pressure. Regardless of which scenario was used, the apparent viscosity required to achieve the pressure difference would align with the shear thickening regime. A plot of the first three injection rates and a plot of the last two injection rates have been displayed in Figure 4.22 and Figure 4.23, respectively, to provide a more detailed view of the results.

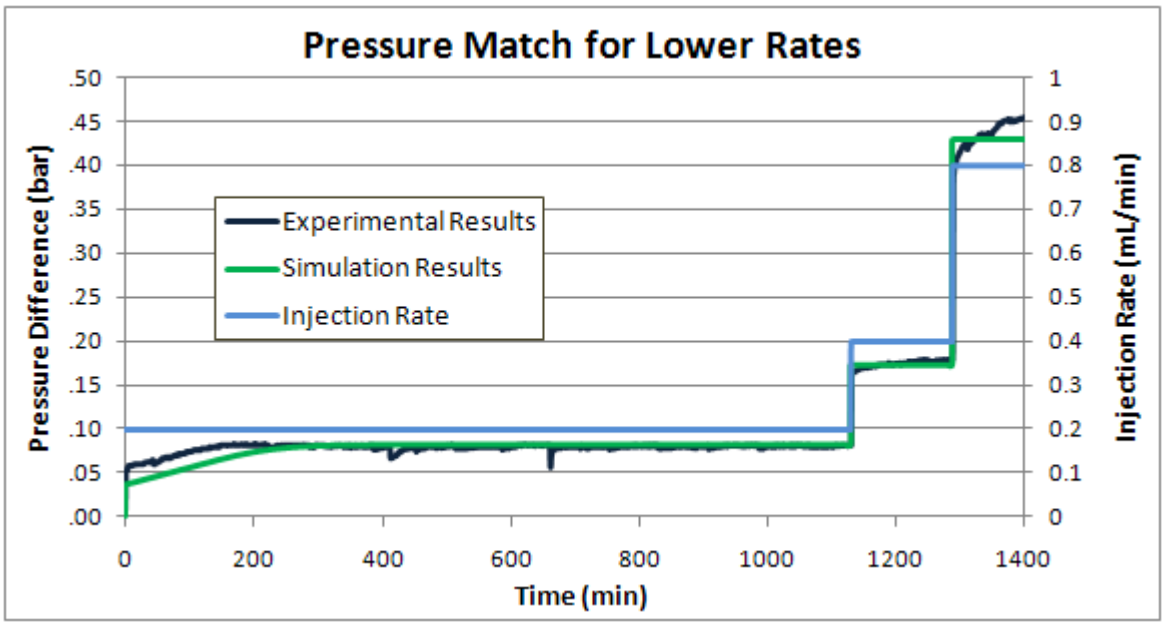

Figure 4.22: Injection rates and pressure results for the lower injection rates that were modeled for the two phase simulation

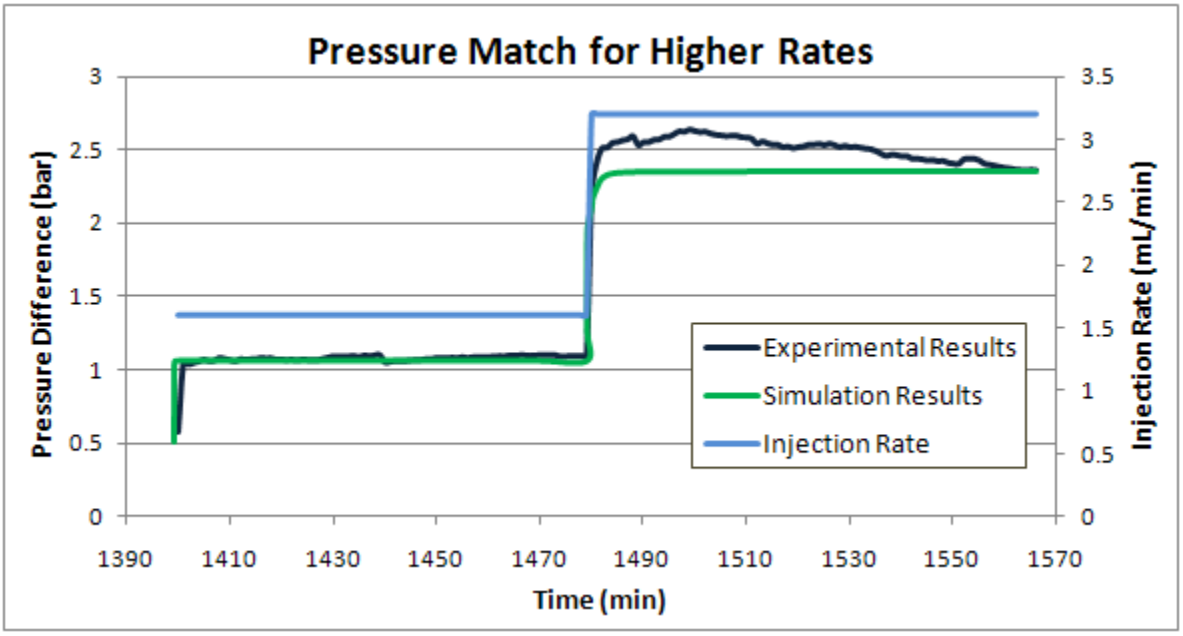

Figure 4.23: Injection rates and pressure results for the higher injection rates that were modeled for the two phase simulation

The simulation resulted in a cumulative oil production of 1.087 mL which was found to closely match the experimental value of 1.1 mL. The error between these two values was only 1.12%, so the cumulative production was considered to be well matched. As can be seen in the graphical results in Figure 2.24, the oil production begins immediately after the injection rate is increased from 1.6 mL/min to 3.2 mL/min. Once the oil production starts, it appears to occur

quite rapidly in a manner that would result from piston-like displacement. Figure 4.25 gives a more detailed view of the cumulative oil production along with the oil production rate.

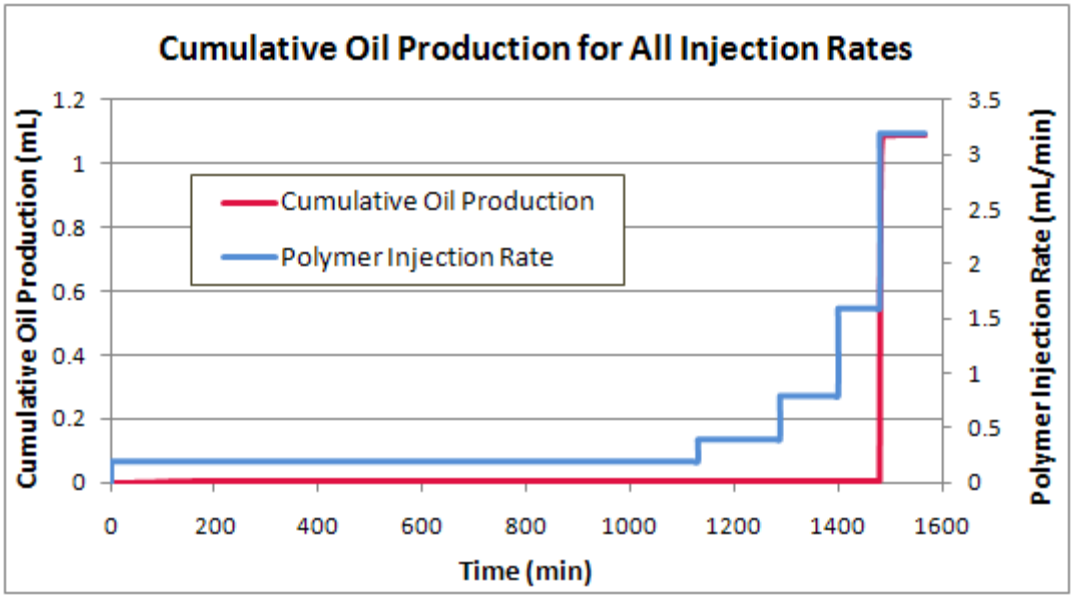

Figure 4.24: Simulated cumulative oil production for the injection rates up to 3.2 mL/min

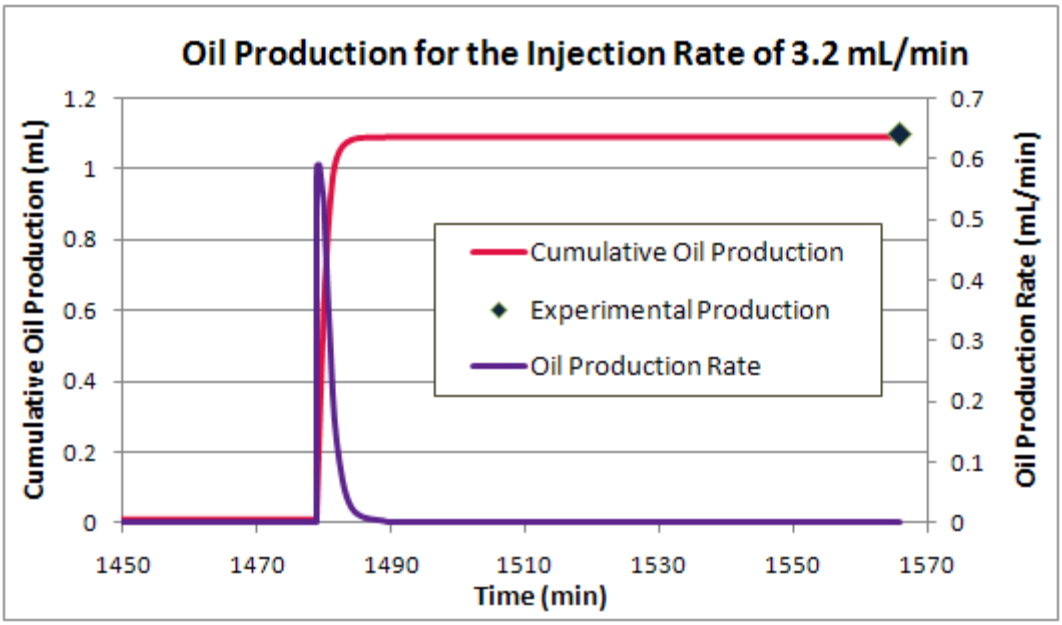

Figure 4.25: A zoomed-in view of the cumulative oil production and oil production rate with the experimental production plotted for comparison

CHAPTER 5 - DISCUSSION

5.1 – SINGLE-PHASE POLYMER FLOOD

From the presented results, it appears that the CMG STARS simulator is capable of modeling the pressure behavior associated with a high molecular weight polymer flood operated under a broad range of injection rates. By manipulating some of the more flexible parameters with in a realistic range, the experimental pressure results for multiple injection rates were well-matched pressure using Simulation 1. Although the initial pressure spikes exhibited in the experimental data were not matched by the simulator, the agreement between the experimental and simulated results were still very good. As previously mentioned, the pressure spikes were probably due to polymer alignment or polymer degradation at the front of the core, and it was not anticipated that the simulator would be able to model this behavior. Two points of interest were identified while working with Simulation 1, the first of which had to do with the pressure instabilities that occurred at the higher injection rates. All of the methods typically used to dampen the fluctuations were used but were not successful for injection rates above 7.5 mL/min.

For the purpose of simulating a field-scale polymer injection process, the pressure instabilities associated with high flow rates probably would not be an issue. The high rates which were tested in the laboratory experiment are typically studied to see the range of a polymers behavior, but are rarely implemented in the field. While that is good news with respect to the field application, it is less than preferable for modeling high rates in the lab.

This leads into point number two which has to do with variation in the RRF value as a function of injection rate. As previously described, the RRF value was used as a tuning parameter to match the steady-state pressure differences of the individual flow rates. Simulating the larger flow rates resulted in pressure fluctuations, so it was not possible to determine an RRF value for these flow rates. The behavior of the RRF values as a function of flow rate displayed a trend very similar to that of the apparent viscosity and RF values. Whether or not there is any physical reason to believe that the RRF values actually follow this sort of trend is something that requires further investigation.

The apparent viscosity values that were used in the previously presented simulation model were calculated by assuming a constant RRF value of 3.6. Aside from being used to determine the apparent viscosity, the RRF value was also accounted for in the adsorption parameters. When history matching the pressure differences, the RRF value associated with the adsorption parameters was changed while the one used to calculate the apparent viscosity was held constant. Since the steady-state pressure drop is affected by all of the parameters included in

the Darcy equation, the RRF adjustments could be making up for any minor errors associated with the other parameters.

Alternatively, the trend of the manipulated RRF values could have a physical basis since it has been suggested that the RRF could vary with flow rate (Chauveteau et al. 2002). Either way, results from a singular simulation cannot definitively prove this behavior, so this could be a subject of future investigations.

The plot displayed in Figure 5.1, shows the resulting pressure match for the situation where the RRF was held at a constant value of 3.6 instead of being treated as a tuning parameter. Since plotting all of the injection rates on a single plot makes it hard to see the discrepancies in the data, only the increasing injection rates are shown.

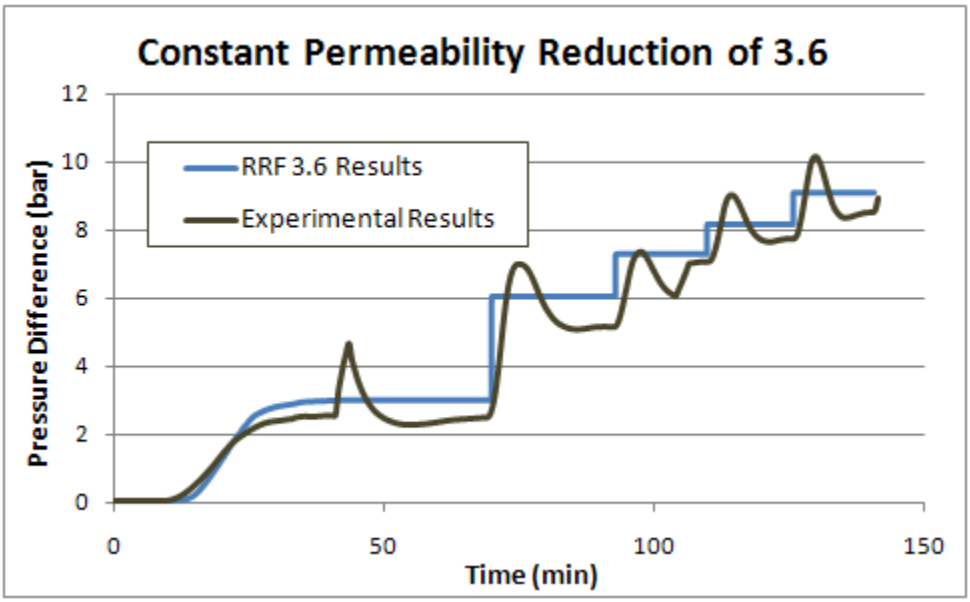

Figure 5.1: Simulated differential pressure results with a constant RRF of 3.6

As can be seen, by holding the RRF at a constant value of 3.6, the steady-state pressure difference is consistently overestimated.

5.2 – TWO-PHASE POLYMER FLOOD

By using experimentally derived input values and realistic ranges of input values for the parameters which were uncertain, a simulation model that matched both pressure and cumulative production data was created. The shape of the relative permeability curves, and the apparent viscosity associated with the different injection rates were among the parameters that carried some uncertainty. Since there was not any data available to model the rate at which the oil was produced, the importance of tuning the relative permeability curves had less to do with manipulating the finer details of the curves to ensure an oil rate was matched and

more to do with ensuring that the cumulative oil production was correct for a given flow rate. Additionally, the state of the fluid saturations in both the simulator and the experiments could be accounted for by a fairly narrow range of values on the relative permeability curves, so those were the primary focus of manipulation rather than the whole curve. Once the relative permeability values were correct for the range of interest, the remainder of the curve was structured to incorporate the range of interest in a seamless manner.

The apparent viscosity table that is used for modeling the polymer viscosity behavior plays a significant role in determining the steady-state pressure difference. Since values were not directly available to model this behavior, the apparent viscosity values were determined from the Darcy equation and an extrapolation method. The values that were used in the model were ultimately selected because they created simulation results that were well matched with the experimental results. This is especially true for the apparent viscosity associated with the last injection rate which was chosen based on a combination of trend-line extrapolation and "guess-and-check," style simulation trials.

From the experimental work conducted by Stavland et al. (2010), there happened to be apparent viscosity data available for the same polymer type that was used in the two phase injection model but at a concentration of 600 ppm instead of 400 ppm. It was decided that an observational comparison of the apparent viscosity values associated with each of the polymer concentrations could provide more insight about the accuracy of the apparent viscosity values created for the 400 ppm polymer. Figure 5.2 displays the apparent viscosity values of the two polymer concentrations as a function of shear rate. In both cases, the conversion between the flow rate and the shear rate was calculated using the absolute permeability.

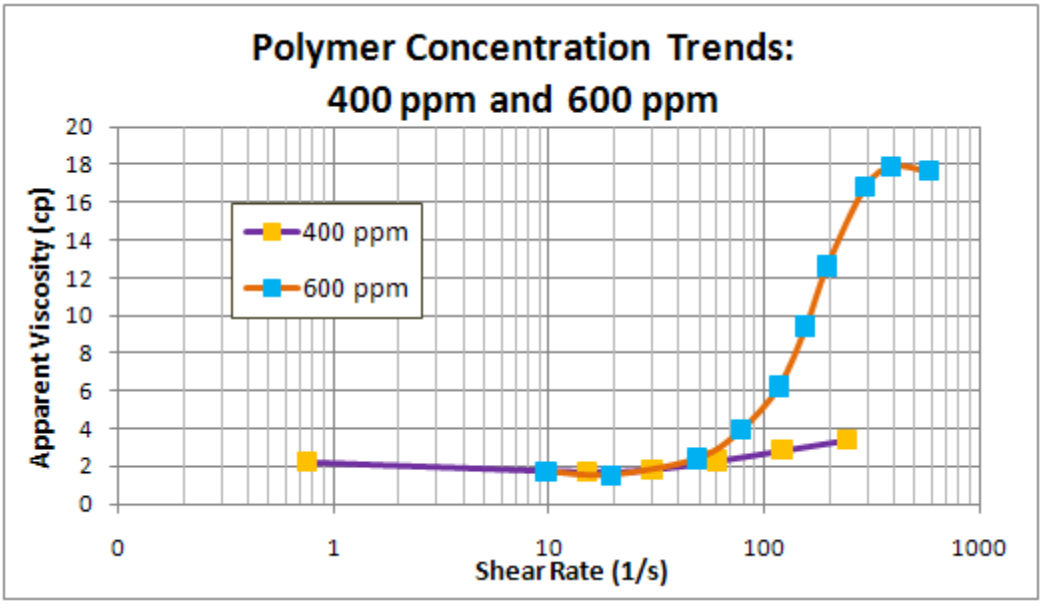

Figure 5.2: Flow regime related transitions and trends in apparent viscosity values for a 400 ppm and a 600 ppm polymer

From the graph it can be seen that while the apparent viscosity for the 600 ppm polymer appears to reach a larger value, the 400 ppm polymer has not yet achieved its maximum viscosity value for the given range of shear rates. It also appears that the 400 ppm polymer transitions to the shear thickening regime for values of shear rate which the 600 ppm polymer is exhibiting shear thinning behavior. This situation seems unrealistic since it is generally expected that, for a given polymer type, the solutions with higher concentrations will not only achieve larger apparent viscosity values but they will also go through the sequence of flow regimes at lower shear rates than the lower concentrations will (Heemskerk et al. 1984). The apparent viscosity behavior displayed in Figure 5.3 for concentrations of 1500 and 600 ppm graphically exemplifies this statement. Again, the polymer type is the same for both solutions, but the concentrations are different.

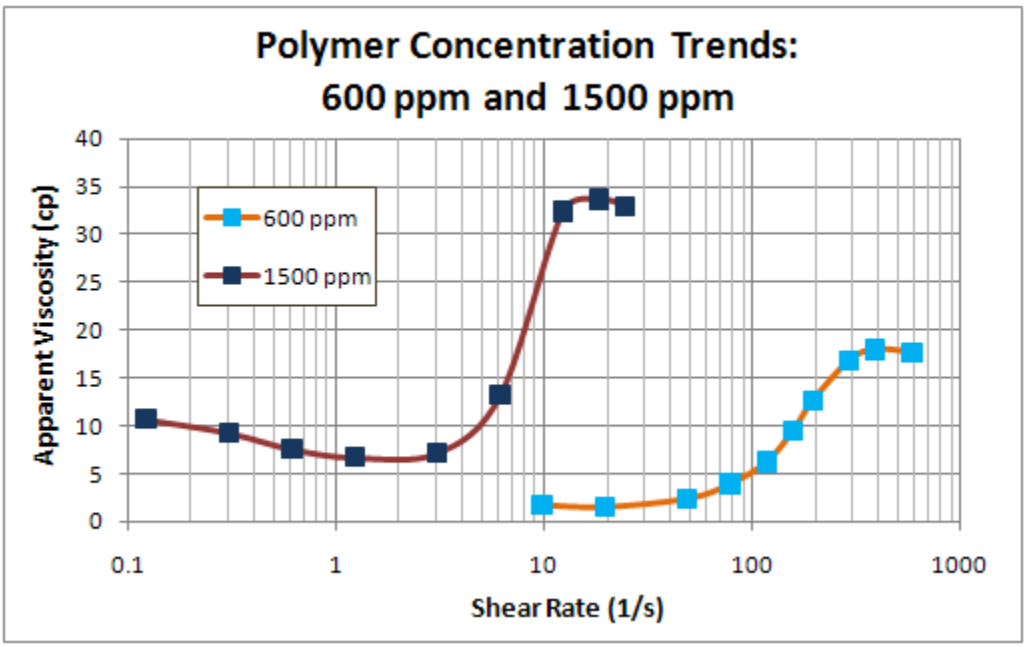

Figure 5.3: Flow regime related transitions and trends in apparent viscosity values for a 600 ppm and a 1500 ppm polymer

Another similarity between these two polymers is that both were injected into 100% water saturated cores. The 400 ppm polymer solution was injected into a core which contained residual oil saturation with the remaining saturation being taken up by water. In addition to the permeability effects due to polymer adsorption, which all of the core flood experienced after polymer injection had taken place, the 400 ppm polymer had another factor affecting the permeability. Before the 400 ppm polymer was injected into the core, it had already been affected by residual oil. In turn, the core had already had developed a permeability scenario that deviated from the absolute permeability before the polymer was injected.

Since the polymer cannot flow in the space occupied by the residual oil, it was decided to adjust the shear rate according to the relative permeability effect from the residual oil. The relative permeability value that was used did not take into account the polymer adsorption effects, so it was believed that using this relative permeability for the case with residual oil saturation would be analogous to using the absolute permeability for the 100% water saturated scenarios.

Figure 5.4 displays the results that were acquired from using this relative permeability to adjust the shear rate of the 400 ppm polymer.

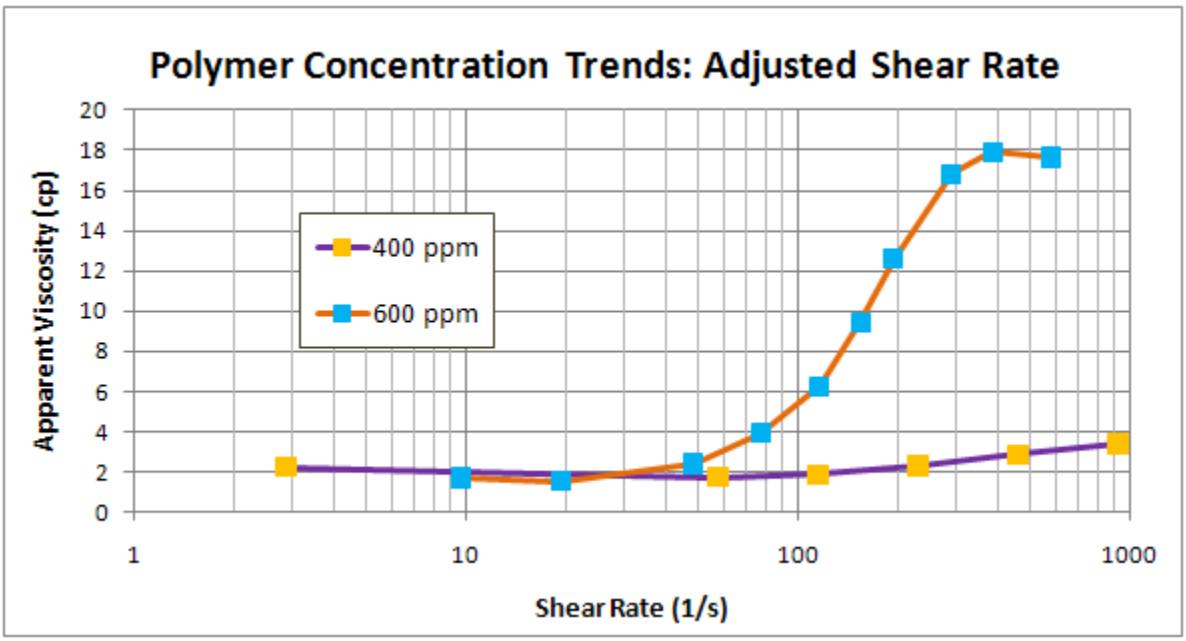

Figure 5.4: "Properly aligned" flow regime transitions and trends for a 400 ppm and a 600 ppm polymer

The locations and development of the flow regimes for the 400 ppm and 600 ppm polymer concentrations presented in this graph reflect the expected behavior much more closely than the previous graph. This could indicate that for the purpose of correlating shear rate values with flow rate values, when residual oil is present, the permeability effects associated with the oil will need to be accounted for. Since this assessment is based on a data set consisting of only one experiment, more investigations will be required before any concrete statements can be made.

Another factor that is at play in this situation is the fact that the 600 ppm flood was conducted in a Berea sandstone core while the 400 ppm flood was conducted in a Bentheim sandstone core. An alpha value of 2.5 was used in the shear rate conversion for the Berea sandstone core. Whether or not there was any physical basis to do so, this same alpha value was also used for the Bentheim sandstone core. If an alpha value of 2.5 is physically inaccurate for the Bentheim sandstone core, then this will also affect the flow rate to shear rate conversion. While it was considered important to mention this point for the sake of completeness, no further work was done with regards to the alpha factor.

CHAPTER 6 – SUMMARY, CONCLUSIONS AND RECCOMMENDATIONS

6.1 – SINGLE-PHASE SIMULATION MODELING

By utilizing the polymer-related simulation capabilities which are currently available in the simulation software, CMG STARS, two sets of experimental data have been modeled and matched using physically realistic input parameters. The first experiment consisted of a single phase polymer injection with injection rates varying from .02 mL/min to 20 mL/min. Within this range of injection rates, the polymer fluid exhibited at least shear thinning, shear thickening, and degradation behavior. Experimental data was used to create a table of velocity and associated viscosity values which accurately described the polymers behavior. Although adsorption data was not available, a sensitivity study preformed for a reasonable range of values was found to be a successful tool for identifying the related adsorption behavior. This study was also useful for gaining a better understanding of how the adsorption model embedded in the simulator could be used to model polymer floods in the core scale (and potentially the field scale). For this portion of the work, the experimental pressure differential in the second core was the available data which was to be matched.

Of the available injection rates, the largest rate successfully modeled was the 7.5 mL/min rate which corresponded to the degradation regime. Other injection rates which exhibited degradation behavior and were also successfully modeled include the 4 mL/min, 5 mL/min, and 6 mL/min rates. It was of particular interest to model the degradation regime, since previously only up to the shear thickening regime had been successfully simulated. Injection rates larger than 7.5 mL/min were not successfully modeled because of the large pressure fluctuations that were produced in the simulator despite attempts to dampen them. It is important to note that the shear thickening and degradation behaviors occur at very high flow rates which rarely if ever occur in the reservoir (Seright 2010). Instead, these high rates, and their associated flow regimes are most likely to be encountered in the near wellbore area, especially in the vicinity of the injection well. All of the injection rates below 5 mL/min were simulated without any problems.

By using the permeability reduction (RRF) value as a tuning parameter, a well matched pressure fit was created. When plotted against flow rate, the permeability reduction values used to match the simulated and experimental pressures created a trend very similar to the one displayed by the apparent viscosity and the mobility reduction. Whether this trend actually reflects a physical characteristic of the permeability reduction is something that can be investigated in further studies.

6.2 – TWO-PHASE SIMULATION MODELING

The two phase experiments consisted of injecting a polymer solution into a single core with residual oil saturation. As the injection rates increased above 3.2 mL/min, some of the oil that was previously considered residual oil was produced which resulted in a decrease in the residual oil saturation and an increase in the water phase saturation. The two phase experiment was conducted for injection rates ranging from .2 mL/min to 18 mL/min. For this work only the rates ranging from .2 mL/min to 3.2 mL/min were simulated. The rate at which two phase flow occurred was of particular interest for this work. Of the rates studied, the 3.2 mL/min injection rate produced 1.1 mL of oil while the lower rates resulted in single phase flow.

Since the availability of experimentally derived adsorption values which could be directly applied to the simulation model was sparse, a sensitivity study was conducted to determine the adsorption behavior. As with the single phase simulation model, conducting a sensitivity study proved to be a successful method for identifying realistic adsorption behavior. Relative permeability curves were constructed based on experimentally derived end-point data. The apparent viscosity behavior was not as defined as it had been for the single phase model. To remedy this, the Darcy equation was implemented for the injection rates that resulted in single phase flow. The apparent viscosity for the injection rate associated with two phase flow was extrapolated by fitting a line through the previously calculated values. It was assumed that the behavior of the unknown apparent viscosity was a continuation of the shear thickening regime, so the options for the extrapolated value were constrained to reflect this assumption. A single experimentally-determined RRF value was used for all of the injection rates which were studied. From the bulk rheology data, an understanding of the frontal mixing behavior was developed and implemented in the simulator. After making minor adjustments to the curvature of the relative permeability behavior as well as minor adjustments to the apparent viscosity associated with the injection rate of 3.2 mL/min, a simulation model was created which matched both the experimental pressure differential and the cumulative oil production of 1.1 mL.

Experimentally derived apparent viscosity results were available for a 600 ppm polymer solution which utilized the same polymer as the one that was simulated. Because the apparent viscosity values that were used in the simulation were developed by the Darcy equation and an educated extrapolation, it was of interest to compare these values with other related data to see if they corroborated.

It was possible to confirm that the apparent viscosity behavior which was developed for the simulation model was realistic by comparing it with the 600 ppm data. While preparing the two data sets for comparison, an observation was made regarding the velocity to shear rate conversion for the two phase data. A misalignment of the 400 ppm flow regimes relative to the

600 ppm flow regimes called to question whether using the absolute permeability value was appropriate for the two phase case. After recalculating the shear rate using the relative permeability value that accounted for the presence of residual saturations, the flow regimes aligned in the expected manner. Whether or not it is physically correct to replace the absolute permeability with the relative permeability in this manner is a topic which can be investigated in further studies.

NOMENCLATURE

μ_U	=	Upper Newtonian Viscosity, cp
μ_L	=	Lower Newtonian Viscosity, cp
μ	=	Viscosity, cp
$\dot{\gamma}$	=	Shear Rate, 1/s
n	=	Shear Thinning Exponent, dimensionless
τ_r	=	Shear Rate at the Lower Newtonian-Shear Thinning Boundary, 1/s
n	=	Shear Thinning Exponent
$\mathcal{E}$	=	Stretch Rate, s
v	=	Interstitial Velocity, m/s
d_p	=	Average Grain Diameter, m
k	=	Permeability, mD
ϕ	=	Porosity, fraction
τ	=	Formation Tortuosity
N_{De}	=	Deborah Number, dimensionless
λ_1	=	Relaxation Time, s
μ_{el}	=	Elongation Viscosity, cp
μ_{max}	=	Maximum Viscosity, cp
μ_2	=	Shear Thickening Viscosity, cp
m	=	Elongation Exponent, dimensionless
λ_2	=	Critical Shear Rate for Shear Thickening, s
μ_3	=	Newtonian Viscosity of the Effluent, cp
μ_0	=	Viscosity at Zero Shear Rate, cp
λ_3	=	Critical Shear Rate for Degradation, s
k	=	Shear Thinning Exponent for Degradation Model
x	=	Tuning Parameter for the Degradation Model

$[\eta_0]$	=	Polymer Intrinsic Viscosity, cp
M_w	=	Molecular Weight, Dalton
R_g	=	Gyration Radius, m
Φ'	=	Universal Constant Equal to 4.2×10^{24}
A	=	Cross Sectional Area, m^2
r	=	Pore Radius, m
d	=	Thickness Close to the Wall (Associated with Polymer Thickness), m
IPV	=	Inaccessible Pore Volume
B	=	Constant that Controls the Apparent Viscosity at Low Shear Rates
RF	=	Mobility Reduction
RRF	=	Permeability Reduction
$\mu_{app,exp}$	=	Experimentally Determined Apparent Viscosity, cp
α	=	Tuning Parameter Associated with the Rock Particles
$\mu_{apparent}$	=	Apparent Viscosity Determined from the Model by Stavland et al. 2010, cp
μ_w	=	Water Viscosity, cp
μ_{app0}	=	Apparent Viscosity at Zero Shear Rate, cp
j	=	Tuning Parameter

REFERENCES

1.) Chauveteau, G., Denys, K. and Zaitoun, A. 2002. New Insight on Polymer Adsorption Under High Flow Rates. Paper SPE 75183, presented at the SPE/DOE Improved Oil Recovery Symposium, Tulsa, Oklahoma, U.S.A., 13-17 April. DOI: 10.2118/75183-MS.

2.) Delshad, M., Kim, D. H., Magbagbeola, O. A., Huh, C., Pope, G. A. and Tarahhom, F. 2008. Mechanistic Interpretation and Utilization of Viscoelastic Behavior of Polymer Solutions for Improved Polymer-Flood Efficiency. Paper SPE 113620, presented at the SPE/DOE Improved Oil Recovery Symposium held in Tulsa, Oklahoma, U.S.A., 19-23 April. DOI: 10.2118/113620-MS.

3.) Green, D. W. and Willhite, G. P. 1998. *Enhanced Oil Recovery.* Henry L. Doherty Memorial Fund of AIME, Society of Petroleum Engineers.

4.) Heemskerk, J., Janssen-van Rosmalen, R., Holtslag, R. J. and Teeuw, D. 1984. Quantification of Viscoelastic Effects of Polyacrylamide Solutions. Paper SPE/DOE 12652, presented at the SPE/DOE Symposium on Enhanced Oil Recovery, Tulsa, Oklahoma, 15-18 April. DOI: 10.2118/12652-MS.

5.) Hirasaki, G. J. and Pope, G. A. 1974. Analysis of Factors Influencing Mobility and Adsorption in the Flow of Polymer Solution through Porous Media. SPE Journal, 337-346, Aug. 1974. DOI: 10.2118/4026-PA.

6.) Moradi, H. 2011. Experimental Investigation of Polymer Flow through Water- and Oil-Wet Porous Media, Thesis, University of Stavanger.

7.) Maerker, J. M. 1975. Shear Degradation of Partially Hydrolyzed Polyacrylamide Solutions. *SPE Journal*, 311-322, Aug. 1975. DOI: 10.2118/5101-PA.

8.) Maerker, J. M. 1976. Mechanical Degradation of Partially Hydrolyzed Polyacrylamide Solutions in Unconsolidated Porous Media. *SPE Journal*, 172-174, Aug 1976. DOI: 10.2118/5672.

9.) Masuda, Y., Tang, K., Miyazawa, M. and Tanaka, S. 1992. 1D Simulation of Polymer Flooding Including the Viscoelastic Effect of Polymer Solution, *SPE Reservoir Engineer*, 247-252, May 1992. DOI: 10.2118/19499-PA.

10.) Morris, C. W. 1978. Mechanical Degradation of Polyacrylamide Solutions in Porous Media. Paper SPE 7064, presented at the SPE Symposium on Improved Methods of Oil Recovery, Tulsa, Oklahoma, U.S.A., 16-17 April 1978. DOI: 10.2118/7064-MS.

11.) Seright, R. S. 1983. The Effects of Mechanical Degradation and Viscoelastic Behavior on Injectivity of Polyacrylamide Solutions. *SPE Journal*, 475-485, June 1983. DOI: 10.2118/9297-PA.

12.) Seright, R. S., Fan, T., Wavrik, K., Balaban, R. 2010. New Insights into Polymer Rheology in Porous Media. Paper SPE 129200, presented at the 2010 SPE Improved Oil Recovery Symposium, Tulsa, Oklahoma, U.S.A, 24-28 April 2010. DOI: 10.2118/129200-MS.

13.) Sorbie, K. S. 1991. *Polymer-Improved Oil Recovery.* Glasgow, Scotland: Blackie and Sons Ltd.

14.) Southwick, J. G. and Manke, C. W. 1988. Molecular Degradation, Injectivity, and Elastic Properties of Polymer Solutions. *SPE Journal*, 1193-1201, November 1988. DOI: 10.2118/15652-PA.

15.) STARS Users Manual, Version 2009.13, Computer Modeling Group, Calgary, Alberta, Canada, 2009.

16.) Stavland, A., Jonsbraaten, H.C. and Lohne, A. 2010. Polymer Flooding – Flow Properties in Porous Media versus Rheological Parameters. Paper SPE 131103, presented at the SPE EUROPE/EAGE Annual Conference and Exhibition, Barcelona, Spain 14-17 June 2010. DOI: 10.2118/131103-MS.

17.) Zaitoun, A. and Kohler, N. 1987. The Role of Adsorption in Polymer Propagation through Reservoir Rocks. Paper SPE 16274, presented at the SPE International Symposium on Oilfield Chemistry, San Antonio, Texas 4-6 February 1987. DOI: 10.2118/16274-MS.
18.) Zaitoun, A. and Chauveteau, G. 1998. Effect of Pore Structure and Residual Oil on Polymer Bridging Adsorption. Paper SPE 39674, presented at SPE/DOE Improved Oil Recovery Symposium, Tulsa, Oklahoma, U.S.A. 19-22 April 1998. DOI: 10.2118/39674-MS.
19.) Zitha, P., Chauveteau, G., Zaitoun, A. 1995. Permeability-Dependent Propagation of Polyacrylamides under Near-Wellbore Flow Conditions. Paper SPE 28955, presented at the SPE International Symposium on Oilfield Chemistry, San Antonio, Texas, 14-17 February 1995. DOI: 10.2118/28955-MS.